2012

Time-domain parameter identification of aeroelastic loads by forced-vibration method for response of flexible structures subject to transient wind

Bochao Cao
Iowa State University

Time-domain parameter identification of aeroelastic loads by forced-vibration method for response of flexible structures subject to transient wind

by

Bochao Cao

A dissertation submitted to the graduate faculty

in partial fulfillment of the requirements for the degree of

DOCTOR OF PHILOSOPHY

Major: Engineering Mechanics

Program of Study Committee:
Partha P. Sarkar, Major Professor
Hui Hu
Peter Sherman
William Gallus
Sivalingam Sritharan

Iowa State University

Ames, Iowa

2012

TABLE OF CONTENTS

ABSTRACT

Slender structures representing civil, mechanical and aerospace systems such as long-span bridges, high-rise buildings, stay cables, power-line cables, high light mast poles, crane-booms and aircraft wings could experience vortex-induced and buffeting excitations below their design wind speeds and divergent self-excited oscillations (flutter) beyond a critical wind speed because these are flexible. Traditional linear aerodynamic theories that are routinely applied for their response prediction are not valid in the galloping, or near-flutter regime, where large-amplitude vibrations could occur and during non-stationary and transient wind excitations that occur, for example, during hurricanes, thunderstorms and gust fronts. The linear aerodynamic load formulation for lift, drag and moment are expressed in terms of aerodynamic functions in frequency domain that are valid for straight-line winds which are stationary or weakly-stationary. Application of the frequency domain formulation is restricted from use in the nonlinear and transient domain because these are valid for linear models and stationary wind. The time-domain aerodynamic force formulations are suitable for finite element modeling, feedback-dependent structural control mechanism, fatigue-life prediction, and above all modeling of transient structural behavior during non-stationary wind phenomena. This has motivated the developing of time-domain models of aerodynamic loads that are in parallel to the existing frequency-dependent models. Parameters defining these time-domain models can be now extracted from wind tunnel tests, for example, the Rational Function Coefficients defining the self-excited wind loads can be extracted using section model tests using the free vibration technique. However, the free vibration method has some limitations because it is difficult to apply at high wind speeds, in turbulent wind environment, or on unstable cross sections with negative aerodynamic damping. In the

current research, new algorithms were developed based on forced vibration technique for direct extraction of the Rational Functions. The first of the two algorithms developed uses the two angular phase lag values between the measured vertical or torsional displacement and the measured aerodynamic lift and moment produced on the section model subject to forced vibration to identify the Rational Functions. This algorithm uses two separate one-degree-of-freedom tests (vertical or torsional) to identify all the four Rational Functions or corresponding Rational Function Coefficients for a two degrees-of-freedom (DOF) vertical-torsional vibration model. It was applied to a streamlined section model and the results compared well with those obtained from earlier free vibration experiment. The second algorithm that was developed is based on direct least squares method. It uses all the data points of displacements and aerodynamic lift and moment instead of phase lag values for more accurate estimates. This algorithm can be used for one-, two- and three-degree-of-freedom motions. A two-degree-of-freedom forced vibration system was developed and the algorithm was shown to work well for both streamlined and bluff section models. The uniqueness of the second algorithms lies in the fact that it requires testing the model at only two wind speeds for extraction of all four Rational Functions. The Rational Function Coefficients that were extracted for a streamlined section model using the two-DOF Least Squares algorithm were validated in a separate wind tunnel by testing a larger scaled model subject to straight-line, gusty and boundary-layer wind.

CHAPTER 1. GENERAL INTRODUCTION

WIND EFFECT ON FLEXIBLE STRUCTURES

When designing flexible structures for wind, dynamic wind loads are of primary interest to structural engineers. The dynamic wind loads can be generally classified as: *self-excited*, *buffeting* and *vortex-shedding induced*.

For a given structure immersed in wind, the motion of the structure perturbs the flow around it such that the modified flow pattern produces additional aerodynamic damping and stiffness loads that are called *self-excited* wind loads. The *self-excited* wind loads will either transfer energy from wind to the structural motion or help in dissipating the kinetic energy of the structure. Above a certain wind speed, the energy increment exceeds the energy dissipation from wind such that the kinetic energy of the structure keeps increasing which makes the structure dynamically unstable. This critical wind speed at which the structure becomes unstable is called *flutter speed*.

Buffeting wind loads are fluctuating loads acting on a structure because of its location in the atmospheric boundary layer. The fluctuating wind loads are induced by turbulence in the up-coming wind and can be calculated based on a statistical description of the turbulence characteristics of the undisturbed flow approaching the structure. Using admittance function formulation proposed by Davenport (1962), the turbulence characteristics can be converted from the wind properties into wind loads on the structure. The frequency-domain admittance function formulation can be also transformed to time-domain indicial function formulation which can be used in time-domain structural analysis.

Shedding of alternating vortices from the top and bottom surfaces of a solid body immersed in wind could be observed in its wake. The shed vortices are accompanied by periodically changing pressure distributions around the bluff body which can induce periodic aerodynamic loads on the body, termed as *vortex-shedding* induced loads. As observed by Strouhal (1878) on a circular cross section cylinder, of a given diameter, the product of vortex-shedding frequency (f_s) and diameter (D) divided by flow velocity (U) is a constant known as Strouhal number (St). The Strouhal number is constant for a given cross section for a wide range of wind speeds. Thus, the vortex-shedding frequency of a cross section increases linearly with the up-coming wind velocity, and when it coincides with a natural frequency of the structure with that cross section, the resonance phenomenon occurs. This phenomenon, known as *lock-in*, appears within a certain range of wind velocity.

LITERATURE REVIEW AND MOTIVATION FOR CURRENT RESEARCH

Due to the development of high-strength material and modern construction technology in civil and construction engineering, the structures are becoming taller and longer. The tallest building in the world, the Burj Khalifa Tower in Dubai, has a height of 828m, while the longest suspension bridge in the world, the Akashi Kaikyo Bridge in Japan has a main span length of 1991m. These very long or tall structures are flexible and very vulnerable to wind loads. Thus, during the design process of these flexible structures, it is definitely necessary to perform structural analysis on them with expecting wind environment, so that large amplitude structural motion and instability of structural response can be avoided in the future.

The aeroelastic behavior of models can be studied either through full structure model test or section model test. A full structure model is a geometrically-scaled three-dimensional model with scaled mechanical properties that can be tested in a wind tunnel subjected to a scaled atmospheric boundary layer flow. The advantage of a full-structure model is that the response and aerodynamic loads of the prototype structure can be easily obtained by simply scaling the measurements of the model and the wind directionality and upstream terrain effects can be determined. However, full structure models are usually very expensive and they need to be tested in wind tunnels with very large test sections. A section model is an appropriately scaled and detailed geometrical model of a typical two-dimensional section of a structure and is commonly used to determine the aeroelastic response characteristics of a prototype structure with a particular cross-sectional shape. The aeroelastic loads and/or response of a section model are used to determine its aeroelastic properties that can be analytically extended to predict the response and loads of the corresponding prototype structure.

In section model structural analysis, the equations of motion for the two-dimensional cross section can be written in Equations (1)-(3).

$$m(\ddot{h} + 2\varsigma_h \omega_h \dot{h} + \omega_h^2 h) = L_b + L_{se} + L_{vs} \tag{1}$$

$$m(\ddot{p} + 2\varsigma_p \omega_p \dot{p} + \omega_p^2 p) = D_b + D_{se} \tag{2}$$

$$I(\ddot{\alpha} + 2\varsigma_\alpha \omega_\alpha \dot{\alpha} + \omega_\alpha^2 \alpha) = M_b + M_{se} + M_{vs} \tag{3}$$

where m and I are the mass and mass moment of inertia per unit length of the structure, h, p and α are vertical, lateral and torsional displacement of the structure as a function of time,

($\dot{}$) and ($\ddot{}$) are corresponding velocity and acceleration, respectively, *L*, *D* and *M* are dynamic lift, drag and moment per unit length applied on the structure, ω and ζ are natural frequency and damping ratio of corresponding degree-of-freedom, and the subscript *b*, *se* and *vs* stand for buffeting load, self-excited load and vortex shedding load, respectively.

In Equations (1)-(3), all the displacements are only functions of time. However, in three-dimensional full structure model, the displacements are functions of time, *t*, as well as spanwise position, *x*. Modal analysis can be used in a full structure analysis where the modal equations have the form of Equations (1)-(3) and the total response of the structure can be calculated as the summation of responses in all modes included in the analysis.

For some structures whose dynamic response in lateral direction is not as prominent as the other two directions, the equations of motion can be simplified such that lateral displacement, *p*, and drag, *D*, are neglected and the equation of motion in the lateral direction is dropped in the analysis.

Flutter Phenomenon of Flexible Structures and Frequency Domain Flutter Analysis

The first famous event that drew people's attention to wind load effects on structures is the collapse of Tacoma Narrows Bridge that happened in 1940. The failure of this bridge was caused by a dramatic aeroelastic instability phenomenon which is called flutter. When a structure moves in wind, sometimes the wind around the structure could do positive work on it and the kinetic energy is transported from wind to the structure, or the wind could also do negative work on the structure and the kinetic energy of the structure is dissipated by its interaction with wind. When energy dissipation in the structural system is larger than the energy generation in the structure from wind, the structure is stable and its motion would get

damped out. Otherwise, the motion of the structure will diverge since the kinetic energy of the structure will keep increasing, and this phenomenon is called flutter. For single mode response of a structural system, the flutter phenomenon could happen when the total damping ratio has decreased to a negative value because of the negative damping brought by the self-excited wind loads. For multi-degree-of-freedom system, the flutter phenomenon could happen even when the total damping in all the modes are positive, since it could be caused by coupling between different modes leading to loss of stiffness.

In 1935, Theodorsen derived a mixed frequency-time domain formulation which is commonly used for the study of unsteady aerodynamic behavior of streamlined airfoil sections. By adopting a generalization of Theodorsen's theory (1935), Scanlan and Tomko (1971) developed a flutter derivative formulation to solve unsteady aerodynamic problems on bluff bodies like civil structures. The original formulation was proposed in a form with two-degree-of-freedom, and was extended to a general three-degree-of-freedom form later as shown in Equations (4)-(6).

$$L_{se} = \frac{1}{2}\rho U^2 B\left[KH_1^*(K)\frac{\dot{h}}{U} + KH_2^*(K)\frac{B\dot{\alpha}}{U} + KH_5^*(K)\frac{\dot{p}}{U} + K^2H_3^*(K)\alpha + K^2H_4^*(K)\frac{h}{B} + K^2H_6^*(K)\frac{p}{B}\right] \tag{4}$$

$$M_{se} = \frac{1}{2}\rho U^2 B^2\left[KA_1^*(K)\frac{\dot{h}}{U} + KA_2^*(K)\frac{B\dot{\alpha}}{U} + KA_5^*(K)\frac{\dot{p}}{U} + K^2A_3^*(K)\alpha + K^2A_4^*(K)\frac{h}{B} + K^2A_6^*(K)\frac{p}{B}\right] \tag{5}$$

$$D_{se} = \frac{1}{2}\rho U^2 B\left[KP_5^*(K)\frac{\dot{h}}{U} + KP_2^*(K)\frac{B\dot{\alpha}}{U} + KP_1^*(K)\frac{\dot{p}}{U} + K^2P_3^*(K)\alpha + K^2P_6^*(K)\frac{h}{B} + K^2P_4^*(K)\frac{p}{B}\right] \tag{6}$$

where ρ = air density, U = mean wind speed, B = width of bridge deck model, K = Bω/U = reduced frequency, where ω = 2πf = circular frequency of vibration, H_i^*, A_i^*, P_i^* (i=1,…,6)

are aeroelastic coefficients known as flutter derivatives that are functions of reduced velocity ($U/fB = 2\pi/K$). The number of flutter derivatives is 18 for a three-degree-of-freedom system, while this number reduces to 8 for a two-degree-of-freedom system.

The flutter derivatives in the formulation mentioned earlier are frequency dependent parameters which need to be extracted from wind tunnel tests. In decades following the early seventies, various methods, including system-identification based ones to extract the flutter derivatives from wind tunnel experiments, were developed by Scanlan and his co-workers (Scanlan and Tomko, 1971, Huston, 1988, Scanlan, 1978, Scanlan and Jones, 1990, Sarkar et al., 1994) and many others. Sarkar et al. (1994)'s Modified Ibrahim Time Domain (MITD) method, Brownjohn and Jakobsen (2001)'s Covariance Block Hankel Matrix (CBHM) method, Gu et al. (2000), Zhu et al. (2002), Gan Chowdhury and Sarkar (2004)'s Iterative Least Squares (ILS) method, Chen et al. (2008), Chen and Kareem (2008), Bartoli et al. (2009), Ding et al. (2010) and a few other efficient methods were developed and accepted as standard methods for the identification of flutter derivatives. All extraction methods can be classified into two types, namely, free vibration and forced vibration, based on the excitation of the section model tests. In free vibration methods, the section model is released from initial displacements and then allowed to vibrate freely in the wind tunnel at fixed wind speed. The section model test can be done in one-degree-of-freedom, two-degree-of-freedom or all three-degree-of-freedom. The test is repeated at several wind speeds and the model displacement time histories that are recorded at an individual wind speed are substituted into a system-identification based algorithm to extract flutter derivatives. In forced vibration methods, the section model is driven to vibrate sinusoidally with fixed amplitude and

frequency. The phase lag between the model displacement time history and the aerodynamic load time history, computed from surface pressure measurement or direct force measurement, is identified and used in the algorithm to extract flutter derivatives. Unlike free vibration tests, two separate one-degree-of-freedom tests need to be conducted to get all 8 flutter derivatives associated with two-degree-of-freedom (vertical and torsional) model formulation.

In flutter analysis, one method known as Scanlan's root-finding approach (Scanlan, 1981) is used where a value of reduced frequency, K, is chosen and the values of flutter derivatives corresponding to that K are obtained from plots of these experimental functions. The values of flutter derivatives are substituted into Equations (4)-(6) and Equations (1)-(3) and a matrix analysis is then performed on the equations of motion where roots of the real and imaginary parts (ω) of determinant of the coefficient matrix multiplying the assumed displacement solution vector are found by equating them to zero. This process is repeated by varying K and the roots (ω) of the real and imaginary parts are plotted as a function of K. The intersection of the two curves defines the critical frequency (ω_c) and critical reduced frequency ($K_c=B\omega_c/U_c$). The critical flutter velocity (U_c) can be easily found using $U_c= B\omega_c/ K_c$.

Time Domain Analysis and Motivation for Current Research

Frequency domain method is suitable to problems corresponding to stationary or weakly-stationary wind input and small amplitudes of structural response. However, to incorporate the nonstationarity of wind environment and nonlinearity of structural vibration in the analysis, time domain formulations for aerodynamic forces (Lin and Ariaratnam, 1980; Scanlan, 1984; Tsiatas and Sarkar, 1988; Scanlan, 1993; Chen and Kareem, 2002) were

proposed and investigated. Moreover, these time domain formulations are also suitable for finite element modeling, feedback-dependent structural control mechanism and fatigue-life prediction.

In time domain, self-excited forces can be directly formulated in indicial functions (Tsiatas and Sarkar, 1988; Caracoglia and Jones, 2003), or they can be first written in Rational Functions (Roger, 1977; Karpel, 1982) in Laplace domain, and then be transformed into time domain. The Rational Function formulation with one lag term for two-degree-of-freedom system can be written as Equation (7) and the corresponding time domain formulation is as Equations (8) and (9).

$$\begin{bmatrix} \hat{L}_{se} \\ \hat{M}_{se} \end{bmatrix} = \begin{bmatrix} \frac{1}{2}\rho U^2 B & 0 \\ 0 & \frac{1}{2}\rho U^2 B^2 \end{bmatrix} \begin{bmatrix} (\underline{A}_0)_{11} + (\underline{A}_1)_{11} p + \frac{F_{11} p}{p+\lambda} & (\underline{A}_0)_{12} + (\underline{A}_1)_{12} p + \frac{F_{12} p}{p+\lambda} \\ (\underline{A}_0)_{21} + (\underline{A}_1)_{21} p + \frac{F_{21} p}{p+\lambda} & (\underline{A}_0)_{22} + (\underline{A}_1)_{22} p + \frac{F_{22} p}{p+\lambda} \end{bmatrix} \begin{bmatrix} \hat{h}/B \\ \hat{\alpha} \end{bmatrix} \tag{7}$$

$$L_{se}(t) = \frac{1}{2}\rho U^2 B \begin{bmatrix} \left((\underline{A}_0)_{11} + (\underline{F})_{11}\right)\frac{h}{B} + (\underline{A}_1)_{11}\frac{\dot{h}}{U} - (\underline{F})_{11}\frac{\lambda U}{B^2}\int_0^t e^{-\frac{U}{B}\lambda(t-\tau)} h(\tau) d\tau \\ + \left((\underline{A}_0)_{12} + (\underline{F})_{12}\right)\alpha + (\underline{A}_1)_{12}\frac{B}{U}\dot{\alpha} - (\underline{F})_{12}\frac{\lambda U}{B}\int_0^t e^{-\frac{U}{B}\lambda(t-\tau)} \alpha(\tau) d\tau \end{bmatrix} \tag{8}$$

$$M_{se}(t) = \frac{1}{2}\rho U^2 B^2 \begin{bmatrix} \left((\underline{A}_0)_{21} + (\underline{F})_{21}\right)\frac{h}{B} + (\underline{A}_1)_{21}\frac{\dot{h}}{U} - (\underline{F})_{21}\frac{\lambda U}{B^2}\int_0^t e^{-\frac{U}{B}\lambda(t-\tau)} h(\tau) d\tau \\ + \left((\underline{A}_0)_{22} + (\underline{F})_{22}\right)\alpha + (\underline{A}_1)_{22}\frac{B}{U}\dot{\alpha} - (\underline{F})_{22}\frac{\lambda U}{B}\int_0^t e^{-\frac{U}{B}\lambda(t-\tau)} \alpha(\tau) d\tau \end{bmatrix} \tag{9}$$

where B= width of the bridge deck, U= mean wind velocity, $p = iK$ is nondimensional Laplace domain variable, K= Bω/U= reduced frequency of the vibration, where ω= 2πf= circular frequency of the vibration, '^' denotes the Laplace transformation of the

corresponding time domain function, L_{se} and M_{se} are self-excited lift and moment, respectively, h is vertical displacement and α is torsional displacement. $\underline{A}_0$, $\underline{A}_1$, $\underline{F}$ and λ are Rational Function Coefficients. $\underline{A}_0$, $\underline{A}_1$ are stiffness matrix and damping matrix, respectively, and $\underline{F}$ is a lag matrix, all of order 2×2, λ is a lag coefficient,

The two-degree-of-freedom flutter derivative formulation can be transformed into Laplace domain as shown in Equation (10).

$$\begin{bmatrix} \hat{L}_{se} \\ \hat{M}_{se} \end{bmatrix} = \begin{bmatrix} \frac{1}{2}\rho U^2 B & 0 \\ 0 & \frac{1}{2}\rho U^2 B^2 \end{bmatrix} \begin{bmatrix} K^2 H_4^*(K) + pKH_1^*(K) & K^2 H_3^*(K) + pKH_2^*(K) \\ K^2 A_4^*(K) + pKA_1^*(K) & K^2 A_3^*(K) + pKA_2^*(K) \end{bmatrix} \begin{bmatrix} \hat{h}/B \\ \hat{\alpha} \end{bmatrix} \quad (10)$$

where H_1^*- H_4^* and A_1^*- A_4^* are flutter derivatives for a two-degree-of-freedom system.

Using relationships between Equation (7) and Equation (10), the coefficients in Rational Function formulation can be obtained from flutter derivatives by approximation techniques; these relationships are defined later in chapters 2 and 3. Rational Function formulation has been applied to bridge aerodynamics by several researchers including Xie (1988), Xiang et al. (1988), Wilde et al. (1996) and Chen et al. (2000). However, this is an indirect way to obtain Rational Function Coefficients since flutter derivatives need to be obtained first from experiments. Thus, to make the process of extracting the rational function coefficients more efficient, Gan Chowdhury and Sarkar (2005) developed a new method based on free vibration of section models where both displacements and surface pressures of the model were simultaneously recorded and used. However, it is known that the free vibration method has some limitations compared to the forced vibration method because it is particularly unsuitable for higher wind velocities, non-stationary flow and larger amplitudes. Thus, a

forced vibration experimental method is required to extract the Rational Functions that will be valid for higher wind speeds and larger amplitudes so that these parameters can be applied to predict the transient response of structures in non-stationary wind flow like tornadoes, microbursts, hurricanes, thunderstorms and gust fronts.

In current research, the forced vibration technique was developed to extract all Rational Function Coefficients for both one degree-of-freedom (one-DOF) and two degree-of-freedom (two-DOF) systems. The analytical approach of the forced vibration technique to identify flutter derivatives is similar in principle to that described in Matsumoto (1996) and Haan (2000). Essentially, while driving the model in a prescribed sinusoidal motion, the pressure is measured on the top and bottom surfaces of the model in the streamwise direction. The pressure signals are integrated to obtain lift and moment time series. Phase angle differences between the motions (the angular and vertical positions) and the aerodynamic forces (the lift and the moment) are estimated that can be used to identify the flutter derivatives. Four flutter derivatives can be identified at a time with a one-DOF motion and hence two separate one-DOF tests are usually done to identify all eight flutter derivatives associated with a two-DOF system. Following on the same principle, a phase-lag-dependent algorithm was developed for a one-DOF (vertical or torsional) system to identify all the Rational Function Coefficients corresponding to one phase-lag term in the formulation.

However, the current forced-vibration techniques for extraction of flutter derivatives (Haan, 2000, Matsumoto, 1996) or the first method developed in current research for extraction of Rational Function Coefficients (Cao and Sarkar, 2010) have some limitations. Firstly, these methods are based on the phase difference between simultaneously obtained displacement

and aerodynamic load time histories. In a recently concluded comparative and sensitivity study (Sarkar et al., 2009), it was shown that in a phase-difference-dependent forced vibration technique to extract the four flutter derivatives based on a pure torsional motion system, the errors in A_2^* and H_2^* could be significant, since slight errors in the phase difference obtained from the experiment gets amplified in the formulation that defines A_2^* and H_2^*. Similar observation was made in the phase-difference-dependent technique to extract Rational Function Coefficients (Cao and Sarkar, 2010). Secondly, these methods were all based on one degree-of-freedom (DOF) motion (vertical or torsional), and aeroelastic coefficients (flutter derivatives or Rational Function Coefficients) associated with two degrees of freedom were obtained by combining results from two separate one DOF tests. Considering there is a physical difference between the aerodynamics of one DOF and two DOF motions, there might be errors introduced in the aeroelastic coefficients obtained by one DOF system because the actual aerodynamic interaction of a two DOF system may not be captured well. Thus, in current research, another forced vibration method that does not use the phase difference is developed to extract all the Rational Function Coefficients simultaneously from a two-DOF dynamic system for the first time. Moreover, the method developed here is more efficient than earlier ones, since it requires data obtained at two wind speeds only to solve for the full set of Rational Function Coefficients.

Time Domain Aeroelastic Load Prediction and Experimental Validation

As mentioned earlier, time domain analysis is necessary for wind engineering problems with nonstationary wind environment or nonlinear structural characteristics and can be used for finite element modeling, feedback-dependent structural control mechanism and fatigue-life

prediction. Thus, many scholars have put their efforts in proposing and investigating time domain formulations for aeroelastic loads (Lin and Ariaratnam, 1980; Scanlan, 1984; Tsiatas and Sarkar, 1988; Scanlan, 1993; Li and Lin, 1995; Scanlan, 2000; Chen et al., 2000; Chen and Kareem, 2002; Salvatori and Borri, 2007; Zhang et al., 2011). However, most of previous research works in time domain analysis area are concentrated on numerical simulations, while experimental validations of time domain formulations are very limited. In current research, a validation procedure is performed through wind tunnel tests on a section model. In the future, based on the experimental procedure carried out in this research work, approaches of revising current time domain formulations for different types of problems (e.g. non-stationary winds, large amplitude motions, etc.) could also possibly be developed.

In current research, self-excited forces were simulated using Rational Function formulation and the coefficients extracted from earlier forced vibration wind tunnel tests. The fluctuating buffeting forces can be modeled using aerodynamic admittance functions (Simiu and Scanlan, 1996; Scanlan and Jones, 1999) in frequency domain and buffeting indicial aerodynamic functions in time domain. Chang et al. (2010) used the relationship between the two formulations for buffeting forces and devised a procedure to identify the buffeting indicial functions of a structural section. This procedure was used here to identify the buffeting indicial functions for the streamlined bridge deck. In this research, these time domain functions for self-excited and buffeting forces were used to predict the total aeroelastic loads acting on a streamlined bridge deck section model with an aspect ratio (B/D) of 15:1 that was subjected to stationary and different gusty winds (ramp-up, ramp-down, bump-shaped), and compared with wind tunnel measurements for validation of these time-domain formulations

of aeroelastic loads. For first set of experiment, smooth winds were applied on the model. In the second set of experiment, two different types of atmospheric boundary layers were generated using spires, chains and roughness blocks in the upstream of the section model to investigate performance of time-domain formulations in turbulent wind cases.

THESIS ORGANIZATION

The current dissertation is written in the format of "Thesis Containing Journal Papers". The dissertation includes four manuscripts out of which three are submitted and under review, and the fourth one is to be submitted to a scholarly journal. In addition, a general introduction chapter appears at the beginning and a general conclusion chapter appears at the end of the dissertation. Because of this "Thesis Containing Journal Papers" format, some repetition might be found in the introduction and experimental set-up parts of each chapter.

The first paper, submitted to Wind and Structures, appears as the second chapter of this dissertation. In this paper, an algorithm is presented for direct extraction of these Rational Functions from section model tests in forced vibration using phase lag. The motivation for using forced-vibration method came from the potential use of these Rational Functions to predict aerodynamic loads and response of flexible structures at high wind speeds and in turbulent wind environment. Numerical tests were performed to verify the robustness and performance of the algorithm under different noise levels that are expected in wind tunnel data. Wind tunnel tests in one degree-of-freedom (vertical/torsional) forced vibration were performed on a streamlined bridge deck section model whose Rational Functions were compared with those obtained by free vibration for the same model.

The second paper, submitted to Engineering Structures, appears as the third chapter of this dissertation. In this paper, a new algorithm that is developed for direct extraction of the Rational Functions from section model tests using forced-vibration technique is presented. The new algorithm can be used to extract all the Rational Functions associated with one, two or three degree-of-freedom motion (vertical, lateral and torsional) of a section model. To validate the new algorithm, forced vibration wind tunnel tests in two degrees of freedom (vertical and torsional) were performed on a streamlined bridge deck section model with width-to-depth ratio B/D = 15:1 and also a bluff rectangular section model with B/D = 5:1. This is a significant improvement from previous forced-vibration methods that require separate one-degree-of-freedom model tests which are dependent on phase angle difference between aerodynamic loads and displacements.

The third paper, submitted to Journal of Engineering Mechanics, appears as the fourth chapter of this dissertation. In this paper, time domain formulations were used to predict aeroelastic loads acting on a rigid bridge deck section model subject to stationary and gusty straight-line winds that are smooth or laminar based on the knowledge of upstream wind speed and model displacement measurements. In this procedure, Rational Function Coefficients are used to formulate the self-excited forces. The coefficients used here were recently obtained from wind tunnel tests performed on a streamlined bridge deck section model with a smaller geometric scale in smooth flow. The results of the validation using a larger section model of this bridge deck subject to a ramp-type gust are presented here.

The fourth paper appears as the fifth chapter of the dissertation. In this paper, to validate time domain formulations in turbulent wind environment, wind tunnel tests were performed with

turbulence generated by two different boundary layer set-ups in the up-stream of the section model. To incorporate gust effects simultaneously on the prediction of wind loads, different types of gusts (ramp-up, ramp-down and bump-shaped) were also generated in the tests.

REFERENCES

Bartoli, G., Contri, S., Mannini, C., Righi, M. (2009). "Toward an improvement in the identification of bridge deck flutter derivatives," J. Eng. Mech., ASCE, 135(8), 771-785.

Brownjohn, J.M.W., Jakobsen, J.B. (2001). "Strategies for aeroelastic parameter identification from bridge deck free vibration data," J. of Wind Eng. and Ind. Aero., 89, 1113-1136.

Cao, B., Sarkar, P.P. (2010). "Identification of rational functions by forced vibration method for time-domain analysis of flexible structures," In Proceedings: The Fifth International Symposium on Computational Wind Engineering, Chapel Hill, May 23-27.

Caracoglia, L., Jones, N.P. (2003). "Time domain vs. frequency domain characterization of aeroelastic forces for bridge deck sections," J. of Wind Eng. and Ind. Aero., 91, 371-402.

Chang, B., Sarkar, P.P. and Phares, B.M., (2010). "A time-domain model for predicting aerodynamic loads on a slender support structures for fatigue design," Journal of Engineering Mechanics, 136(6), 736-746.

Chen, C., Wu, J., Chen, J. (2008). "Prediction of flutter derivatives by artificial neural networks," J. Wind Eng. Ind. Aerodyn., 96, 1925-1937.

Chen, X., Matsumoto, M., and Kareem, A. (2000). "Time domain flutter and buffeting response analysis of bridges," J Eng Mech, 126(1), 7-16.

Chen, X. and Kareem, A. (2002). "Advances in modeling of aerodynamic forces on bridge decks," J. Eng. Mech., ASCE, 128 (11), 1193-1205.

Chen, X., Kareem, A. (2008). "Identification of critical structural modes and flutter derivatives for predicting coupled bridge flutter," J. Wind Eng. Ind. Aerodyn., 96, 1856-1870.

Davenport, A.G. (1962). "Buffeting of a suspension bridge by storm winds," J. Structural Eng., ASCE, 88 (3), 233-268.

Ding, Q., Zhou, Z., Zhu, L., Xiang, H. (2010). "Identification of flutter drivatives of bridge decks with free vibration technique," J. Wind Eng. Ind. Aerodyn., 98, 911-918.

Gan Chowdhury, A., Sarkar, P.P. (2003). "A new technique for identification of eighteen flutter derivatives using a three-degree-of-freedom section model," Eng. Struct., 25(14), 1763-1772.

Gan Chowdhury, A., Sarkar, P.P. (2004). "Identification of eighteen flutter derivatives of an airfoil and a bridge deck," Wind and Struct., 7(3), 187-202.

Gan Chowdhury, A., Sarkar, P.P. (2005). "Experimental identification of rational function coefficients for time-domain flutter analysis," Eng. Struct., 27(9), 1349-1364.

Gu, M., Zhang, R., Xiang, H. (2000). "Identification of flutter derivatives of bridge decks." J. Wind Eng. Ind. Aerodyn., 84, 151-162.

Haan, F.L. (2000). “The effects of turbulence on the aerodynamics of long-span bridges,” Ph.D. Dissertation. Notre Dame (Indiana, USA): University of Notre Dame.

Haan, F.L., Sarkar, P.P. (2006). “Development of an active gust generation mechanism on a wind tunnel for wind engineering and industrial aerodynamics applications,” Wind and Struct., 9(5), 369-386.

Huston D.R., Bosch, H.R., Scanlan, R.H. (1988). “The effects of fairings and of turbulence on the flutter derivatives of a notably unstable bridge deck,” J. of Wind Eng. and Ind. Aero., 29(1-3), 339-349.

Karpel, M. (1982). “Design for active flutter suppression and gust alleviation using state-space aeroelastic modeling,” J. of Aircraft 19(3), 221–227.

Matsumoto, M. (1996). “Aerodynamic damping of prisms,” Journal of Wind Engineering and Industrial Aerodynamics, 59(2-3), 159-175.

Li, Q.C. and Lin, Y.K. (1995). “New stochastic theory for bridge stability in turbulent flow.” J. Eng. Mech., 121(1), 102-116.

Lin, Y.K. and Ariaratnam, S.T. (1980). “Stability of bridge motion in turbulent winds,” J. of Struct. Mech., 8 (1), 1-15.

Roger, K. (1977). “Airplane math modeling methods for active control design,” AGARD-CP-228.

Salvatori, L., and Borri, C. (2007). “Frequency and time-domain methods for the numerical modeling of full-bridge aeroelasticity.” Comput. Struct., 85, 675-687.

Sarkar, P.P., Jones, N.P., Scanlan, R.H. (1994). "Identification of aeroelastic parameters of flexible bridges," J. Eng. Mech., 120(8), 1718-1742.

Sarkar, P.P., Gan Chowdhury, A., Gardner, T.B. (2004). "A novel elastic suspension system for wind tunnel section model studies," J. of Wind Eng. and Ind. Aero., 92, 23-40.

Sarkar, P.P., Caracoglia, L., Haan Jr., F.L., Sato, H., Murakoshi, J. (2009). "Comparative and sensitivity study of flutter derivatives of selected bridge deck sections, Part1: Analysis of inter-laboratory experimental data," Eng. Struct., 31(1), 158-169.

Scanlan, R.H., Tomko, J.J. (1971). "Airfoil and bridge deckflutter derivatives," J. Eng. Mech. Div., 97(6), 1717-1733.

Scanlan, R.H. (1978). "The action of lexible bridges under wind, I: flutter theory," J. Sound Vib. 60(2), 187-199.

Scanlan, R.H. (1981). "State-of-the-art methods for calculating flutter, vortex induced, and buffeting response of bridge structures." Federal Highway Administration Report No. FHWA/RD 80/50.

Scanlan, R.H. (1984). "Role of indicial functions in buffeting analysis of bridges," J. of Struc. Eng., 110 (7).

Scanlan, R.H. (1993). "Problematics in formulation of wind-force models for bridge decks," J. Eng. Mech., ASCE, 119 (7), 1353-1375.

Scanlan, R.H., Jones, N.P. (1990). "A minimum design methodology for evaluating bridge flutter and buffeting response," J. of Wind Eng. and Ind. Aero.,36(2), 1341-1353.

Scanlan, R.H. and Jones, N.P. (1999). "A form of aerodynamic admittance for use in bridge aeroelastic analysis. J. Fluids and Struct., 13, 1017-1027.

Scanlan, R.H. (2000). "Motion-related body force functions in two-dimensional low-speed flow." J. Fluids Struct., 14, 49-63.

Sengupta, A., Sarkar, P.P. (2008). "Experimental measurement and numerical simulation of an impinging jet with application to thunderstorm microburst winds," J. of Wind Eng. and Ind. Aero.,96(3), 345-365.

Shinozuka, M. (1971). "Simulation of multivariate and multidimensional random processes," The Journal of the Acoustical Society of America, 49, 357-368.

Simiu, E. and Scanlan, R.H. (1996). "Wind effects on structures: fundamentals and applications to design," 3rd ed., John Wiley & Sons, New York, NY.

Strouhal, V. (1878). "On one particular way of tone generation," Annalen der Physik und Chemie (Leipzig), ser. 3.

Tsiatas, G., Sarkar, P.P. (1988). "Motion stability of long-span bridges under gusty winds," J. of Eng. Mech., ASCE, 114(2).

Wilde K., Fujino Y., Masukawa J. (1996). "Time domain modeling of bridge deck flutter," Struct Eng/Earthq Eng, JSCE 13(2): 93-104.

Xiang H., Xie J., Lin Z. (1988). "Aerodynamic study on a proposed cable-stayed bridge in Shanghai, China," J Wind Eng Ind Aerodyn 29:419-427.

Xie J. (1988). “CVR method for identification of nonsteady aerodynamic model,” J Wind Eng Ind Aerodyn 29:389-397.

Yang, W.W. and Chang, T.Y.P., 1998. Numerical simulation of turbulent fluctuations along the axis of a bridge. Eng. Struct., The Journal of Earthquake, Wind and Ocean Engineering, 20 (9): pp. 837-848.

Zhang, Z., Chen, Z., Cai, Y., Ge, Y. (2011). “Indicial functions for bridge aeroelastic forces and time-domain flutter analysis.” J. Bridge Eng., ASCE, 16(4), 546-557.

Zhu, L.D., Xu, Y.L., Zhang, F., Xiang, H.F. (2002). “Tsing Ma bridge deck under skew winds- Part II: flutter derivatives.” J. Wind Eng. Ind. Aerodyn., 90, 807-837.

CHAPTER 2. EXTRACTION OF RATIONAL FUNCTIONS BY FORCED VIBRATION METHOD FOR TIME-DOMAIN ANALYSIS OF LONG-SPAN BRIDGES

A paper submitted to Wind and Structures

Bochao Cao[1a], Partha P. Sarkar [1b*]

[1] *2271 Howe Hall, Department of Aerospace Engineering, Iowa State University, Ames, IA, 50011-2271, USA*

Abstract: Rational Functions are used to express the self-excited aerodynamic forces acting on a flexible structure for use in time-domain flutter analysis. The Rational Function Approximation (RFA) approach involves obtaining of these Rational Functions from the frequency-dependent flutter derivatives by using an approximation. In the past, an algorithm was developed to directly extract these Rational Functions from wind tunnel section model tests in free vibration. In this paper, an algorithm is presented for direct extraction of these Rational Functions from section model tests in forced vibration. The motivation for using forced-vibration method came from the potential use of these Rational Functions to predict aerodynamic loads and response of flexible structures at high wind speeds and in turbulent wind environment. Numerical tests were performed to verify the robustness and performance of the algorithm under different noise levels that are expected in wind tunnel data. Wind tunnel tests in one degree-of-freedom (vertical/torsional) forced vibration were performed on

[*b] Corresponding author: Professor, E-mail: ppsarkar@iastate.edu
[a] Graduate Research Assistant, E-mail: cbc@iastate.edu

a streamlined bridge deck section model whose Rational Functions were compared with those obtained by free vibration for the same model.

Keywords: flutter analysis, time-domain method, rational function approximation, forced vibration, long-span bridges

1 INTRODUCTION

Analysis to predict wind-induced flutter instability of flexible structures is usually conducted in frequency domain, since the self-excited aerodynamic forces induced by motion of structures are expressed by the well-known flutter derivatives (Scanlan and Tomko 1971) that are functions of reduced frequency. Flutter derivatives can be identified at discrete reduced frequencies (or reduced velocities) through either free vibration (Chowdhury and Sarkar 2003, Chen et al. 2008, Chen and Kareem 2008, Bartoli et al. 2009, Ding et al. 2010) or forced vibration (Matsumoto 1996, Haan 2000) method using section models in wind tunnels. However, when dealing with wind interacting with nonlinear structures or structures excited by non-stationary winds, the time-domain method (Lin and Ariaratnam 1980, Scanlan 1993, Chen and Kareem 2002, Caracoglia and Jones 2003, Zhang et al. 2011) is more suitable and preferable. Roger (1977) developed a Rational Function Approximation (RFA) using least squares (LS) method for approximation of self-excited forces with rational functions in Laplace domain that can be used in time-domain analysis. These functions can be indirectly extracted from experimentally obtained flutter derivatives using approximation techniques. Karpel (1982) developed another RFA formulation using minimum state method known as MS-RFA that involves lesser computational work while maintaining higher

accuracy of approximation compared to LS-RFA by Roger. RFA formulation has been applied to bridge aerodynamics by several researchers including Chen et al. (2000). To accelerate the process of extraction of Rational Functions, Chowdhury and Sarkar (2005) developed a method through which Rational Functions can be extracted directly from free vibration experiments in a wind tunnel at fewer wind velocities compared to those used for extracting flutter derivatives. It is known that the free vibration method has some limitations compared to the forced vibration method, particularly, at higher wind velocities and for turbulent flow. This provides the motivation of developing a forced vibration method to extract the Rational Functions from wind tunnel tests.

In this paper, a new algorithm for forced vibration experimental method is developed for direct extraction of Rational Functions. Results from both numerical simulation and wind tunnel tests are presented to validate the algorithm. A streamlined bridge deck section model with a chord-to-thickness ratio of about 15:1 was used as an example.

2 FORMULATION AND ALGORITHM

In two degree-of-freedom (DOF), self-excited forces acting on the structure can be calculated from flutter derivative formulation as given below:

$$L_{se}(t) = \frac{1}{2}\rho U^2 B\left[\mathrm{K}H_1^*(K)\frac{\dot{h}}{U} + \mathrm{K}H_2^*(K)\frac{B\dot{\alpha}}{U} + \mathrm{K}^2 H_3^*(K)\alpha + \mathrm{K}^2 H_4^*(K)\frac{h}{B}\right] \quad (1)$$

$$M_{se}(t) = \frac{1}{2}\rho U^2 B^2\left[\mathrm{K}A_1^*(K)\frac{\dot{h}}{U} + \mathrm{K}A_2^*(K)\frac{B\dot{\alpha}}{U} + \mathrm{K}^2 A_3^*(K)\alpha + \mathrm{K}^2 A_4^*(K)\frac{h}{B}\right] \quad (2)$$

where L_{se} = self-excited lift, M_{se} = self-excited torsional moment, ρ = air density, U = mean wind speed, B = width of bridge deck model, $K = B\omega/U$ = reduced frequency, where $\omega = 2\pi f$

= circular frequency of the vibration, h(t,x) = vertical displacement, α(t,x) = torsional displacement, (˙) = d( )/dt, H_i^*, A_i^* (i=1,…,4) = flutter derivatives which are aeroelastic coefficients changing with reduced frequency.

Applying Laplace transformation on Equations (1) and (2):

$$\begin{bmatrix} \hat{L}_{se} \\ \hat{M}_{se} \end{bmatrix} = \underline{V}_f \underline{\tilde{Q}} \underline{\hat{q}} = \begin{bmatrix} \frac{1}{2}\rho U^2 B & 0 \\ 0 & \frac{1}{2}\rho U^2 B^2 \end{bmatrix} \begin{bmatrix} \mathrm{K}^2 H_4^*(K) + p.\mathrm{K} H_1^*(K) & \mathrm{K}^2 H_3^*(K) + p.\mathrm{K} H_2^*(K) \\ \mathrm{K}^2 A_4^*(K) + p.\mathrm{K} A_1^*(K) & \mathrm{K}^2 A_3^*(K) + p.\mathrm{K} A_2^*(K) \end{bmatrix} \begin{bmatrix} \hat{h}/B \\ \hat{\alpha} \end{bmatrix} \tag{3}$$

where p = iK = nondimensional Laplace domain variable, and '^' denotes the Laplace transformation of the corresponding time domain function. By Karpel (1982)'s minimum state RFA formulation with neglect of second order term, the matrix $\underline{\tilde{Q}}$ can be approximated by $\underline{Q}$, which is a matrix of rational functions in Laplace domain, as given below:

$$\underline{Q}(p) = \underline{A}_0 + \underline{A}_1 p + \underline{D}\left(p\underline{I} + \underline{R}\right)^{-1} \underline{E} p \tag{4}$$

where $\underline{A}_0, \underline{A}_1$ are stiffness matrix and damping matrix, respectively, $\underline{D}$ and $\underline{E}$ are lag matrices, $\underline{R}$ is a diagonal matrix with diagonal elements of lag coefficients, and the dimension of the matrix $\underline{R}$ is the number of lag terms. Since Chowdhury and Sarkar (2005) showed that, the formulation with even one lag term works well for streamlined and bluff bridge decks, in this paper, only formulation with one lag term is used. With only one lag term, Equation (4) can be written as given below:

$$\underline{Q}(p) = \begin{bmatrix} \underline{Q}_{11} & \underline{Q}_{12} \\ \underline{Q}_{21} & \underline{Q}_{22} \end{bmatrix} = \underline{A}_0 + \underline{A}_1 p + \begin{bmatrix} \underline{D}_{11} \\ \underline{D}_{21} \end{bmatrix} \frac{p}{p+\lambda} \begin{bmatrix} \underline{E}_{11} & \underline{E}_{12} \end{bmatrix} = \underline{A}_0 + \underline{A}_1 p + \frac{p}{p+\lambda} \begin{bmatrix} \underline{F}_{11} & \underline{F}_{12} \\ \underline{F}_{21} & \underline{F}_{22} \end{bmatrix} = \underline{A}_0 + \underline{A}_1 p + \frac{p}{p+\lambda} \underline{F} \tag{5}$$

where $\underline{A}_0, \underline{A}_1, \underline{F}$ and λ are referred here as Rational Function Coefficients.

Substituting Equation (5) into Equation (3), self-excited aerodynamic forces in Laplace domain can be obtained:

$$\hat{L}_{se} = \frac{1}{2}\rho U^2 B\left[\left(\left(\underline{A}_0\right)_{11} + \left(\underline{A}_1\right)_{11} p + \frac{\underline{F}_{11} p}{p+\lambda}\right) \quad \left(\left(\underline{A}_0\right)_{12} + \left(\underline{A}_1\right)_{12} p + \frac{\underline{F}_{12} p}{p+\lambda}\right)\right]\hat{\underline{q}} \tag{6}$$

$$\hat{M}_{se} = \frac{1}{2}\rho U^2 B^2\left[\left(\left(\underline{A}_0\right)_{21} + \left(\underline{A}_1\right)_{21} p + \frac{\underline{F}_{21} p}{p+\lambda}\right) \quad \left(\left(\underline{A}_0\right)_{22} + \left(\underline{A}_1\right)_{22} p + \frac{\underline{F}_{22} p}{p+\lambda}\right)\right]\hat{\underline{q}} \tag{7}$$

To obtain higher accuracy, formulation with two lag terms could be used, as derived in Chowdhury (2004).

Applying inverse Laplace transformation on Equations (6) and (7), time domain formulations can be obtained as given below:

$$\dot{L}_{se} + \lambda\frac{U}{B}L_{se} = \frac{1}{2}\rho U^2 B\left(\left(\frac{U}{B}\right)\underline{\psi}_1\underline{q} + \underline{\psi}_2\dot{\underline{q}} + \left(\frac{B}{U}\right)\underline{\psi}_3\ddot{\underline{q}}\right) \tag{8}$$

$$\dot{M}_{se} + \lambda\frac{U}{B}M_{se} = \frac{1}{2}\rho U^2 B^2\left(\left(\frac{U}{B}\right)\underline{\psi}_4\underline{q} + \underline{\psi}_5\dot{\underline{q}} + \left(\frac{B}{U}\right)\underline{\psi}_6\ddot{\underline{q}}\right) \tag{9}$$

where $\underline{\psi}_1 = \left[\lambda\left(\underline{A}_0\right)_{11} \quad \lambda\left(\underline{A}_0\right)_{12}\right]$, $\underline{\psi}_2 = \left[\left(\underline{A}_0\right)_{11} + \lambda\left(\underline{A}_1\right)_{11} + \underline{F}_{11} \quad \left(\underline{A}_0\right)_{12} + \lambda\left(\underline{A}_1\right)_{12} + \underline{F}_{12}\right]$,

$\underline{\psi}_3 = \left[\left(\underline{A}_1\right)_{11} \quad \left(\underline{A}_1\right)_{12}\right]$, $\underline{\psi}_4 = \left[\lambda\left(\underline{A}_0\right)_{21} \quad \lambda\left(\underline{A}_0\right)_{22}\right]$,

$\underline{\psi}_5 = \left[\left(\underline{A}_0\right)_{21} + \lambda\left(\underline{A}_1\right)_{21} + \underline{F}_{21} \quad \left(\underline{A}_0\right)_{22} + \lambda\left(\underline{A}_1\right)_{22} + \underline{F}_{22}\right]$, $\underline{\psi}_6 = \left[\left(\underline{A}_1\right)_{21} \quad \left(\underline{A}_1\right)_{22}\right]$

In a forced vibration method, the model is constrained to vibrate in one-DOF, vertical, torsional or horizontal motion, where the displacement is a sinusoidal motion at a prescribed amplitude and frequency. For the current study, experiments in vertical and torsional degrees of freedom were performed to validate the new method, respectively.

In vertical motion experiment, the displacements h and α can be written as:

$$h = h_0\cos\left(\omega_h t\right),\ \alpha = 0 \tag{10}$$

At a certain mean wind velocity, U_1, since there is a lag between self-excited aerodynamic loads (lift and moment) and the corresponding displacement, the self-excited loads can be written as:

$$L_{se} = L_{h0}^1 \cos\left(\omega_h t - \phi_{Lh}^1\right) \tag{11}$$

$$M_{se} = M_{h0}^1 \cos\left(\omega_h t - \phi_{Mh}^1\right) \tag{12}$$

Substituting Equations (10) and (11) into Equation (8):

$$\begin{aligned} &-L_{h0}^1 \omega_h \sin(\omega_h t - \phi_{Lh}^1) + \lambda \frac{U_1}{B} L_{h0}^1 \cos(\omega_h t - \phi_{Lh}^1) \\ &= \frac{1}{2}\rho U_1^{\,2} B\left(\left(\frac{U_1}{B}\right)\left(\underline{\psi_1}\right)_1 \frac{h_0 \cos(\omega_h t)}{B} - \left(\underline{\psi_2}\right)_1 \frac{h_0 \omega_h \sin(\omega_h t)}{B} - \left(\frac{B}{U_1}\right)\left(\underline{\psi_3}\right)_1 \frac{h_0 \left(\omega_h\right)^2 \cos(\omega_h t)}{B}\right) \end{aligned} \tag{13}$$

By matching coefficients of $\sin(\omega_h t)$ and $\cos(\omega_h t)$ above, following equations can be obtained:

$$\begin{aligned} \left[\omega_h B \sin\phi_{Lh}^1 + \lambda U_1 \cos\phi_{Lh}^1\right]\frac{L_{h0}^1}{h_0} &= \frac{1}{2}\rho\left(U_1\right)^2 B\left(\left(\frac{U_1}{B}\right)\left(\underline{\psi_1}\right)_1 - \left(\frac{B}{U_1}\right)\left(\underline{\psi_3}\right)_1 \left(\omega_h\right)^2\right) \\ \left[\omega_h B \cos\phi_{Lh}^1 - \lambda U_1 \sin\phi_{Lh}^1\right]\frac{L_{h0}^1}{h_0} &= \frac{1}{2}\rho\left(U_1\right)^2 B\left(\underline{\psi_2}\right)_1 \omega_h \end{aligned} \tag{14a}$$

Equations (14a) can be re-written in matrix form:

$$\begin{bmatrix} \frac{1}{2}\rho\left(U_1\right)^3 & 0 & -\frac{1}{2}\rho U_1 B^2\left(\omega_h\right)^2 & -U_1\frac{L_{h0}^1}{h_0}\cos\phi_{Lh}^1 \\ 0 & \frac{1}{2}\rho\left(U_1\right)^2 B\omega_h & 0 & U_1\frac{L_{h0}^1}{h_0}\sin\phi_{Lh}^1 \end{bmatrix} \begin{bmatrix} \left(\underline{\psi_1}\right)_1 \\ \left(\underline{\psi_2}\right)_1 \\ \left(\underline{\psi_3}\right)_1 \\ \lambda \end{bmatrix} = \omega_h \frac{B}{h_0}\begin{bmatrix} L_{h0}^1 \sin\phi_{Lh}^1 \\ L_{h0}^1 \cos\phi_{Lh}^1 \end{bmatrix} \tag{14b}$$

Since the above equations have four unknowns, $\left(\underline{\psi_1}\right)_1$ to $\left(\underline{\psi_3}\right)_1$ and λ, it cannot be solved. However, if similar equations are written for two more wind velocities, U_2 and U_3, and

combined with Equation (14b) , the following matrix of six equations in terms of the four unknowns can be obtained:

$$\underline{C_{h1}}\,\underline{X_{h1}} = \underline{D_{h1}} \tag{15}$$

where $\underline{C_{h1}} = \begin{bmatrix} \frac{1}{2}\rho(U_1)^3 & 0 & -\frac{1}{2}\rho U_1 B^2(\omega_h)^2 & -U_1\frac{L^1_{h0}}{h_0}\cos\phi^1_{Lh} \\ 0 & \frac{1}{2}\rho(U_1)^2 B\omega_h & 0 & U_1\frac{L^1_{h0}}{h_0}\sin\phi^1_{Lh} \\ \frac{1}{2}\rho(U_2)^3 & 0 & -\frac{1}{2}\rho U_2 B^2(\omega_h)^2 & -U_2\frac{L^2_{h0}}{h_0}\cos\phi^2_{Lh} \\ 0 & \frac{1}{2}\rho(U_2)^2 B\omega_h & 0 & U_2\frac{L^2_{h0}}{h_0}\sin\phi^2_{Lh} \\ \frac{1}{2}\rho(U_3)^3 & 0 & -\frac{1}{2}\rho U_3 B^2(\omega_h)^2 & -U_3\frac{L^3_{h0}}{h_0}\cos\phi^3_{Lh} \\ 0 & \frac{1}{2}\rho(U_3)^2 B\omega_h & 0 & U_3\frac{L^3_{h0}}{h_0}\sin\phi^3_{Lh} \end{bmatrix}$, $\underline{D_{h1}} = \omega_h\frac{B}{h_0}\begin{bmatrix} L^1_{h0}\sin\phi^1_{Lh} \\ L^1_{h0}\cos\phi^1_{Lh} \\ L^2_{h0}\sin\phi^2_{Lh} \\ L^2_{h0}\cos\phi^2_{Lh} \\ L^3_{h0}\sin\phi^3_{Lh} \\ L^3_{h0}\cos\phi^3_{Lh} \end{bmatrix}$,

and $\underline{X_{h1}} = \begin{bmatrix} (\underline{\psi_1})_1 \\ (\underline{\psi_2})_1 \\ (\underline{\psi_3})_1 \\ \lambda \end{bmatrix}$

By Least Squares method, the unknown vector $\underline{X_{h1}}$ can be solved as:

$$\underline{X_{h1}} = \left[\underline{C_{h1}}^T\,\underline{C_{h1}}\right]^{-1}_{4\times4}\left[\underline{C_{h1}}^T\,\underline{D_{h1}}\right]_{4\times1} \tag{16a}$$

Similarly, by substituting Equations (10) and (12) into Equation (9), the unkown vector $\underline{X_{h2}}$ can be solved as:

$$\underline{X_{h2}} = \left[\underline{C_{h2}}^T\,\underline{C_{h2}}\right]^{-1}_{4\times4}\left[\underline{C_{h2}}^T\,\underline{D_{h2}}\right]_{4\times1} \tag{16b}$$

where $\underline{C_{h2}} = \begin{bmatrix} \frac{1}{2}\rho(U_1)^3 B & 0 & -\frac{1}{2}\rho U_1 B^3(\omega_h)^2 & -U_1\frac{M^1_{h0}}{h_0}\cos\phi^1_{Mh} \\ 0 & \frac{1}{2}\rho(U_1)^2 B^2\omega_h & 0 & U_1\frac{M^1_{h0}}{h_0}\sin\phi^1_{Mh} \\ \frac{1}{2}\rho(U_2)^3 B & 0 & -\frac{1}{2}\rho U_2 B^3(\omega_h)^2 & -U_2\frac{M^2_{h0}}{h_0}\cos\phi^2_{Mh} \\ 0 & \frac{1}{2}\rho(U_2)^2 B^2\omega_h & 0 & U_2\frac{M^2_{h0}}{h_0}\sin\phi^2_{Mh} \\ \frac{1}{2}\rho(U_3)^3 B & 0 & -\frac{1}{2}\rho U_3 B^3(\omega_h)^2 & -U_3\frac{M^3_{h0}}{h_0}\cos\phi^3_{Mh} \\ 0 & \frac{1}{2}\rho(U_3)^2 B^2\omega_h & 0 & U_3\frac{M^3_{h0}}{h_0}\sin\phi^3_{Mh} \end{bmatrix}$,

$\underline{D_{h2}} = \omega_h \frac{B}{h_0}\begin{bmatrix} M^1_{h0}\sin\phi^1_{Mh} \\ M^1_{h0}\cos\phi^1_{Mh} \\ M^2_{h0}\sin\phi^2_{Mh} \\ M^2_{h0}\cos\phi^2_{Mh} \\ M^3_{h0}\sin\phi^3_{Mh} \\ M^3_{h0}\cos\phi^3_{Mh} \end{bmatrix}$, and $\underline{X_{h2}} = \begin{bmatrix} (\underline{\psi_4})_1 \\ (\underline{\psi_5})_1 \\ (\underline{\psi_6})_1 \\ \lambda \end{bmatrix}$

In this algorithm, data from experiments at only three wind speeds (U_1 to U_3) are needed which is the minimum requirement for the least squares method. However, to increase the accuracy of the algorithm, data collected at more number of wind speeds could be included. This will add more number of rows in the matrix $\underline{C_{hi}}$ and vector $\underline{D_{hi}}$.

Finally, from vectors $\underline{X_{h1}}$ and $\underline{X_{h2}}$, $(\underline{A_0})_{11}$, $(\underline{A_0})_{21}$, $(\underline{A_1})_{11}$, $(\underline{A_1})_{21}$, $(\underline{F})_{11}$, $(\underline{F})_{21}$ and λ can be obtained, and Q_{11} and Q_{21} can be obtained from Equation (5). Following a similar procedure, using data from forced vibration experiments under torsional motion of the model $(\underline{A_0})_{12}$, $(\underline{A_0})_{22}$, $(\underline{A_1})_{12}$, $(\underline{A_1})_{22}$, $(\underline{F})_{12}$, $(\underline{F})_{22}$ and λ, as well as Q_{12} and Q_{22}, can be obtained. It is noted that λ for the vertical motion case and torsional motion case may not be the same.

Thus, this algorithm will require simultaneous measurements of the displacements (h or α) along with the surface pressures on the model that will help compute the self-excited forces, lift (L_{se}) and moment (M_{se}). Amplitudes of the self-excited forces (L_{se} and M_{se}) that are computed from pressures and their phase lags (ϕ's) with respect to displacement (h or α) along with amplitude and frequency of the displacement and the mean wind speeds are used as input to the algorithm.

3 EXPERIMENTAL SET-UP

3.1 *Wind tunnel used*

The experiments were performed in the Bill James Open-Return Wind Tunnel, which is located in the Wind Simulation and Testing Laboratory (WiST Lab) in the Department of Aerospace Engineering at Iowa State University. This wind tunnel has a test section of 0.915m (3.0ft) width by 0.762m (2.5ft) height and its maximum wind velocity is 75 m/s (246 ft/s).

3.2 *Model, suspension system and forced vibration mechanism*

A streamlined bridge deck section model was used in the experiment as shown in Fig. 1 and 2. The model is composed of a shallow box girder section and two semi-circular fairings at the edges. The length, chord length and thickness of the model are about 0.533m, 0.3m, and 0.02m, respectively. The three-DOF model suspension system and two Plexiglas end plates that were used to reduce the edge defects on the model are shown in Fig. 2. This system was developed by Sarkar et al. (2004). The suspension system enables vertical, horizontal and torsional motions of the model. In the current experiments, sinusoidal vertical and torsional motions of the model with constant amplitudes and frequencies are realized by the driving

mechanism connected to the model suspension system with four aluminum rods as shown in Fig. 2. The entire mechanism is driven by two motors which are placed above the test section, as seen in Fig. 3. By changing the rotating speed of two motors using two separate controllers, the two frequencies of model vibration in two degrees of freedom can be changed independently.

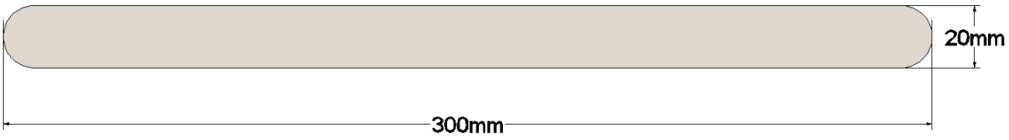

Figure 1. Cross section of the streamlined bridge deck model used in the experiment

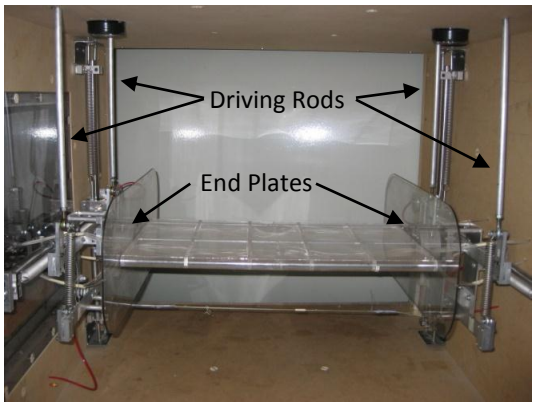

Figure 2. Bridge deck model and suspension system

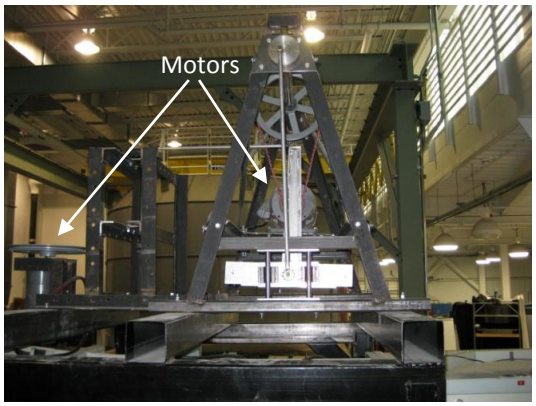

Figure 3. Driving mechanism

3.3 *Displacement measurement*

The vertical displacement of the model was measured by measuring the elastic force in each of two springs which is connected to the model at one end and a strain gage force transducer at the other end. The torsional displacement was measured by measuring the torque at one end of the model shaft using a torque transducer which is mounted on the suspension system. LabView was used for data acquisition, where the sampling rate was set at 625Hz.

3.4 *Aerodynamic force measurement*

The algorithm stated in this paper, in addition to the displacement time histories, requires the time histories of aerodynamic forces acting on the model while it is vibrating. Therefore, surface pressures were measured on the model including the fairings through a row of pressure taps located on the upper and lower surfaces of the model along the mid-plane. In total, forty-two pressure taps were used in this test, equally distributed on both the surfaces. The pressure taps are denser on the upstream side than the downstream side of the model. Two 64-channel pressure modules (Scanivalve ZOC33/64 Px) were used to measure the pressure. The sampling rate for pressure measurement was 312.5Hz (half of displacement sampling rate) in the experiment. To synchronize the pressure data with the displacement data, the pressure transducers were set to work in external-trigger mode. The LabView program that was used for displacement data acquisition, was programmed to output a digital signal when the displacement data acquisition started, so that the pressure data acquisition system would receive this external signal and get triggered to start the acquisition of pressure. A separate program RAD (Scanivalve) was used to collect the pressure data.

4 RESULTS AND DISCUSSIONS

4.1 *Numerical tests and results*

To validate the algorithm as presented here, numerical tests were done before using it with wind tunnel data. Firstly, the displacement time history of the model was generated as a sinusoidal function with the same amplitude and frequency as those of the wind tunnel tests. Secondly, the first derivative of the displacement history was generated through central difference method. Using the flutter derivatives for the cross section mentioned here (Chowdhury and Sarkar, 2003, 2004), the aerodynamic lift and moment time histories (L_{se} and M_{se}) were generated. Using the lift, moment and displacement time histories as input, rational function coefficients were extracted using the algorithm developed here. The relationship between rational function coefficients and flutter derivatives, as given below, were used to calculate the flutter derivatives for comparison with those used:

$$H_1^* = imag(Q_{11})/\mathrm{K}^2,\ H_4^* = real(Q_{11})/\mathrm{K}^2,\ \ A_1^* = imag(Q_{21})/\mathrm{K}^2,\ A_4^* = real(Q_{21})/\mathrm{K}^2$$

$$H_2^* = imag(Q_{12})/K^2,\ H_3^* = real(Q_{12})/K^2,\ A_2^* = imag(Q_{22})/K^2,\ A_3^* = real(Q_{22})/K^2 \qquad (17)$$

An excellent agreement between the two sets of flutter derivatives proved the feasibility of the algorithm for extraction of rational function coefficients.

However, in a wind tunnel experiment, the test data can be contaminated with noise. Therefore, to test the robustness of the algorithm, white noise time histories with a normal probability distribution were scaled and added to the displacement and force time histories that were generated, and then rational function coefficients were extracted from these noisy data using the algorithm. The standard deviation of the noise time histories was chosen as 10%

and 20% of the respective signal amplitudes. The flutter derivatives extracted using Equation (17) from these noisy data were compared with those extracted from the original numerical data, and the percentage errors (root mean square) were calculated as shown in Table 1. In Table 1, it is seen that H_4*, A_4*, H_2* and A_2* are more sensitive to the noise in the data than the rest of the flutter derivatives. However, the errors in all eight flutter derivatives change marginally even with the doubling of noise amplitudes.

Table 1 Percentage errors for derivatives drawn from noisy data

Noise Amplitudes	H_1*	H_4*	A_1*	A_4*	H_2*	H_3*	A_2*	A_3*
10%	0.3	5.0	0.2	1.8	0.9	0.2	1.1	1.0
20%	0.4	6.2	0.3	3.6	2.1	0.3	1.8	1.0

4.2 *Experimental results*

For vertical DOF forced vibration of the bridge deck model, wind tunnel tests were performed at wind speeds of 4m/s, 6.7m/s and 11.1m/s, while for torsional DOF forced vibration, measurements were carried out at wind speeds of 3.6m/s, 10.2m/s and 15.2m/s. The model was forced to vibrate at 2.44Hz for vertical motion and 3.28 Hz for torsional motion. The rational functions Q_{11}, Q_{21}, Q_{12} and Q_{22}, as obtained by the algorithm and method mentioned here, are shown in Fig. 4. For the purpose of validation of the rational functions obtained using the proposed algorithm, these were converted to corresponding flutter derivatives of the streamlined bridge section and compared with those obtained earlier by free vibration method (Chowdhury and Sarkar, 2003). However, error envelopes need to be assessed for each of these two data sets before the comparison. All eight flutter derivatives (H_1* to H_4*, A_1* to A_4*) were calculated using the obtained rational functions (Equation (17))

and error envelopes of these flutter derivatives were obtained using perturbed rational functions that were extracted using modified phase lag angles,$\phi_{Lh}, \phi_{Mh}, \phi_{L\alpha}$and $\phi_{M\alpha}$, with ±7% error added to their obtained values. Similarly, error envelopes for flutter derivative data sets that were obtained by free vibration method (Chowdhury and Sarkar, 2003) were calculated by adding ±7% errors to the original phase lag angles, $\phi_{Lh}, \phi_{Mh}, \phi_{L\alpha}$and $\phi_{M\alpha}$, obtained from the numerically generated displacement and force time histories without noise as in Section 4.1. Both sets of flutter derivatives and their corresponding error envelopes are plotted for comparison in Fig. 5.

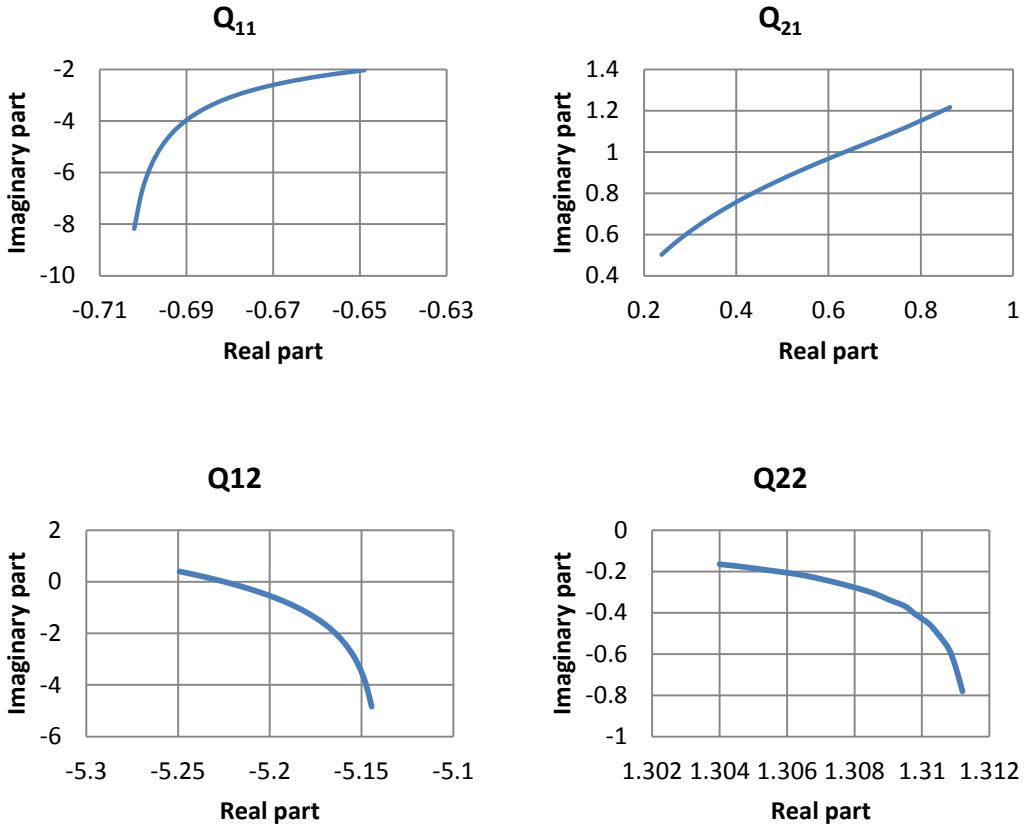

Figure 4. Experimentally obtained Rational Functions

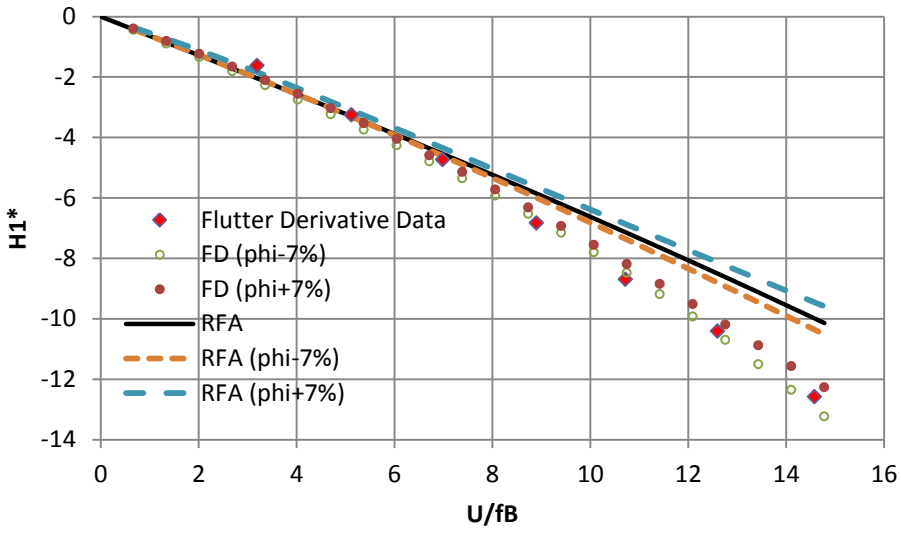
H1*
U/fB
Flutter Derivative Data
FD (phi-7%)
FD (phi+7%)
RFA
RFA (phi-7%)
RFA (phi+7%)
0
-2
-4
-6
-8
-10
-12
-14
0
2
4
6
8
10
12
14
16

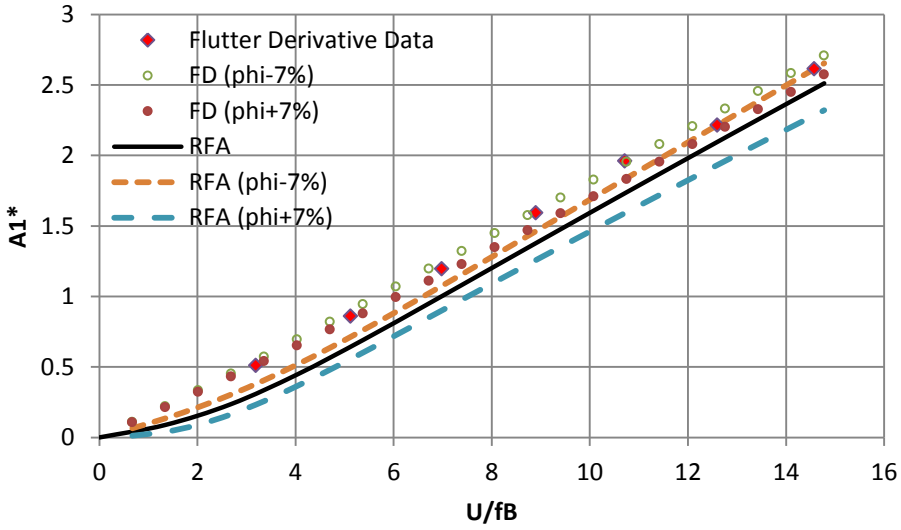
A1*
U/fB
Flutter Derivative Data
FD (phi-7%)
FD (phi+7%)
RFA
RFA (phi-7%)
RFA (phi+7%)
3
2.5
2
1.5
1
0.5
0
0
2
4
6
8
10
12
14
16

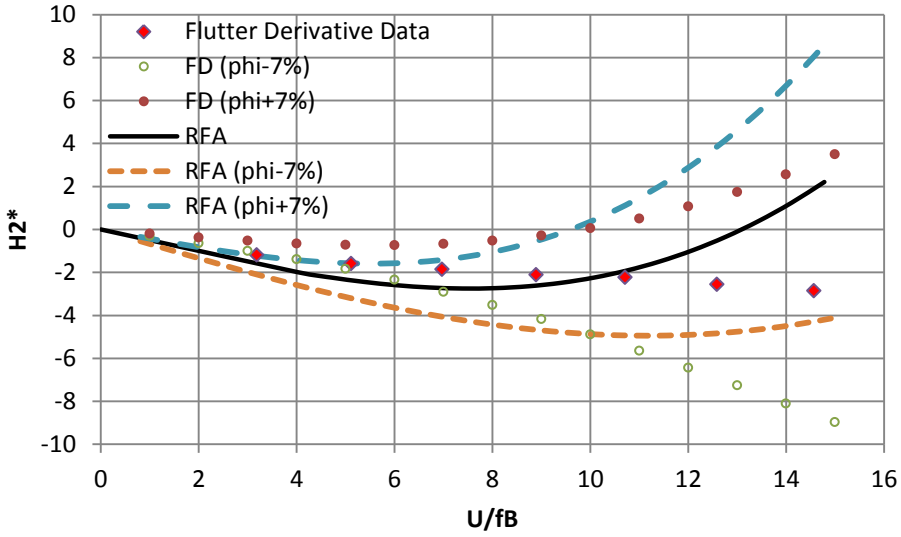
Flutter Derivative Data
FD (phi-7%)
FD (phi+7%)
RFA
RFA (phi-7%)
RFA (phi+7%)
H2*
U/fB
10
8
6
4
2
0
-2
-4
-6
-8
-10
0
2
4
6
8
10
12
14
16

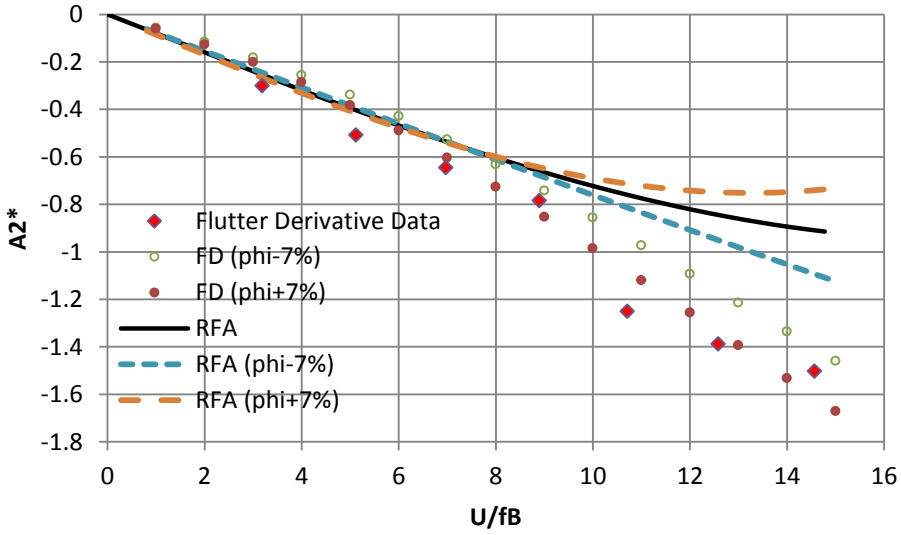
Flutter Derivative Data
FD (phi-7%)
FD (phi+7%)
RFA
RFA (phi-7%)
RFA (phi+7%)
A2*
U/fB
0
-0.2
-0.4
-0.6
-0.8
-1
-1.2
-1.4
-1.6
-1.8
0
2
4
6
8
10
12
14
16

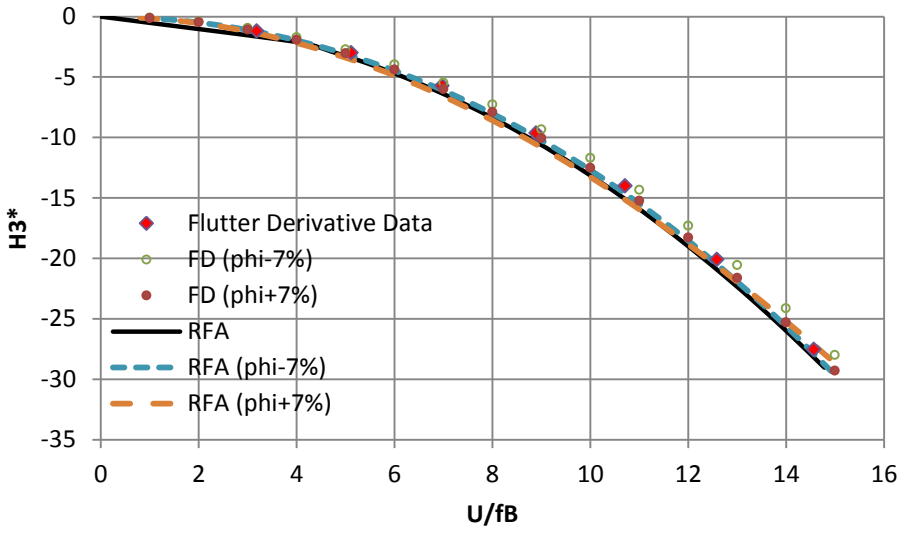
H3*
U/fB
Flutter Derivative Data
FD (phi-7%)
FD (phi+7%)
RFA
RFA (phi-7%)
RFA (phi+7%)
0
-5
-10
-15
-20
-25
-30
-35
0
2
4
6
8
10
12
14
16

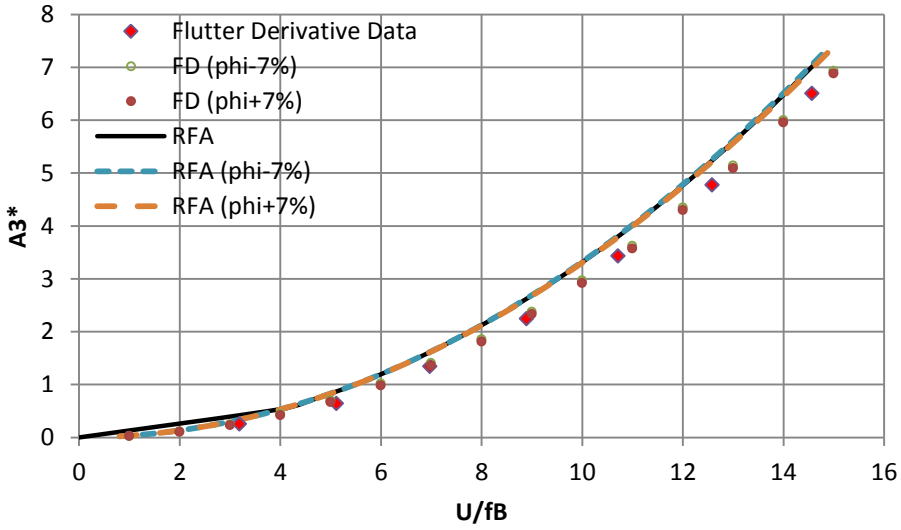
A3*
U/fB
Flutter Derivative Data
FD (phi-7%)
FD (phi+7%)
RFA
RFA (phi-7%)
RFA (phi+7%)
8
7
6
5
4
3
2
1
0
0
2
4
6
8
10
12
14
16

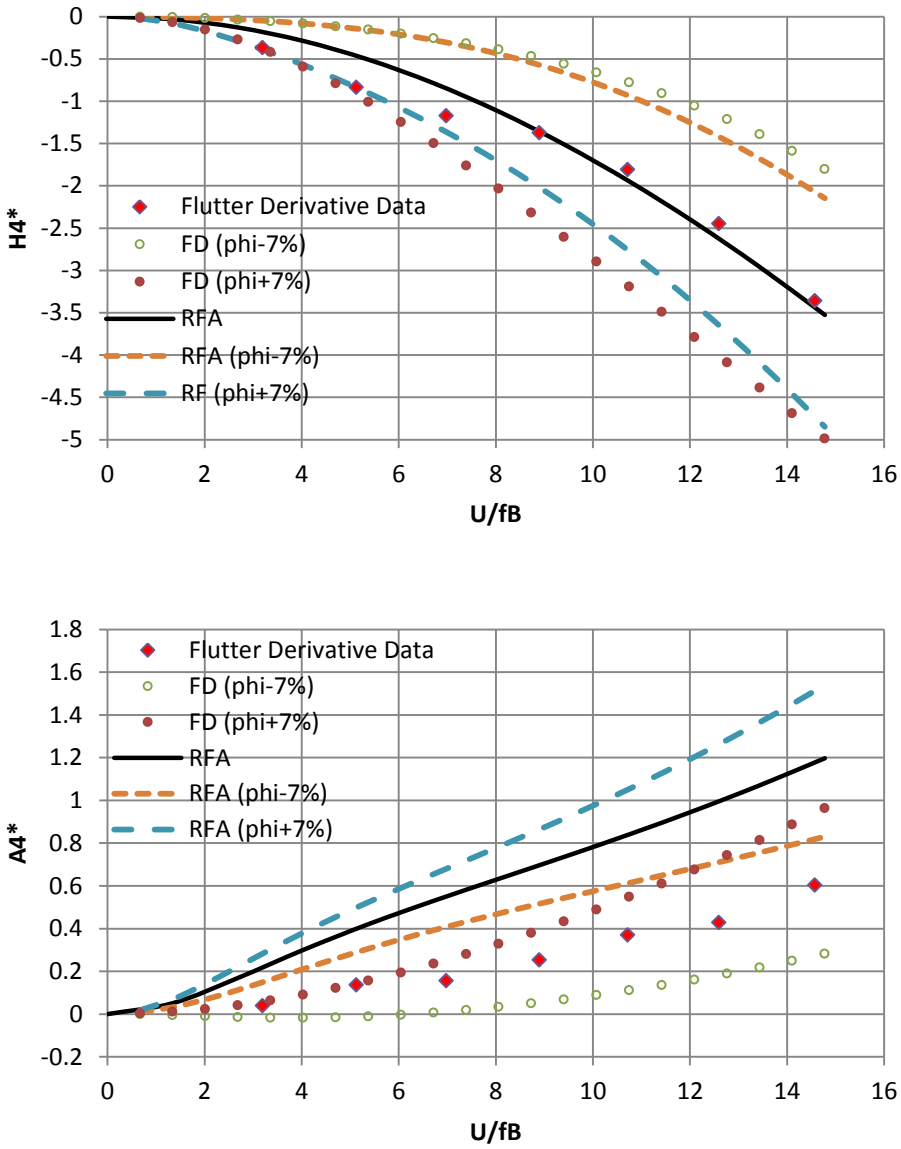

Figure 5. Comparison of experimentally obtained flutter derivatives and those from experimental Rational Functions

These plot show that H_4*, A_1*, H_3* and A_3* match very well with earlier flutter derivative data obtained by free vibration method. H_1*, H_2* and A_2* curves match well for low reduced velocities and there are some differences at higher reduced velocities. This could be because

the free vibration method need not be very accurate at high wind speeds when aerodynamic damping is positive and large. This difference could be also attributed to the fact that the free-vibration experiments were of two-DOF (vertical and torsional) while the forced vibration experiments stated here were two separate one-DOF motion experiments (vertical and torsional, respectively) for extraction of all eight flutter derivatives. It could be a combination of both reasons. The worst comparison is the A_4*curves. The A_4* extracted from RFA method here is almost twice of that free vibration method. This could be because of the difference in degrees of freedom or it could be because A_4* is more sensitive to the noise in the experimental data as concluded by numerical tests (Table 1). However, in Fig. 5, all the 7% error bands for flutter derives from RFA (rational function approximation) data overlap with corresponding 7% error bands for free vibration flutter derivative data. Moreover, from error bands plotted in Fig. 5, it is seen that H_4*, A_4* and H_2* are more sensitive to the phase difference than other flutter derivatives. This is similar to the results presented in Table 1. Actually, it has been shown by Sarkar et al. (2009) that, in forced vibration technique to extract flutter derivatives, slight error in estimation of the phase difference between aerodynamic loads and displacements obtained from experiments could get amplified in some of the flutter derivatives (A_2* and H_2* in Sarkar et al., 2009), which is similar to what is observed here in H_4*, A_4*, H_2* and A_2* plots in Fig. 5.

To further validate the method, the flutter speed of the streamlined bridge deck section model was predicted using time domain simulation and Rational Function Coefficients extracted here. The flutter speed obtained here was compared with that obtained by Gan Chowdhury and Sarkar (2005) for the same model using Rational Functions (free vibration) and flutter derivatives (free vibration) and shown in Table 2. To investigate the effect of error

in phase difference on the prediction of flutter speed, the Rational Functions, obtained by adding ±2% errors to the exact value of $\phi_{Lh}, \phi_{Mh}, \phi_{L\alpha}$ and $\phi_{M\alpha}$, calculated from the numerically generated displacement and aerodynamic load time histories using Gan Chowdhury and Sarkar's (2005) flutter derivative data, were also used to predict flutter speed of the bridge deck, and the results are listed in Table 2.

Table 2. Comparison of flutter speeds of the streamlined bridge deck section model obtained by different set of parameters

	Flutter Derivatives (Gan Chowdhury and Sarkar, 2005) Free vibration	Rational Functions (Gan Chowdhury and Sarkar, 2005) Free vibration	Rational Functions (Obtained in this paper) Forced vibration	Rational Functions (Obtained by adding ±2% error to flutter derivative data) Forced vibration
Flutter Speed, U_{cr} (m/s)	32.4	31.8	34.5	32.9 (-2%), 32.8 (+2%)

It can be seen from the table that the comparison of predicted flutter speed is good, though some of the flutter derivatives, especially A_4*, do not match very well with those extracted earlier, as shown in Fig. 5. Moreover, by ±2% error test, it is shown that slight error in phase difference, $\phi_{Lh}, \phi_{Mh}, \phi_{L\alpha}$ and $\phi_{M\alpha}$, could lead to a change in predicted flutter speed.

Overall, this algorithm demonstrated the feasibility of direct extraction of rational functions by the forced vibration method.

5 CONCLUSION

In this paper, a new method has been introduced to directly extract rational function coefficients or rational functions from forced vibration experiment. Through numerical tests, it has been shown that the algorithm is feasible for extraction of rational function coefficients and it is quite robust. The validation results of the obtained rational functions show that flutter derivatives extracted from this RFA method are generally in good agreement with those from earlier free vibration experimental results, given their sensitivity to noise in the signals. In the future, all eight flutter derivatives will be extracted simultaneously using a two-DOF forced-vibration system to eliminate the influence of single DOF (if any) on the final results. Moreover, to avoid the amplification of the error induced from phase difference identification in the algorithm as discussed previously, a new algorithm which is based on the system identification on the whole time histories rather than just the phase differences and amplitudes of time histories will be developed and validated by wind tunnel tests.

6 REFERENCES

Bartoli, G., Contri, S., Mannini, C., Righi, M. (2009), "Toward an improvement in the identification of bridge deck flutter derivatives", J. Eng. Mech., ASCE, 135(8), 771-785.

Caracoglia, L., Jones, N.P. (2003), "Time domain vs. frequency domain characterization of aeroelastic forces for bridge deck sections", J. Wind Eng. Ind. Aerodyn., 91, 371-402

Chen, C., Wu, J., Chen, J. (2008), "Prediction of flutter derivatives by artificial neural networks", J. Wind Eng. Ind. Aerodyn., 96, 1925-1937.

Chen, X., Matsumoto, M., Kareem, A. (2000), "Time domain flutter and buffeting response analysis of bridges", J. Eng. Mech., ASCE, 126(1), 7-16.

Chen, X., Kareem, A. (2002), "Advances in modeling of aerodynamic forces on bridge decks", J. Eng. Mech., ASCE, 128(11), 1193-1205.

Chen, X., Kareem, A. (2008), "Identification of critical structural modes and flutter derivatives for predicting coupled bridge flutter", J. Wind Eng. Ind. Aerodyn., 96, 1856-1870.

Ding, Q., Zhou, Z., Zhu, L., Xiang, H. (2010), "Identification of flutter drivatives of bridge decks with free vibration technique", J. Wind Eng. Ind. Aerodyn., 98, 911-918.

Gan Chowdhury, A., Sarkar, P.P. (2003), "A new technique for identification of eighteen flutter derivatives using a three-degree-of-freedom section model", Eng. Struct., 25(14), 1763-1772.

Gan Chowdhury, A. (2004), "Identification of Frequency domain and time domain aeroelastic parameters for flutter analysis of flexible structures", PhD dissertation. Ames (IA), Iowa State University.

Gan Chowdhury, A., Sarkar, P.P. (2004), "Identification of eighteen flutter derivatives of an airfoil and a bridge deck", Wind and Struct., 7(3), 187-202.

Gan Chowdhury, A., Sarkar, P.P. (2005), "Experimental identification of rational function coefficients for time-domain flutter analysis", Eng. Struct., 27(9), 1349-1364.

Haan, F.L. (2000), "The effects of turbulence on the aerodynamics of long-span bridges", Ph.D. dissertation. Notre Dame (IN, USA), University of Notre Dame.

Lin, Y.K., Ariaratnam, S.T. (1980), "Stability of bridge motion in turbulent winds", J. Struct. Mech., 8(1), 1-15.

Karpel, M. (1982), "Design for active flutter suppression and gust alleviation using state-space aeroelastic modeling", J. of Aircraft, 19(3), 221–227.

Matsumoto, M. (1996), "Aerodynamic damping of prisms", J. Wind Eng. Ind. Aerodyn., 59(2-3):159-175.

Roger, K. (1977), "Airplane math modeling methods for active control design", AGARD-CP-228.

Sarkar, P.P., Gan Chowdhury, A., Gardner, T.B. (2004), "A novel elastic suspension system for wind tunnel section model studies", J. Wind Eng. Ind. Aerodyn. 92, 23-40.

Sarkar, P.P., Caracoglia, L., Haan Jr., F.L., Sato, H., Murakoshi, J. (2009), "Comparative and sensitivity study of flutter derivatives of selected bridge deck sections, Part1: Analysis of inter-laboratory experimental data", Eng. Struct., 31(1): 158-169.

Scanlan, R.H., Tomko, J.J. (1971), "Airfoil and bridge deckflutter derivatives", J. Eng. Mech. Div., 97(6):1717-1733.

Scanlan, R.H. (1993), "Problematics in formulation of wind-force models for bridge decks", J. Eng. Mech., ASCE 119(7), 1353-1375.

Zhang, Z., Chen, Z., Cai, Y., Ge, Y. (2011), "Indicial functions for bridge aeroelastic forces and time-domain flutter analysis", J. Bridge Eng., ASCE 16(4), 546-557.

Figure Captions

Table Captions

CHAPTER 3. IDENTIFICATION OF RATIONAL FUNCTIONS USING TWO-DEGREE-OF-FREEDOM MODEL BY FORCED VIBRATION METHOD

A paper submitted to Engineering Structures

Bochao Cao[a], Partha P. Sarkar[a,*]

[a] *Wind Simulation & Testing Laboratory, Department of Aerospace Eng., Iowa State University, Ames IA 50011, USA*

Keywords: rational functions, self-excited forces, two-degree-of-freedom model, forced vibration method, streamlined section model, bluff section model.

Abstract

In prediction of self-excited forces and flutter instability of flexible structures, time domain method has distinct advantages. Rational Functions that are used to formulate self-excited aerodynamic forces in time domain were indirectly extracted from experimentally obtained flutter derivatives in the past. Recently, an algorithm was published to directly extract the Rational Functions from wind tunnel section model tests in free vibration. To overcome the limitations of free vibration technique, a new algorithm that is developed for direct extraction of the Rational Functions from section model tests using a forced-vibration

(*) Corresponding author: Partha P. Sarkar, Professor and Director, Wind Simulation and Testing Laboratory, Department of Aerospace Engineering, Iowa State University, 2271 Howe Hall, Room 1200, Ames, IA 50011-2271 USA. Email: ppsarkar@iastate.edu, tel. (515) 294-0719

technique is presented here. The new algorithm can be used to extract all the Rational Functions associated with one, two or three degree-of-freedom motion (vertical, lateral and torsional) of a section model. To validate the new algorithm, forced vibration wind tunnel tests in two degrees of freedom (vertical and torsional) were performed on a streamlined bridge deck section model with width-to-depth ratio B/D = 15:1 and also a bluff rectangular section model with B/D = 5:1. This is a significant improvement from other forced-vibration methods that require separate one-degree-of-freedom model tests which are dependent on phase angle difference between aerodynamic loads and displacements.

1. Introduction

In design of long-span bridges, it is important to identify whether there is aeroelastic instability (flutter) at wind speeds below the design wind speed. Scanlan and Tomko [1] developed a technique to carry out flutter analysis in frequency domain using experimentally obtained flutter derivatives. This laid the foundation for the development of various efficient methods to extract flutter derivatives from wind tunnel experiments, such as Scanlan [2] and Sarkar et al. [3]'s Modified Ibrahim Time Domain (MITD) method, Brownjohn and Jakobsen [4]'s Covariance Block Hankel Matrix (CBHM) method, and Gan Chowdhury and Sarkar [5]'s Iterative Least Squares (ILS) method, and many other methods. In recent years, time domain analysis (e.g., [6]-[10]) has been gaining popularity. In time domain analysis, the equations of motion are frequency independent so structural and aerodynamic nonlinearities can be incorporated. For time domain analysis, the self-excited forces acting on a flexible structure can be approximately represented by Rational Functions in Laplace domain. Roger [11] formulated the least squares Rational Function Approximation (LS-RFA) formulation,

and Karpel [12] developed the minimum state Rational Function Approximation (MS-RFA) formulation. Using these RFA formulations, one can obtain Rational Function Coefficients from flutter derivatives by approximation techniques. RFA formulation has been applied to bridge aerodynamics by several researchers including Xie [13], Xiang et al. [14], Wilde et al. [15] and Chen et al. [16]. However, this is an indirect way to obtain Rational Function Coefficients since flutter derivatives need to be obtained first from experiments that need to be repeated for several wind speeds. Thus, to make the process of extracting the Rational Function Coefficients more efficient, Gan Chowdhury and Sarkar [17] developed a new method based on free vibration of section models where both displacements and surface pressures of the model were simultaneously recorded and used. It is known that the free vibration method has some limitations compared to the forced vibration method because it is particularly unsuitable for higher wind speeds, large amplitudes of motion, turbulent flow, aerodynamically unstable cross sections and flow regimes where vortex-shedding dominates the excitation. This provided the motivation to develop a forced vibration experimental method to extract the Rational Functions. However, the current forced-vibration techniques for extraction of flutter derivatives [18,19] or Rational Function Coefficients [20] have some limitations. Firstly, these techniques are based on the *phase difference* between simultaneously obtained displacement and aerodynamic load time histories. In a recently concluded comparative and sensitivity study [21], it was shown that in a phase-difference-dependent forced vibration technique to extract the four flutter derivatives based on a pure torsional motion system, the errors in A_2^* and H_2^* could be significant, since slight errors in the phase difference obtained from the experiment gets amplified in the formulation that defines A_2^* and H_2^*. Similar observation was made in the phase-difference-dependent

technique to extract Rational Function Coefficients [20]. Secondly, earlier forced vibration techniques were all based on one degree-of-freedom (DOF) motion (vertical or torsional), and aeroelastic coefficients (flutter derivatives or Rational Function Coefficients) associated with two degrees of freedom were obtained by combining results from two separate one DOF tests. Considering there is a physical difference between the aerodynamics of one DOF and two DOF motions, there might be errors introduced in the aeroelastic coefficients obtained by one DOF system because the actual aerodynamic interaction of a two DOF system may not be captured well. Thus, in this paper, a forced vibration method that does not use the *phase difference* is described to extract all the Rational Function Coefficients simultaneously from a two-DOF dynamic system for the first time. Moreover, the method developed in this paper is more efficient than earlier ones, since it requires data obtained at two wind speeds only to solve for the full set of Rational Function Coefficients.

2. Formulation and Algorithm

Using Minimum State Rational Function Approximation (MS-RFA) formulation, Karpel [12] derived the following Laplace domain formulation of aerodynamic self-excited forces:

$$\begin{bmatrix} \hat{L}_{se} \\ \hat{M}_{se} \end{bmatrix} = \underline{V}_f \underline{\underline{Q}}\hat{\underline{q}} = \begin{bmatrix} \frac{1}{2}\rho U^2 B & 0 \\ 0 & \frac{1}{2}\rho U^2 B^2 \end{bmatrix} \cdot \begin{bmatrix} (\underline{A}_0)_{11} + (\underline{A}_1)_{11} p + \frac{(\underline{F})_{11} p}{p+\lambda} & (\underline{A}_0)_{12} + (\underline{A}_1)_{12} p + \frac{(\underline{F})_{12} p}{p+\lambda} \\ (\underline{A}_0)_{21} + (\underline{A}_1)_{21} p + \frac{(\underline{F})_{21} p}{p+\lambda} & (\underline{A}_0)_{22} + (\underline{A}_1)_{22} p + \frac{(\underline{F})_{22} p}{p+\lambda} \end{bmatrix} \begin{bmatrix} \hat{h}/B \\ \hat{\alpha} \end{bmatrix} \quad (1)$$

where B= width of the bridge deck, U= mean wind velocity, $p = iK$ is nondimensional Laplace domain variable, K= Bω/U= reduced frequency of the vibration, where ω= 2πf= circular frequency of the vibration, '^' denotes the Laplace transformation of the corresponding time domain function, L_{se} and M_{se} are self-excited lift and moment, respectively, h is vertical displacement and α is torsional displacement. $\underline{Q}$ is Rational Function matrix consisting of four Rational Functions and $\underline{A}_0$, $\underline{A}_1$, $\underline{F}$ and λ are Rational Function Coefficients. $\underline{A}_0$, $\underline{A}_1$ are stiffness matrix and damping matrix, respectively, and $\underline{F}$ is a lag matrix, all of order 2×2, λ is a lag coefficient, and $\hat{\underline{q}} = [\hat{h}/B \quad \hat{\alpha}]^T$ is the displacement vector. Multiplying both sides with p+λ, and applying inverse Laplace transformation on both sides of Equation (1), two time-domain equations for lift and moment can be obtained respectively as:

$$\dot{L}_{se} + \lambda_L \frac{U}{B} L_{se} = \frac{1}{2}\rho U^2 B\left(\left(\frac{U}{B}\right)\underline{\psi}_1 \underline{q} + \underline{\psi}_2 \dot{\underline{q}} + \left(\frac{B}{U}\right)\underline{\psi}_3 \ddot{\underline{q}}\right) \tag{2}$$

$$\dot{M}_{se} + \lambda_M \frac{U}{B} M_{se} = \frac{1}{2}\rho U^2 B^2\left(\left(\frac{U}{B}\right)\underline{\psi}_4 \underline{q} + \underline{\psi}_5 \dot{\underline{q}} + \left(\frac{B}{U}\right)\underline{\psi}_6 \ddot{\underline{q}}\right) \tag{3}$$

where $\underline{\psi}_1 = \left[\lambda_L\left(\underline{A}_0\right)_{11} \quad \lambda_L\left(\underline{A}_0\right)_{12}\right]$, $\underline{\psi}_2 = \left[\left(\underline{A}_0\right)_{11} + \lambda_L\left(\underline{A}_1\right)_{11} + \left(\underline{F}\right)_{11} \quad \left(\underline{A}_0\right)_{12} + \lambda_L\left(\underline{A}_1\right)_{12} + \left(\underline{F}\right)_{12}\right]$,

$\underline{\psi}_3 = \left[\left(\underline{A}_1\right)_{11} \quad \left(\underline{A}_1\right)_{12}\right]$, $\underline{\psi}_4 = \left[\lambda_M\left(\underline{A}_0\right)_{21} \quad \lambda_M\left(\underline{A}_0\right)_{22}\right]$,

$\underline{\psi}_5 = \left[\left(\underline{A}_0\right)_{21} + \lambda_M\left(\underline{A}_1\right)_{21} + \left(\underline{F}\right)_{21} \quad \left(\underline{A}_0\right)_{22} + \lambda_M\left(\underline{A}_1\right)_{22} + \left(\underline{F}\right)_{22}\right]$, $\underline{\psi}_6 = \left[\left(\underline{A}_1\right)_{21} \quad \left(\underline{A}_1\right)_{22}\right]$.

Equations (1-3) are slightly modified forms of those mentioned in [17]. Equations (2) and (3) can be rewritten in matrix form as:

$$\begin{bmatrix} \underline{\psi_1} & \underline{\psi_2} & \underline{\psi_3} & -\lambda_L \end{bmatrix} \begin{bmatrix} \frac{1}{2}\rho U^2 B\left(\frac{U}{B}\right)\underline{q} \\ \frac{1}{2}\rho U^2 B\underline{\dot{q}} \\ \frac{1}{2}\rho U^2 B\left(\frac{B}{U}\right)\underline{\ddot{q}} \\ \frac{U}{B}\underline{L_{se}} \end{bmatrix} = \underline{\dot{L}_{se}} \tag{4}$$

$$\begin{bmatrix} \underline{\psi_4} & \underline{\psi_5} & \underline{\psi_6} & -\lambda_M \end{bmatrix} \begin{bmatrix} \frac{1}{2}\rho U^2 B^2\left(\frac{U}{B}\right)\underline{q} \\ \frac{1}{2}\rho U^2 B^2\underline{\dot{q}} \\ \frac{1}{2}\rho U^2 B^2\left(\frac{B}{U}\right)\underline{\ddot{q}} \\ \frac{U}{B}\underline{M_{se}} \end{bmatrix} = \underline{\dot{M}_{se}} \tag{5}$$

Let $\underline{A_L} = \begin{bmatrix} \underline{\psi_1} & \underline{\psi_2} & \underline{\psi_3} & -\lambda_L \end{bmatrix}$, $\underline{X_L} = \begin{bmatrix} \frac{1}{2}\rho U^2 B\left(\frac{U}{B}\right)\underline{q} \\ \frac{1}{2}\rho U^2 B\underline{\dot{q}} \\ \frac{1}{2}\rho U^2 B\left(\frac{B}{U}\right)\underline{\ddot{q}} \\ \frac{U}{B}\underline{L_{se}} \end{bmatrix}$, $\underline{b_L} = \underline{\dot{L}_{se}}$,

$\underline{A_M} = \begin{bmatrix} \underline{\psi_4} & \underline{\psi_5} & \underline{\psi_6} & -\lambda_M \end{bmatrix}$, $\underline{X_M} = \begin{bmatrix} \frac{1}{2}\rho U^2 B^2\left(\frac{U}{B}\right)\underline{q} \\ \frac{1}{2}\rho U^2 B^2\underline{\dot{q}} \\ \frac{1}{2}\rho U^2 B^2\left(\frac{B}{U}\right)\underline{\ddot{q}} \\ \frac{U}{B}\underline{M_{se}} \end{bmatrix}$, $\underline{b_M} = \underline{\dot{M}_{se}}$.

Thus,

$$\underline{\underline{A}}_L \underline{\underline{X}}_L = \underline{\dot{L}}_{se}, \qquad \underline{\underline{A}}_M \underline{\underline{X}}_M = \underline{\dot{M}}_{se} \tag{6}$$

It can be seen that all the Rational Function Coefficients that need to be identified are included in $\underline{\underline{A}}_L$ and $\underline{\underline{A}}_M$. Therefore, the problem reduces to extracting $\underline{\underline{A}}_L$ and $\underline{\underline{A}}_M$ from a two-DOF test. In a forced vibration experiment, displacement and aeroelastic force time histories are recorded, and their derivatives can be obtained by finite difference method applied to original time histories. Thus, vectors $\underline{\underline{X}}_L$, $\underline{\underline{X}}_M$, $\underline{b}_L$ and $\underline{b}_M$ in the above equations can be formulated. Finally, vectors $\underline{\underline{A}}_L$ and $\underline{\underline{A}}_M$ can be solved by Least Squares method as:

$$\underline{\underline{A}}_L = \left(\underline{b}_L \underline{\underline{X}}_L^{\,T}\right)\left(\underline{\underline{X}}_L \underline{\underline{X}}_L^{\,T}\right)^{-1}, \qquad \underline{\underline{A}}_M = \left(\underline{b}_M \underline{\underline{X}}_M^{\,T}\right)\left(\underline{\underline{X}}_M \underline{\underline{X}}_M^{\,T}\right)^{-1} \tag{7}$$

3. Experimental Set-Up

3.1. Description of Wind Tunnel Used

The experiments were performed in the Bill James Open-Return Wind Tunnel, which is located in the Wind Simulation and Testing Laboratory (WiST Lab) in the Department of Aerospace Engineering at Iowa State University. This wind tunnel has a test section of 0.915m (3.0ft) width by 0.762m (2.5ft) height and its maximum wind velocity is 75 m/s (246 ft/s).

3.2. Model, Suspension System and Forced Vibration Mechanism

To validate the method stated in this paper, experiments were carried out on both a streamlined model and a bluff model. The streamlined bridge deck section model was used in both one-DOF experiment and two-DOF experiment as shown in Figure 1 and Figure 2 (see also [22]). The streamlined model is composed of a shallow box girder section and two semi-circular fairings at the edges. The length, chord length and thickness of the model are about

0.533m, 0.3m, and 0.02m, respectively. The bluff section model is rectangular with a width-to-depth ratio (B/D) of 5:1, and the length, chord length and thickness of the model are about 0.533m, 0.16m, and 0.032m, respectively (see also [21]). To reduce the edge effects, two plexiglass end plates were used on both models as seen in Figure 2.

The three-DOF model suspension system used in this experiment is shown in Figure 2. This system, developed by Sarkar et al. [23], enables vertical, horizontal and torsional motions of the model. To realize forced sinusoidal motions of the section model with constant amplitude and frequency in the experiments, a driving mechanism (Figure 3) was used. The driving mechanism is placed above the test section. It consists of two motors, which are used to drive vertical and torsional motions of the model, respectively. The section model is driven by four aluminum rods which are connected with the driving mechanism, as seen in Figure 2. Thus, vertical, torsional, or combined vertical-torsional two-DOF sinusoidal motion of the section model can be generated using this driving mechanism. Moreover, by changing the rotating speed of two motors using two separate controllers, the two frequencies of model vibration in two degrees of freedom can be changed independently.

3.3. Displacement Measurement

The vertical displacement of the model was measured by measuring the elastic force in each of two springs which is connected to the model at one end and a strain gage force transducer at the other end. The torsional displacement was measured by measuring the torque at one end of the model shaft using a torque transducer which is mounted on the suspension system. LabVIEW was used for data acquisition, where the sampling rate was set at 625Hz.

3.4. Aeroelastic Force Measurement

The algorithm stated in this paper requires time histories of aeroelastic forces acting on the model while it vibrates, in addition to the displacement time histories of the model. Therefore, surface pressures were measured on the model through a row of pressure taps located on the upper and lower surfaces of the model along the mid-plane for both streamlined and bluff models. In total, forty-two pressure taps for streamlined model and thirty-two pressure taps for bluff model were used in the test. The pressure taps are equally distributed on the top and bottom surfaces and they are denser on the upstream side than the downstream side of the models. Two 64-channel pressure modules (Scanivalve ZOC33/64 Px) were used to measure the pressure. The sampling rate for pressure measurement was 312.5Hz (half of displacement sampling rate) in the experiment. To synchronize the pressure data with the displacement data, the pressure transducers were set to work in external-trigger mode. LabVIEW (National Instrument) was used for displacement data acquisition and a separate program RAD (Scanivalve) was used to collect the pressure data. LabVIEW was programmed to output a digital signal when the displacement data acquisition started so that the pressure data acquisition system would get externally triggered to synchronously start the pressure data acquisition. The total sampling time was set as 10 seconds for all the tests.

4. Numerical Tests

4.1. Numerical Simulation and Noise Test

Before conducting the wind tunnel tests, numerical tests were carried out first to confirm that the algorithm developed here works well in extracting Rational Function Coefficients of bridge decks with both streamlined and bluff cross sections. In the numerical tests, flutter

derivatives of a bluff rectangular (B/D=5:1) section model as extracted in [19] were used to generate lift and moment time histories at two wind speeds with given vertical and torsional displacement time histories as sinusoidal functions. The generated lift and moment were substituted in the algorithm to extract Rational Function Coefficients for the model, and the Rational Function matrix which contains four Rational Functions was computed using following formulation:

$$\underline{Q} = \begin{bmatrix} \left(\underline{A}_0\right)_{11} + \left(\underline{A}_1\right)_{11} p + \dfrac{\left(\underline{F}\right)_{11} p}{p+\lambda} & \left(\underline{A}_0\right)_{12} + \left(\underline{A}_1\right)_{12} p + \dfrac{\left(\underline{F}\right)_{12} p}{p+\lambda} \\ \left(\underline{A}_0\right)_{21} + \left(\underline{A}_1\right)_{21} p + \dfrac{\left(\underline{F}\right)_{21} p}{p+\lambda} & \left(\underline{A}_0\right)_{22} + \left(\underline{A}_1\right)_{22} p + \dfrac{\left(\underline{F}\right)_{22} p}{p+\lambda} \end{bmatrix} \tag{8}$$

To assess the accuracy of the extracted Rational Functions, they were converted to flutter derivatives using following relationships:

$$H_1^* = imag\left(\underline{Q}_{11}\right)/\mathrm{K}^2, H_4^* = real\left(\underline{Q}_{11}\right)/\mathrm{K}^2, \;\; A_1^* = imag\left(\underline{Q}_{21}\right)/\mathrm{K}^2, \; A_4^* = real\left(\underline{Q}_{21}\right)/\mathrm{K}^2$$

$$H_2^* = imag\left(\underline{Q}_{12}\right)/K^2, H_3^* = real\left(\underline{Q}_{12}\right)/K^2, \; A_2^* = imag\left(\underline{Q}_{22}\right)/K^2, \; A_3^* = real\left(\underline{Q}_{22}\right)/K^2 \tag{9}$$

The obtained flutter derivatives (referred RFA) were compared with the original ones used at the beginning of the simulation as shown in Figure 4. As can be seen in the plots, all eight flutter derivatives compare very well with the original ones, which proves that the Rational Function formulation with only one lag term as used here is accurate enough to approximate flutter derivatives of a bluff cross section model, even at high reduced velocities where some flutter derivatives could have complex trends. Moreover, this comparison shows that the algorithm developed here can work very well in extracting Rational Function Coefficients from forced vibration experimental data. To quantitatively assess the error in the

obtained Rational Function Coefficients, they were converted to flutter derivatives at exact reduced velocities where original experimental data in [19] were obtained and the error function as given by Equation (10) was calculated to evaluate the percentage error:

$$err = \frac{\sum_{j=1}^{8}\left[\sqrt{\sum_{i=1}^{N}\left(X_i^{(j)} - X_i^{0(j)}\right)^2} \Big/ \sqrt{\sum_{i=1}^{N}\left(X_i^{0(j)}\right)^2}\right]}{8} \times 100\% \tag{10}$$

where $X_i^{(j)}$ is the j'th flutter derivative of the model calculated from Rational Functions and evaluated at the i'th reduced velocity point, and X(1)-X(8) correspond to H1*-H4* and A1*-A4*, respectively, and $X_i^{0(j)}$ is the corresponding original flutter derivative value given in [19], and N is the number of the reduced velocity points involved in the calculation. Using this error function, the percentage error was calculated as 8.14% which is acceptable considering data at only two wind velocities were used in the simulation to extract all the Rational Function Coefficients and the accuracy will certainly be improved by introducing data from more number of wind velocities.

Some noise tests were performed to test the robustness of the algorithm. White noise with different standard deviations was added to the numerically generated displacement and corresponding load (lift, moment) time histories obtained by using the original flutter derivatives given in [19]. The standard deviation of the noise was chosen as certain percentage (2%, 5% and 10%) of time history amplitudes of displacements (h, α) and loads. The flutter derivatives from the obtained Rational Functions from the noisy data were compared with ones extracted from the numerically generated time histories without any noise, and the errors were computed using Equation (10), except the $X_i^{0(j)}$ here is the flutter derivative obtained from noise-free time histories and the $X_i^{(j)}$ is obtained from contaminated

ones. The results are listed in Table 1 which shows a percentage error below 10% even with a 10% noise. Thus, the algorithm is reasonably robust.

4.2. Effect of Time Step on Accuracy of the Algorithm

In the algorithm, the displacement time histories need to be numerically differentiated twice to get acceleration time histories and also the first derivatives of the load time histories need to be evaluated using numerical method. Thus, the time step chosen in the finite difference method to calculate numerical derivatives could affect the accuracy of the extracted coefficients, especially when noise is present in the data. In current research, second order central difference method was used to evaluate derivatives. To investigate the consistency of the algorithm with different time steps chosen, numerical tests were carried out with larger time steps and also with 5% noise added to the displacement and load time histories.

The time step in the original numerical test was set as 0.0032s which coincides with the experimental sampling period, and the ones used in current test were 0.005s and 0.01s which are about twice and three times of the original one. The coefficients extracted from 5% noise contaminated time histories and with two larger time steps were compared with ones extracted from clean time histories and with original time step. The errors were calculated using Equation (10) as in the noise tests. It turns out that the percentage error for time step of 0.005s is 4.18% and that for time step of 0.01s is 6.54% which are both acceptable, although time steps are about two to three times the original time step of 0.0032s.

4.3. Experimental Error Estimate and Resulted Error in the Coefficients

In addition to electronic noise, errors could also be introduced into real experimental data either through equipment error or operational error from experimentalists. In this section,

numerical tests were performed to confirm the algorithm could still work well when both noise and errors are present in the data.

For current algorithm, the input data are model displacements, h and α, aerodynamic loads, L and M, and the input parameters are wind velocity, U, and air density, ρ. In this numerical test, error was directly added to the specified parameters and the amplitudes for time history data.

In the experiment, the model displacements were obtained by measuring spring forces as mentioned earlier under experimental set-up and thus errors could be introduced from the error in the force transducers and the calibration of transducers. Moreover, considering that angle measurement could have more error than length measurement, 3% error is given to vertical displacement, h, while 5% error is given to torsional displacement, α. The errors in the aerodynamic loads could come from the pressure transducers, the pressure tubing, and the error from numerical method used to integrate surface pressure into loads. Considering that integration of pressures to calculate moment could have more error than those from calculating lift, 3% error is assigned to lift, while 5% error is assigned to moment. The air density depends on the temperature and atmospheric pressure and does not change much, so only 1% error is assigned. Finally, the error in the wind velocity could come from the measurement of the dynamic pressure using Pitot tube and the error in the air density, thus 3% error is assigned. In the test, 5% noise and two combinations of errors, all positive or all negative, were given to simulate real experimental environment. The resulting flutter derivatives are plotted in Figure 4 (referred RFA_noise & errors (+/-)) to compare with the results from clean data and the original flutter derivative data. It can be seen in the plots that the errors in the extracted aeroelastic parameters increase with reduced velocity, however,

this occurs in a very small range. The errors were also quantified by error Equation (10), which are 5.90% for the negative error case and 6.88% for the positive error case. Thus, even with estimated errors and noise added in the data, the algorithm can still be used to accurately extract all the coefficients.

5. Experimental Results and Discussion

For the streamlined bridge deck section model, wind tunnel tests were performed at five wind speeds: 2.8m/s, 5.8m/s, 8.6m/s, 11.7m/s, 14.4m/s. The model was forced to move in two DOFs (vertical and torsional) at frequencies that were both around 2.5Hz. Data obtained at two wind velocities, 2.8m/s and 14.4m/s, were used in the algorithm to solve for all the Rational Function Coefficients. The results are given below:

$$\underline{A}_0 = \begin{bmatrix} 0.3273 & -6.2384 \\ -0.0970 & 1.3818 \end{bmatrix},\ \underline{A}_1 = \begin{bmatrix} -3.7549 & -1.4947 \\ 0.8510 & -0.3819 \end{bmatrix},\ \underline{F} = \begin{bmatrix} -0.9484 & 1.3397 \\ 0.2689 & -0.1682 \end{bmatrix},$$

$$\lambda_L = 0.1843,\ \lambda_M = 0.2239$$

For the bluff rectangular section model, experiments were carried out at wind speeds of 2.9m/s, 5.9m/s, 8.7m/s, 11.6m/s, 14.6m/s. In these tests, the model was forced to vibrate in the same way and at same frequencies as what was set in the experiment of streamlined model. Data obtained at wind speeds of 5.9m/s and 14.6m/s were used in the algorithm to extract all the Rational Function Coefficients for this bluff section model, which are given below:

$$\underline{A}_0 = \begin{bmatrix} -0.0618 & -7.9085 \\ -0.0387 & -0.6258 \end{bmatrix},\ \underline{A}_1 = \begin{bmatrix} -0.7820 & 7.3997 \\ -1.7649 & -1.0621 \end{bmatrix},\ \underline{F} = \begin{bmatrix} -10.4613 & -5.7309 \\ -1.5021 & 2.9637 \end{bmatrix},$$

$$\lambda_L = 1.2048,\ \lambda_M = 0.7091$$

To validate the obtained Rational Function Coefficients, they were converted to flutter derivatives using Equation (9) as what was done in the numerical tests. The flutter derivatives computed using Rational Functions for the streamlined model were compared with those directly extracted from a free vibration experiment carried out by Gan Chowdhury and Sarkar [17] on the same model and plotted in Figure 5. While the flutter derivatives obtained from Rational Functions for the bluff rectangular model were compared with those directly extracted from a forced vibration experiment by Matsumoto [19] on a model with the same shape and same aspect ratio, B/D=5. The flutter derivatives for the bluff model were plotted in Figure 6.

It can be seen from Figure 5 that, all flutter derivatives for the streamlined section model that are converted from Rational Functions match with directly extracted ones very well, except for H_2*. In an earlier research by Cao and Sarkar [20] where the same streamlined model was discussed, similar phenomenon was observed and some numerical tests have been performed there on the flutter derivatives of this model. The tests showed that, for this model, H_2^* derivative is most sensitive to the error in the input time histories. Moreover, in that study, the H_2* curve changed from the original shape to a shape similar to what was obtained here with just 7% error added to the time histories generated by the original flutter derivatives.

The comparison of flutter derivatives for the bluff section model, as shown in Figure 6, is a little worse than that of the streamlined model, however the comparison of H_1*, A_4*, H_3* and A_3* is quite good, while the comparison of H_4*, A_1*, H_2* and A_2* is good for low reduced velocity region (less than 10) but slightly off at higher reduced velocities.

By directly applying inverse Laplace transformation on both sides of Equation (1), the following formulations for self-excited lift and moment (aeroelastic forces) in time domain can be obtained:

$$L_{se}(t)=\frac{1}{2}\rho U^2 B\left[\begin{array}{l}\left(\left(\underline{A}_0\right)_{11}+\left(\underline{F}\right)_{11}\right)\frac{h}{B}+\left(\underline{A}_1\right)_{11}\frac{\dot{h}}{U}-\left(\underline{F}\right)_{11}\frac{\lambda_L U}{B^2}\int_0^t e^{-\frac{U}{B}\lambda_L(t-\tau)}h(\tau)d\tau \\ +\left(\left(\underline{A}_0\right)_{12}+\left(\underline{F}\right)_{12}\right)\alpha+\left(\underline{A}_1\right)_{12}\frac{B}{U}\dot{\alpha}-\left(\underline{F}\right)_{12}\frac{\lambda_L U}{B}\int_0^t e^{-\frac{U}{B}\lambda_L(t-\tau)}\alpha(\tau)d\tau\end{array}\right] \tag{11}$$

$$M_{se}(t)=\frac{1}{2}\rho U^2 B^2\left[\begin{array}{l}\left(\left(\underline{A}_0\right)_{21}+\left(\underline{F}\right)_{21}\right)\frac{h}{B}+\left(\underline{A}_1\right)_{21}\frac{\dot{h}}{U}-\left(\underline{F}\right)_{21}\frac{\lambda_M U}{B^2}\int_0^t e^{-\frac{U}{B}\lambda_M(t-\tau)}h(\tau)d\tau \\ +\left(\left(\underline{A}_0\right)_{22}+\left(\underline{F}\right)_{22}\right)\alpha+\left(\underline{A}_1\right)_{22}\frac{B}{U}\dot{\alpha}-\left(\underline{F}\right)_{22}\frac{\lambda_M U}{B}\int_0^t e^{-\frac{U}{B}\lambda_M(t-\tau)}\alpha(\tau)d\tau\end{array}\right] \tag{12}$$

The above formulations can be used to predict self-excited forces and flutter speed in time domain. Aeroelastic self-excited forces can be calculated using Equations (11) and (12) at all wind speeds generated in the experiments using the model displacements h and α as recorded, their first derivatives as calculated by finite difference method and the Rational Function Coefficients as extracted. The numerically generated aerodynamic force time histories were compared with those obtained experimentally at wind speeds other than those used in the extraction procedure of Rational Function Coefficients to verify the accuracy of the method. For the streamlined model, comparisons of lift and moment time histories at wind speed of 11.7m/s are shown in Figure 7 and Figure 8, respectively. For the bluff model, comparisons of the lift and moment time histories at wind speed of 11.6m/s are shown in Figure 9 and Figure 10, respectively. As can be observed in the plots for the streamlined model, both lift and moment time histories matched very well, while the matching is slightly worse for the bluff section model. In the plots for the bluff section model, the amplitudes of

predicted lift and moment time histories (by Rational Functions) are slightly smaller than those of experimentally measured ones, especially for the lift. To better compare these time histories, cross-correlation coefficient, $\rho_{xy,}$ and percentage peak error, $err_{peak,}$ defined as below were calculated and listed in Table 2.

$$\rho_{\mathrm{xy}} = \frac{\frac{1}{n}\sum_{i=1}^{n} x_i y_i}{\sigma_x \sigma_y} \tag{13}$$

$$err_{peak} = \frac{\frac{1}{n}\sum_{i=1}^{n}\left(\hat{x}_i - \hat{y}_i\right)^2}{\sqrt{\frac{1}{n}\sum_{i=1}^{n}\hat{x}_i^2}\sqrt{\frac{1}{n}\sum_{i=1}^{n}\hat{y}_i^2}} \times 100\% \tag{14}$$

where x is experimentally obtained time history, y is simulated time history, $\hat{x}_i(i = 1,2,\dots)$ are peak values of time history x, and $\hat{y}_i(i = 1,2,\dots)$ are peak values of time history y. From Table 2, it is shown that cross-correlation coefficients for all the time histories are close to 1 which means the comparisons of the whole time histories are good, while the coefficients for lift time histories are lower than those for moment time histories, and the coefficients for the bluff section model are lower than those for the streamlined section model. The percentage peak errors for streamlined model time histories are very low, while those for bluff model time histories are much larger, especially for the moment time history. This shows the similar trend as shown in the cross-correlation coefficient results that the comparisons for the streamlined model time histories are better than those for the bluff model time histories. Actually, a similar trend can also be found in earlier flutter derivative studies (e.g., [21]).

For further validation, the flutter speed of the streamlined section model was predicted using time domain simulation and Rational Function Coefficients obtained in this experiment.

In flutter speed prediction, after substituting Rational Functions into right hand side load term, the time domain equations of motion were solved at each time step with given wind speeds, and the wind speed was increased continuously until a diverging solution was obtained. The flutter speed obtained here was compared with that obtained by Gan Chowdhury and Sarkar [17] on the same model using Rational Functions (free vibration) and flutter derivatives and shown in Table 3. Moreover, to investigate the difference between Rational Function Coefficients extracted from one-DOF and two-DOF forced vibration tests, the flutter speed obtained earlier by Cao and Sarkar [20] from two separate one-DOF forced vibration tests was also included in Table 3. As seen in this table, the comparison is good. Similarly, the flutter speed of the bluff section model was also predicted using Rational Function Coefficients obtained in this paper, and compared with that predicted using flutter derivatives obtained by Matsumoto [19], as shown in Table 4. It can be seen that the flutter speed comparison for bluff section model is good, though slightly worse than the streamlined model case.

5. Conclusion

In this paper, a new algorithm has been developed for direct extraction of all the Rational Function Coefficients for one, two or three-DOF forced vibration wind tunnel tests on a section model. The algorithm does not use phase angle difference between displacement and aeroelastic force time histories in the extraction procedure like in previous methods available in the literature. Thus, the error introduced in all the parameters from error in identification of one parameter, i.e. phase angle difference, is eliminated in this algorithm. Rather this new algorithm uses all the recorded data points to identify the unknown parameters in a least

square sense that minimizes the error originating from the noisy signals. The proposed algorithm is more efficient than others since it requires data collected at two wind speeds only to extract the full set of Rational Function Coefficients for a two-DOF system. As part of the validation process, the Rational Functions obtained in this paper were converted into flutter derivatives and were compared with directly extracted ones obtained in earlier experiments by other scholars, for both streamlined and bluff section models. The comparison is well, especially for the streamlined model case. Moreover, it was shown that the Rational Function Coefficients obtained using this algorithm can be used to accurately predict the self-excited forces acting on a section model at a given wind speed, for both a streamlined cross section and a bluff cross section. Further, the flutter speed of the streamlined cross section bridge deck model was predicted using Rational Function Coefficients obtained here and has been shown to match with earlier results. In the future, to validate the application of Rational Functions to predict the response of a bridge deck in a non-stationary wind environment, free vibration tests in a gusty wind (ramp down function applied to mean speed) was performed on a streamlined section model with the same geometry as the model used in this paper but with a larger scale. The results of this validation are quite favorable and will be presented separately.

Notations

The following symbols were used in this paper: The following symbols were used in this paper:

$L_{se}(t)$	aerodynamic self-excited lift in Laplace domain
$M_{se}(t)$	aerodynamic self-excited moment in Laplace domain
ρ	air density
U	mean wind speed, m/s
B	width of the bridge deck
D	height of bridge deck
B/D	aspect ratio of bridge deck model
K	(=Bω/U), reduced frequency of the vibration
p	($= iK$), nondimensional Laplace domain variable
$\widehat{h}$	vertical displacement in Laplace domain
$\widehat{\alpha}$	torsional displacement in Laplace domain
$\underline{Q}$	Matrix of Rational Functions
$\widehat{q}$	displacement vector in Laplace domain
$\underline{A}_0, \underline{A}_1, \underline{F}, \lambda$	Rational Function Coefficients
$L_{se}(t)$	aerodynamic self-excited lift in time domain
$M_{se}(t)$	aerodynamic self-excited moment in time domain
$\underline{\psi}_1, ..., \underline{\psi}_6$	vectors that include all the Rational Function Coefficients
$A_1^*, ..., A_4^*$	flutter derivatives per unit length, aerodynamic moment
$H_1^*, ..., H_4^*$	flutter derivatives per unit length, lift force
$h(t)$	vertical displacement in time domain
$\alpha(t)$	torsional displacement in time domain
τ	dummy time variable in the integration
ρ_{xy}	cross-correlation coefficient
err_{peak}	percentage peak error
x	experimentally obtained time history
y	simulated time history
$\hat{x}_i$	peak values of time history x
$\hat{y}_i$	peak values of time history y

References

[1] Scanlan, R.H., Tomko, J.J., 1971. Airfoil and bridge deckflutter derivatives. J Eng Mech Div 97(6):1717-1733.

[2] Scanlan, R.H., 1978. The action of lexible bridges under wind, I: flutter theory. J Sound Vib 60(2):187-199.

[3] Sarkar, P.P., Jones, N.P., Scanlan, R.H., 1994. Identification of aeroelastic parameters of flexible bridges. J Eng Mech 120(8):1718-1742.

[4] Brownjohn, J.M.W., Jakobsen, J.B., 2001. Strategies for aeroelastic parameter identification from bridge deck free vibration data. J Wind Eng Ind Aerodyn 89:1113-1136.

[5] Gan Chowdhury, A., Sarkar, P.P., 2003. A new technique for identification of eighteen flutter derivatives using a three-degree-of-freedom section model. Eng Struct 25(14):1763-1772.

[6] Lin, Y.K., Ariaratnam, S.T., 1980. Stability of bridge motion in turbulent winds. J Struct Mech 8(1), 1-15.

[7] Scanlan, R.H., 1984. Role of indicial functions in buffeting analysis of bridges. J Struct Eng 110(7).

[8] Scanlan, R.H., 1993. Problematics in formulation of wind-force models for bridge decks. J Eng Mech, ASCE 119(7), 1353-1375.

[9] Chen, X., Kareem, A., 2002. Advances in modeling of aerodynamic forces on bridge decks. J Eng Mech, ASCE 128(11), 1193-1205.

[10] Caracoglia, L., Jones, N.P., 2003. Time domain vs. frequency domain characterization of aeroelastic forces for bridge deck sections. J Wind Eng Ind Aerodyn 91, 371-402

[11] Roger, K., 1977. Airplane math modeling methods for active control design. AGARD-CP-228.

[12] Karpel, M., 1982. Design for active flutter suppression and gust alleviation using state-space aeroelastic modeling. J Aircraft 19(3):221-227.

[13] Xie J., 1988. CVR method for identification of nonsteady aerodynamic model. J Wind Eng Ind Aerodyn 29:389-397.

[14] Xiang H., Xie J., Lin Z., 1988. Aerodynamic study on a proposed cable-stayed bridge in Shanghai, China. J Wind Eng Ind Aerodyn 29:419-427.

[15] Wilde K., Fujino Y., Masukawa J., 1996. Time domain modeling of bridge deck flutter. Struct Eng/Earthq Eng, JSCE 13(2): 93-104.

[16] Chen, X., Matsumoto, M., and Kareem, A., 2000. Time domain flutter and buffeting response analysis of bridges. J Eng Mech, 126(1), 7-16.

[17] Gan Chowdhury, A., Sarkar, P.P., 2005. Experimental identification of rational function coefficients for time-domain flutter analysis. Eng Struct 27(9), 1349-1364.

[18] Haan Jr., F.L., 2000. The effects of turbulence on the aerodynamics of long-span bridges. Dissertation, University of Notre Dame, Notre Dame, Indiana.

[19] Matsumoto, M., 1996. Aerodynamic damping of prisms. J Wind Eng Ind Aerodyn 59(2-3):159-175.

[20] Cao, B., Sarkar, P.P., 2010. Identification of rational functions by forced vibration method for time-domain analysis of flexible structures. In Proceedings: The Fifth International Symposium on Computational Wind Engineering, Chapel Hill.

[21] Sarkar, P.P., Caracoglia, L., Haan Jr., F.L., Sato, H., Murakoshi, J., 2009. Comparative and sensitivity study of flutter derivatives of selected bridge deck sections, Part1: Analysis of inter-laboratory experimental data. Eng Struct 31(1): 158-169.

[22] Gan Chowdhury, A., Sarkar, P.P., 2004. Identification of eighteen flutter derivatives of an airfoil and a bridge deck. Wind and Struct 7(3), 187-202.

[23] Sarkar, P.P., Gan Chowdhury, A., Gardner, T.B., 2004. A novel elastic suspension system for wind tunnel section model studies. J Wind Eng Ind Aerodyn 92(1):23-40.

List of Tables

List of Figures

Table 1. Percentage errors shown in noise tests

	2% noise	5% noise	10% noise
err (%) Eqn. 10	1.74	3.92	9.39

Table 2. Parameters for time history comparisons

	ρ_{xy}	err_{peak}
Lift (streamlined model)	0.8498	1.55%
Moment (streamlined model)	0.8815	0.40%
Lift (bluff model)	0.8783	6.96%
Moment (bluff model)	0.8141	38.22%

Table 3. Comparison of flutter speeds of the streamlined section model obtained by different set of parameters

	Flutter Derivatives (Free vibration, [7])	Rational Functions (Free vibration, [7])	Rational Functions (Forced vibration, 1DOF, [3])	Rational Functions (Forced vibration, 2DOF, current)
Flutter speed, U_{cr} (m/s)	32.4	31.8	34.5	32.4

Table 4. Comparison of flutter speeds of the bluff section model obtained by different set of parameters

	Flutter Derivatives (Forced vibration, 1DOF, [11])	Rational Functions (Forced vibration, 2DOF, current)
Flutter speed, U_{cr} (m/s)	19.5	21.7

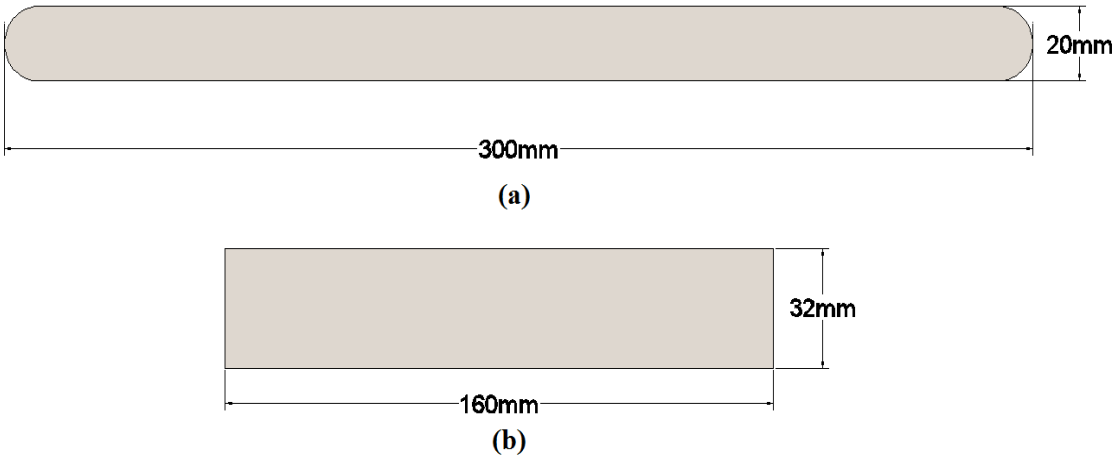

Figure 1. Cross section of models used in the experiments: (a) streamlined and (b) bluff

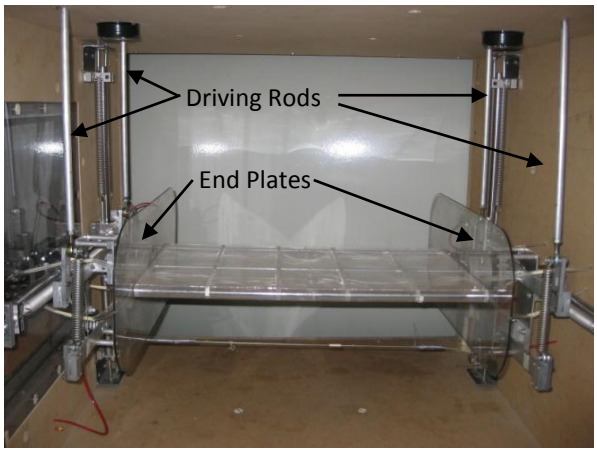

Figure 2. Model and suspension system

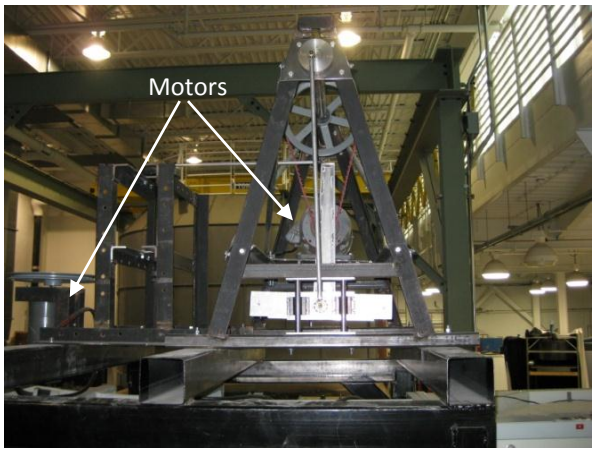

Figure 3. Driving mechanism

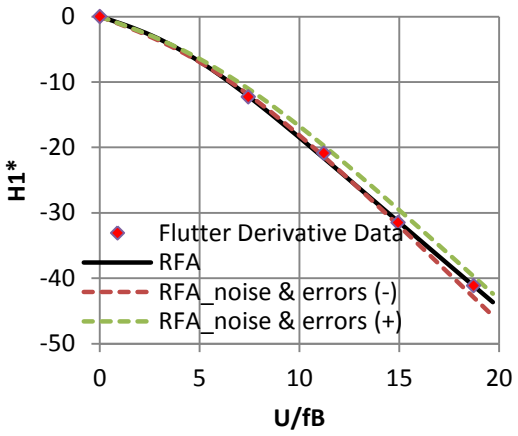
H1*
U/fB
Flutter Derivative Data
RFA
RFA_noise & errors (-)
RFA_noise & errors (+)

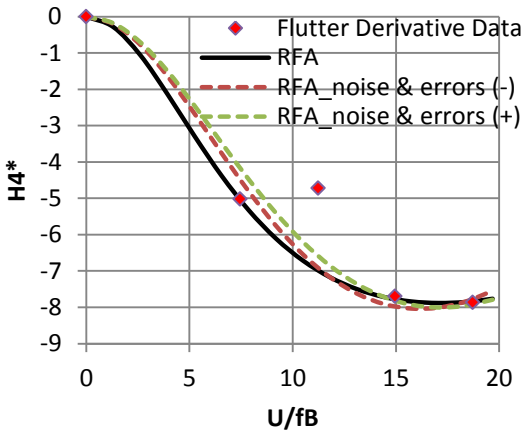
H4*
U/fB
Flutter Derivative Data
RFA
RFA_noise & errors (-)
RFA_noise & errors (+)

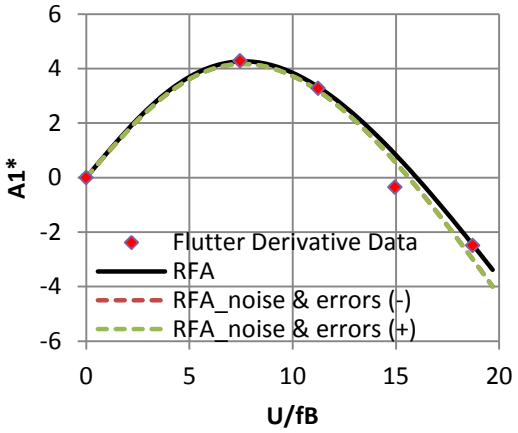
A1*
U/fB
Flutter Derivative Data
RFA
RFA_noise & errors (-)
RFA_noise & errors (+)

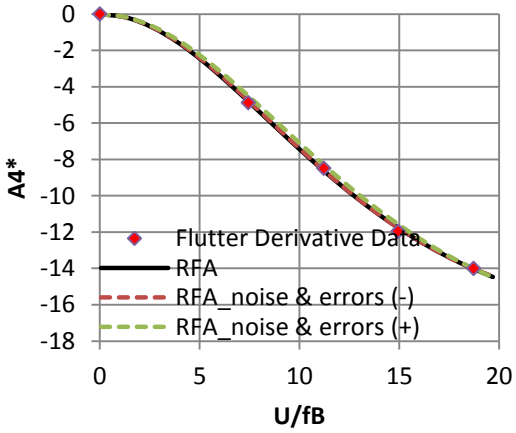
A4*
U/fB
Flutter Derivative Data
RFA
RFA_noise & errors (-)
RFA_noise & errors (+)

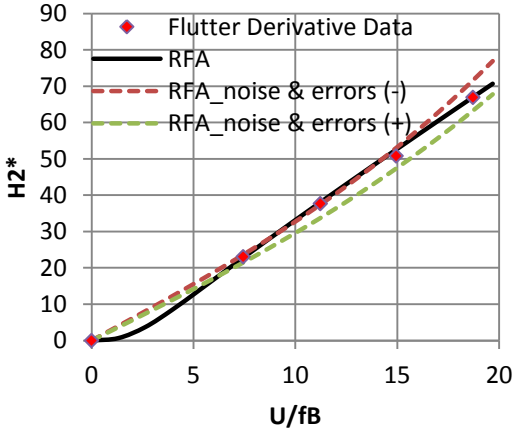
H2*
U/fB
Flutter Derivative Data
RFA
RFA_noise & errors (-)
RFA_noise & errors (+)

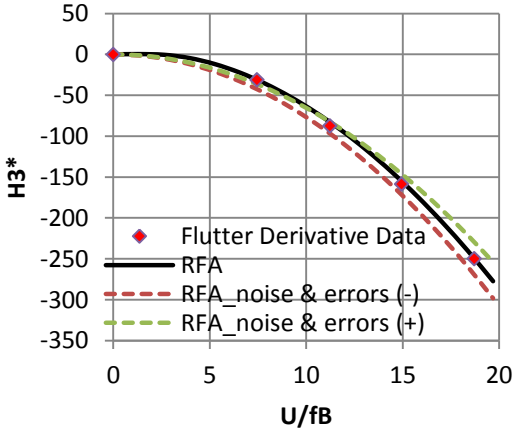
H3*
U/fB
Flutter Derivative Data
RFA
RFA_noise & errors (-)
RFA_noise & errors (+)

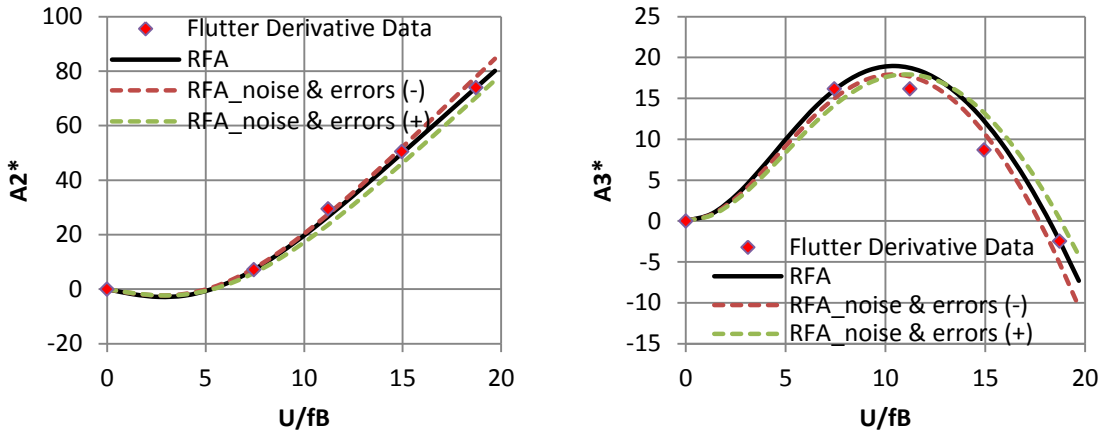

Figure 4. Numerically extracted Ration Function Coefficients from clean time histories and the time histories polluted by noises and with errors added

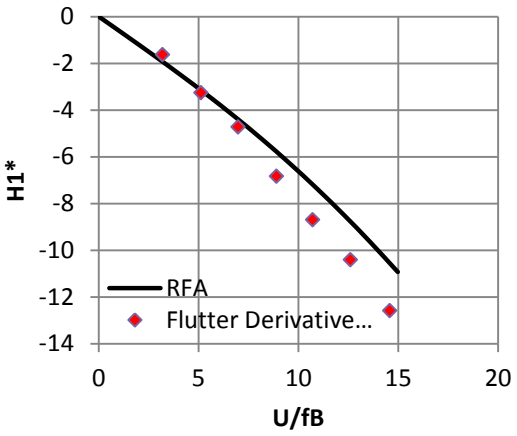
H1*
U/fB
RFA
Flutter Derivative...

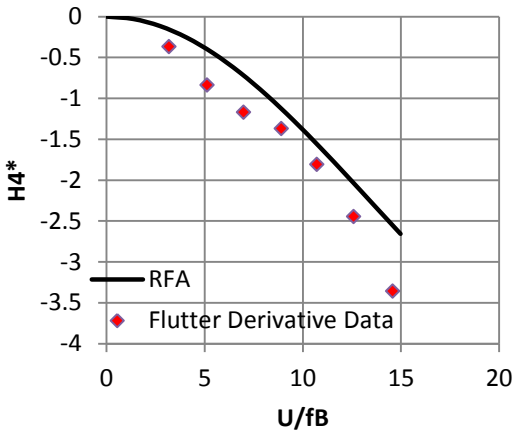
H4*
U/fB
RFA
Flutter Derivative Data

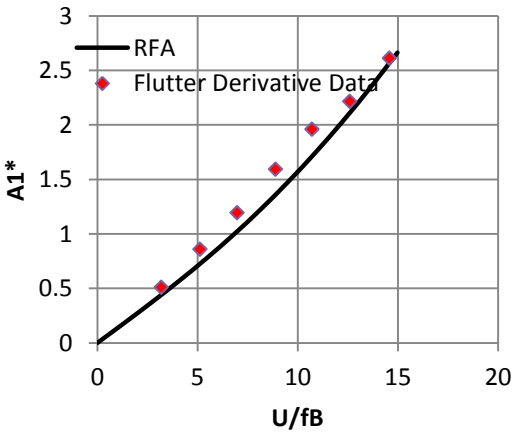
A1*
U/fB
RFA
Flutter Derivative Data

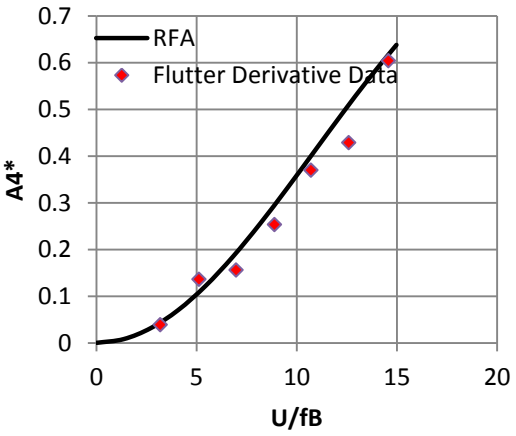
A4*
U/fB
RFA
Flutter Derivative Data

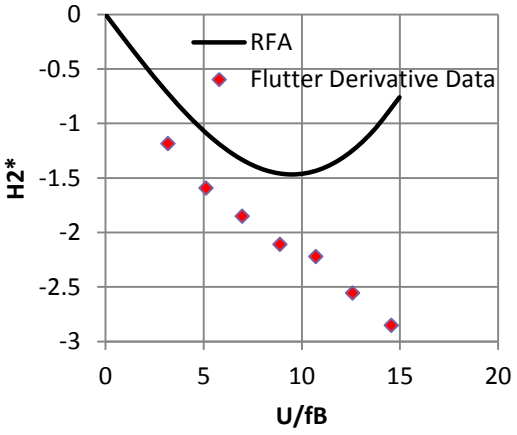
H2*
U/fB
RFA
Flutter Derivative Data

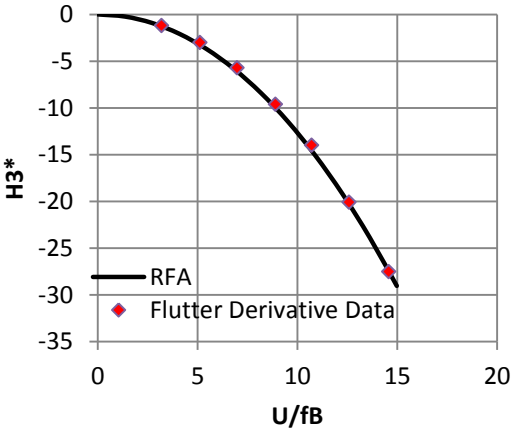
H3*
U/fB
RFA
Flutter Derivative Data

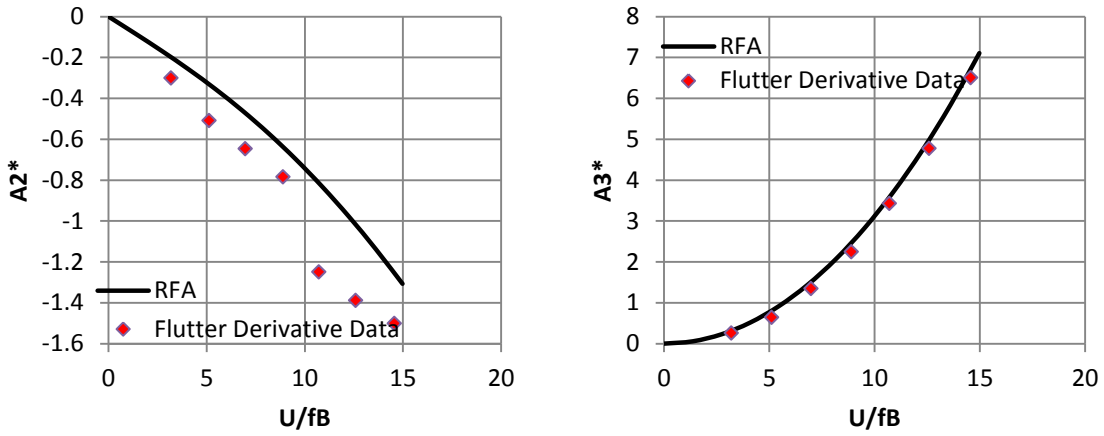

Figure 5. Comparison of experimentally obtained flutter derivatives [17] and those from Rational Functions for the streamlined section model

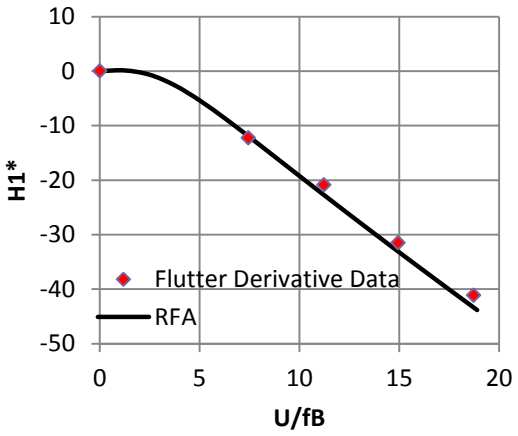
H1*
U/fB
Flutter Derivative Data
RFA

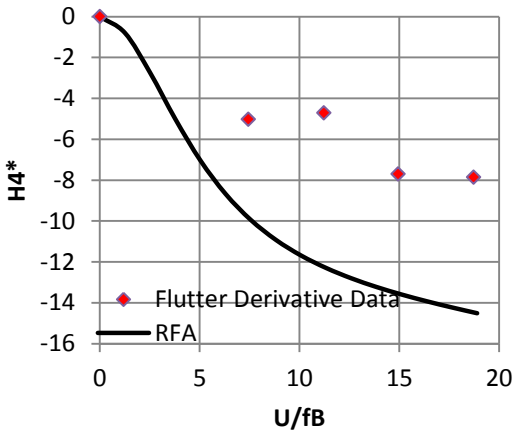
H4*
U/fB
Flutter Derivative Data
RFA

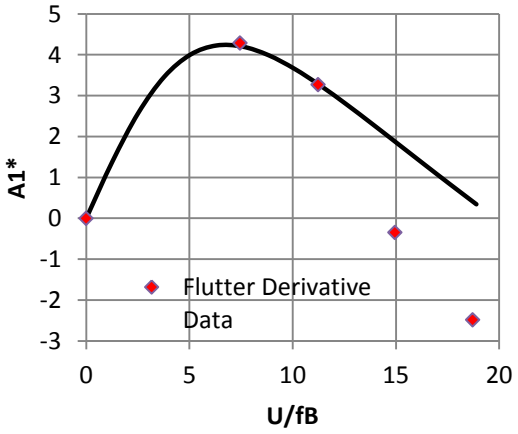
A1*
U/fB
Flutter Derivative Data

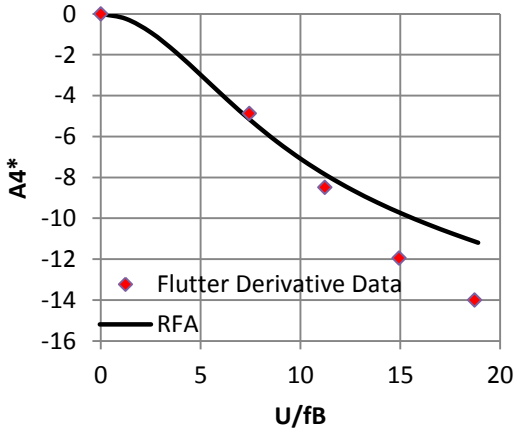
A4*
U/fB
Flutter Derivative Data
RFA

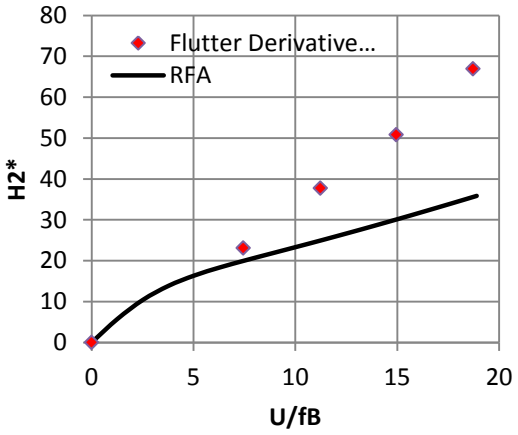
H2*
U/fB
Flutter Derivative...
RFA

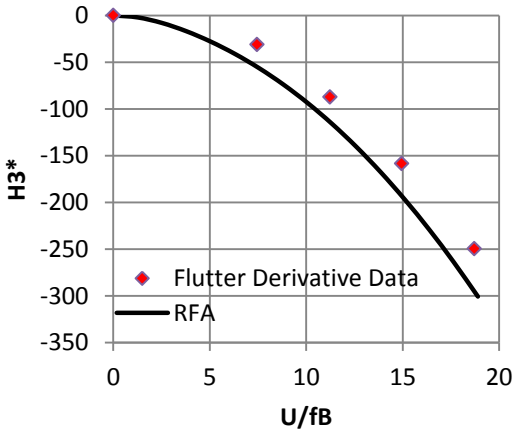
H3*
U/fB
Flutter Derivative Data
RFA

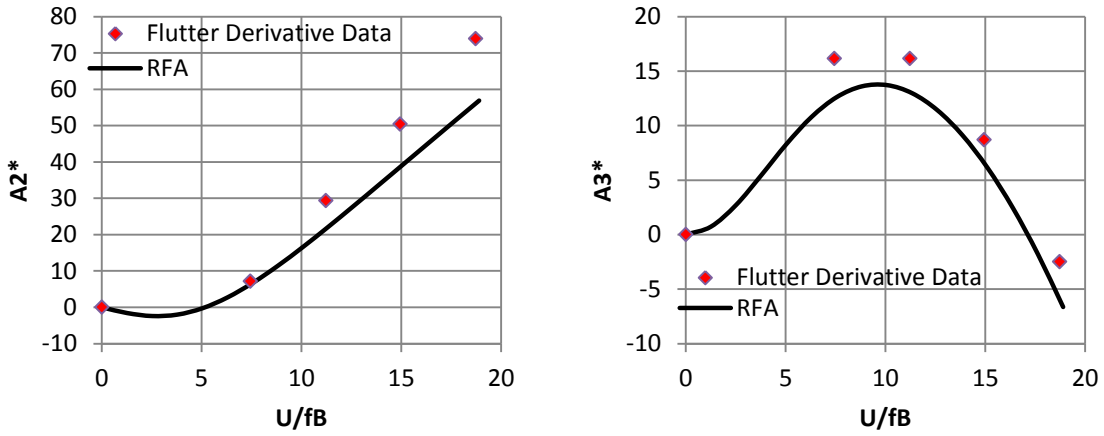

Figure 6. Comparison of experimentally obtained flutter derivatives [19] and those from Rational Functions for the bluff section model

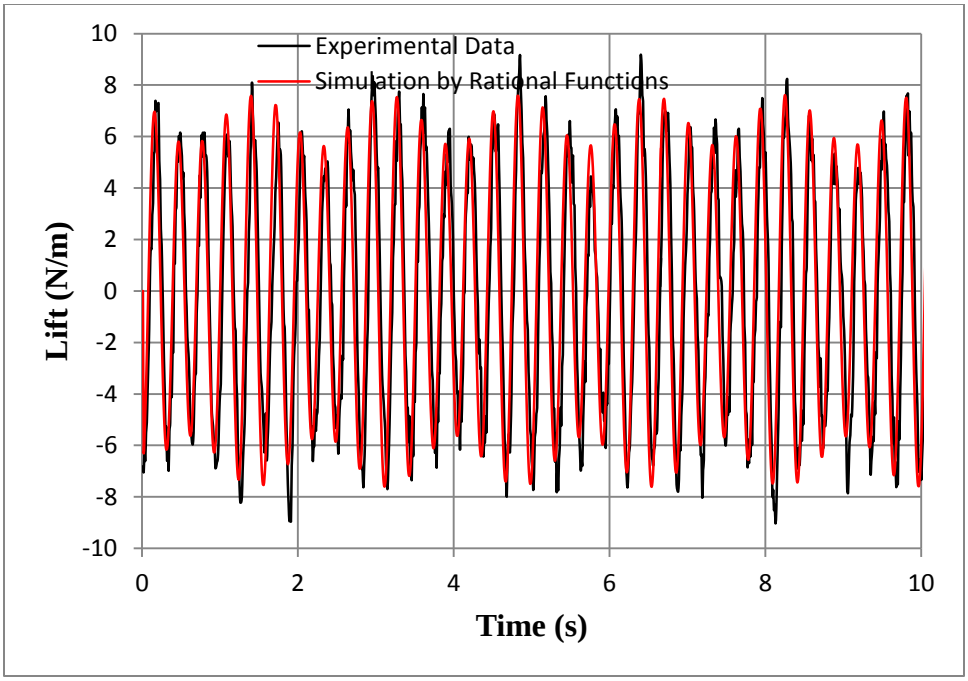

Figure 7. Lift time histories for the streamlined section model at velocity of 11.7m/s

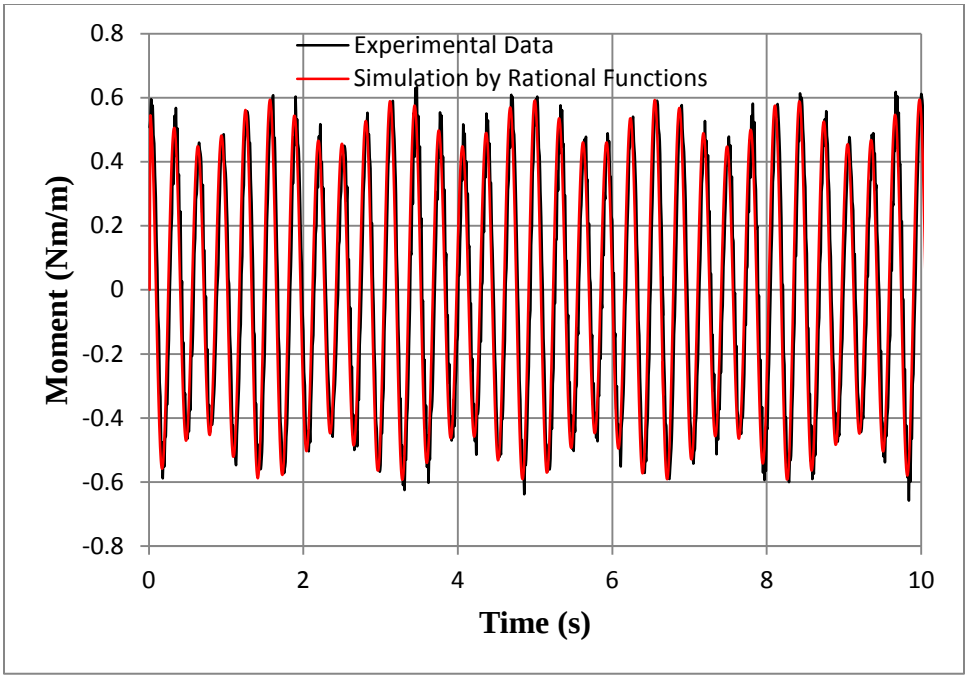

Figure 8. Moment time histories for the streamlined section model at velocity of 11.7m/s

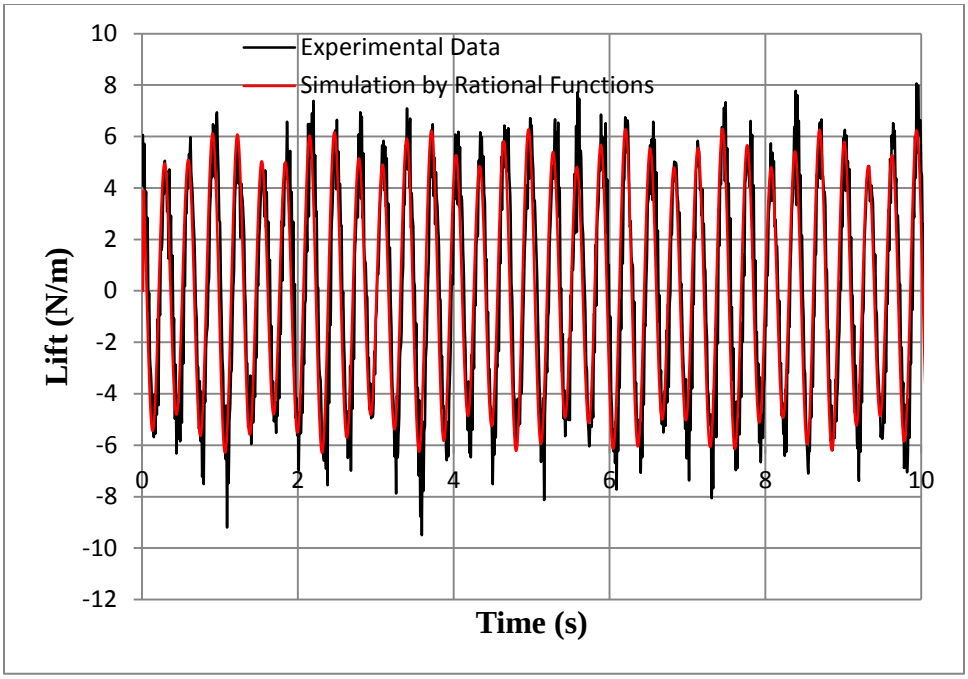

Figure 9. Lift time histories for the bluff section model at velocity of 11.6m/s

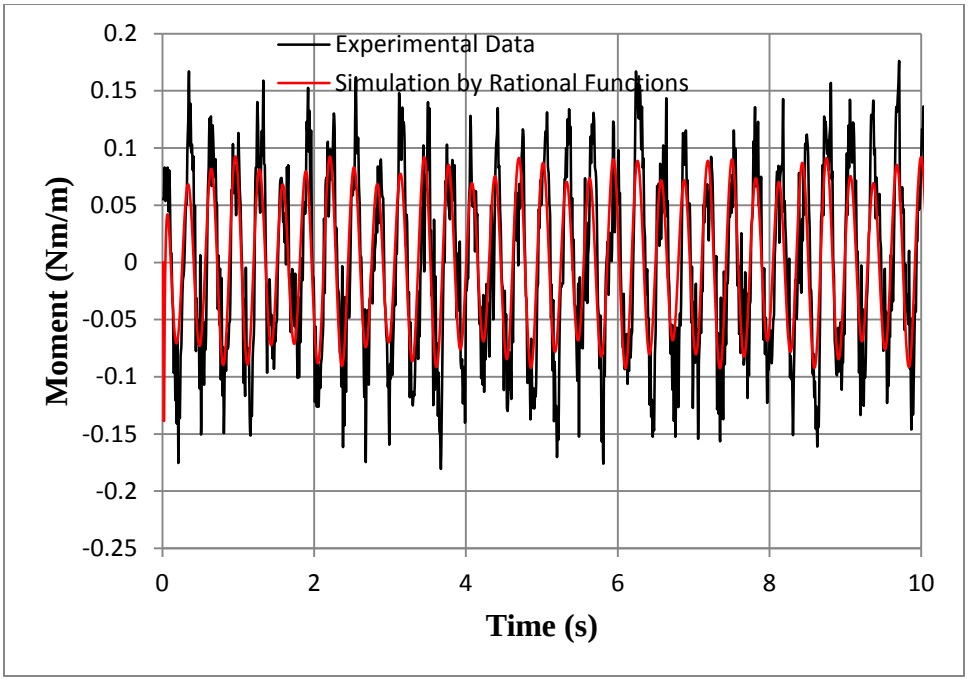

Figure 10. Moment time histories for the bluff section model at velocity of 11.6m/s

CHAPTER 4. TIME-DOMAIN AEROELASTIC LOADS AND RESPONSE OF FLEXIBLE BRIDGES IN GUSTY WIND: PREDICTION AND EXPERIMENTAL VALIDATION

A paper submitted to Journal of Engineering Mechanics, ASCE

Bochao Cao[1] and Partha P. Sarkar[2]

Abstract: Flexible bridges could experience vortex-induced and buffeting excitations below their design wind speeds and divergent self-excited oscillations (flutter) beyond a critical wind speed. For regular straight-line winds which are stationary or weakly-stationary, frequency domain formulation is routinely used for flutter analysis of bridges. However, when evaluating performance of flexible bridges subjected to gusty winds that are transient in nature, the frequency-domain formulation is not applicable and hence time-domain methods should be used. In this paper, time domain formulations were used to predict aeroelastic loads acting on a rigid bridge deck section model subject to stationary and gusty straight-line winds based on the knowledge of upstream wind speed and model displacement measurements. In this procedure, Rational Functions and indicial functions are used to formulate self-excited forces and buffeting forces, respectively. These functions used here were recently obtained from wind tunnel tests performed on a streamlined bridge deck section model with a smaller geometric scale. The results of the validation using a larger section model of this bridge deck subject to a ramp-type gust are presented here.

CE Database keywords: long-span bridges, time-domain formulation, rational functions, buffeting indicial functions, aeroelastic load prediction, gusty wind

Introduction

In traditional method of flutter analysis of flexible structures subjected to regular straight-line winds, self-excited forces were formulated using Scanlan (1971)'s flutter derivative formulation. This is a mixed-domain (frequency domain and time domain) formulation, since flutter derivatives used in the formulation are functions of reduced frequencies. Thus, this

[1] Graduate Research Assistant, Dept. of Aerospace Engineering; cbc@iastate.edu
[2] Professor, Dept. of Aerospace Engineering; corresponding author; ppsarkar@iastate.edu
2271 Howe Hall, Iowa State University, Ames, IA 50011-2271

formulation for self-excited forces cannot be substituted in equations of motion to continuously solve for response time histories of flexible structures below flutter speed or capture its transient response in gusty winds. To incorporate the nonstationarity of wind environment and nonlinearity of structural vibration in the analysis, time domain formulations for aerodynamic forces (Lin and Ariaratnam, 1980; Scanlan, 1984; Tsiatas and Sarkar, 1988; Scanlan, 1993; Li and Lin, 1995; Scanlan, 2000; Chen et al., 2000; Chen and Kareem, 2002; Salvatori and Borri, 2007; Zhang et al., 2011) were proposed and investigated. Moreover, these time domain formulations are also suitable for finite element modeling, feedback-dependent structural control mechanism and fatigue-life prediction. However, previous research on use of time domain analysis method in bridge aerodynamics is limited to numerical simulations without any experimental validation. In the current study, validation tests are performed on a section model in a wind tunnel to verify the aerodynamic time-domain load models in stationary and gusty winds. Apart from increasing confidence levels of the time-domain aerodynamic load model presented here, the experimental procedure in this research can be used for studying problems related to non-stationary winds such as large amplitude motions or buffeting response in boundary-layer wind. In time domain, self-excited forces can be directly formulated in indicial functions (Tsiatas and Sarkar, 1988; Caracoglia and Jones, 2003), or they can be first written in Rational Functions (Roger, 1977; Karpel, 1982) in Laplace domain, and then be transformed into time domain. Using corresponding relationship between Laplace domain and frequency domain formulations of these self-excited forces, Rational Function Coefficients can be indirectly extracted from experimentally obtained flutter derivatives. However, to accelerate the process of extraction of Rational Function Coefficients, methods based on free vibration experiment (Chowdhury

and Sarkar, 2005) and forced vibration experiment (Cao and Sarkar, 2010) were developed. These methods require experimental data recorded at much fewer wind velocities compared to those used for extracting flutter derivatives. The Rational Function Coefficients used in this paper were obtained by a forced vibration method described in Cao and Sarkar (2010). The fluctuating buffeting forces can be modeled using aerodynamic admittance functions (Simiu and Scanlan, 1996; Scanlan and Jones, 1999) in frequency domain and buffeting indicial aerodynamic functions in time domain. Chang et al. (2010) used the relationship between the two formulations for buffeting forces and devised a procedure to identify the buffeting indicial functions of a structural section. This procedure was used here to identify the buffeting indicial functions for the streamlined bridge deck. In the current paper, these time domain functions for self-excited and buffeting forces were used to predict the total aeroelastic loads acting on a streamlined bridge deck section model with an aspect ratio (B/D) of 15:1 that was subjected to both stationary and ramp-shaped gusty winds, and compared with wind tunnel measurements for validation of these time-domain formulations of aeroelastic loads.

Time Domain Equations for Aeroelastic Loads

In most analysis, motion in two degrees of freedom (vertical or across-wind and torsional) are considered sufficient but occasionally all three degrees of freedom including the lateral or along-wind are necessary for accurate analysis. For flexible long span bridges, vertical-torsional modes have routinely been used, except for cable-stayed bridges, where lateral mode needs to be included in the analysis. In this paper, only self-excited and buffeting loads

were included in the total aeroelastic load terms that appear on the right-hand side of the two-degree-of-freedom (vertical-torsional) equations of motion written as:

$$m(\ddot{h} + 2\varsigma_h \omega_h \dot{h} + \omega_h^2 h) = L_{ae} = L_b + L_{se} \tag{1}$$

$$I(\ddot{\alpha} + 2\varsigma_\alpha \omega_\alpha \ddot{\alpha} + \omega_\alpha^2 \alpha) = M_{ae} = M_b + M_{se} \tag{2}$$

where m= mass per unit length; I= mass moment of inertia about the centroidal axis per unit length; h(t,x)= vertical displacement; α(t,x)= torsional displacement; ω_h, ς_h = natural frequency and damping ratio of vibration for dominant vertical or cross-wind mode; $\omega_\alpha, \varsigma_\alpha$ = natural frequency and damping ratio of vibration for dominant torsional mode; ($\dot{}$)= d( )/dt; ($\ddot{}$)= d^2( )/dt^2; L_{ae}= total aeroelastic lift; M_{ae}= total aeroelastic moment; L_b= buffeting lift component; L_{se}= self-excited lift component; M_b= buffeting torsional moment; M_{se}= self-excited torsional moment.

Equations for Self-Excited Aeroelastic Loads

Self-excited lift and moment for a bridge-deck section in time domain, as obtained by transforming Rational Function formulation from Laplace domain, can be written as:

$$\begin{aligned} L_{se}(t) = \frac{1}{2}\rho U^2 B \Bigg[& \left(\left(\underline{A}_0\right)_{11} + \left(\underline{F}\right)_{11}\right)\frac{h}{B} + \left(\underline{A}_1\right)_{11}\frac{\dot{h}}{U} - \left(\underline{F}\right)_{11}\frac{\lambda_L U}{B^2}\int_0^t e^{-\frac{U}{B}\lambda_L(t-\tau)} h(\tau)d\tau \\ & + \left(\left(\underline{A}_0\right)_{12} + \left(\underline{F}\right)_{12}\right)\alpha + \left(\underline{A}_1\right)_{12}\frac{B}{U}\dot{\alpha} - \left(\underline{F}\right)_{12}\frac{\lambda_L U}{B}\int_0^t e^{-\frac{U}{B}\lambda_L(t-\tau)}\alpha(\tau)d\tau \Bigg] \end{aligned} \tag{3}$$

$$\begin{aligned} M_{se}(t) = \frac{1}{2}\rho U^2 B^2 \Bigg[& \left(\left(\underline{A}_0\right)_{21} + \left(\underline{F}\right)_{21}\right)\frac{h}{B} + \left(\underline{A}_1\right)_{21}\frac{\dot{h}}{U} - \left(\underline{F}\right)_{21}\frac{\lambda_M U}{B^2}\int_0^t e^{-\frac{U}{B}\lambda_M(t-\tau)} h(\tau)d\tau \\ & + \left(\left(\underline{A}_0\right)_{22} + \left(\underline{F}\right)_{22}\right)\alpha + \left(\underline{A}_1\right)_{22}\frac{B}{U}\dot{\alpha} - \left(\underline{F}\right)_{22}\frac{\lambda_M U}{B}\int_0^t e^{-\frac{U}{B}\lambda_M(t-\tau)}\alpha(\tau)d\tau \Bigg] \end{aligned} \tag{4}$$

where ρ= air density, B= width of the bridge deck, U= mean wind velocity, $\underline{A}_0, \underline{A}_1$ are stiffness matrix and damping matrix, respectively, and $\underline{F}$ is a lag matrix, all of order 2×2, λ_L and λ_M are lag coefficients. The elements of $\underline{A}_0, \underline{A}_1, \underline{F}$ matrices and λ_L, λ_M are known as Rational Function Coefficients.

Equations for Buffeting Loads

In time domain, buffeting lift and moment can be formulated using buffeting indicial functions in terms of non-dimensional time, s = Ut/B, as follows:

$$L_b(s) = \frac{1}{2}\rho U^2 B \frac{C_D + C_L^{'}}{U} \int_0^s w(\sigma)\phi_{wL}^{'}(s-\sigma)d\sigma \tag{5}$$

$$M_b(s) = \frac{1}{2}\rho U^2 B^2 \frac{C_M^{'}}{U} \int_0^s w(\sigma)\phi_{wM}^{'}(s-\sigma)d\sigma \tag{6}$$

where $\phi_{wL}^{'}(s)$ and $\phi_{wM}^{'}(s)$ = derivatives of buffeting indicial functions, $\phi_{wL}(s)$ and $\phi_{wM}(s)$, respectively, C_L = lift coefficient, α = angle of attack, C_M' = $dC_M/d\alpha$, C_M = moment coefficient, w(s) = turbulent velocity in vertical direction. Since the section model used in the current work is symmetric, the lift and moment coefficients C_L and C_M are both zero at angle of attack α=0. Thus, as can be seen in Equations (5) and (6), the along-wind turbulence (u) term that enter through C_L and C_M drops out.

The functions, $\phi_{wL}^{'}(s)$ and $\phi_{wM}^{'}(s)$, expressed in non-dimensional time, s = Ut/B, take the following form:

$$\phi_{xx}^{'} = A_1 \cdot e^{-A_2 \cdot s} + A_3 \cdot e^{-A_4 \cdot s} \tag{7}$$

where A_1 to A_4 are constants.

Rational and Indicial Functions for a Streamlined Bridge Deck

A streamlined bridge deck section that is a thin rectangular section with semi-circular fairings at its both edges with an aspect ratio (B/D, B =total width and D=depth) of 15:1 was used in the experiments described in this paper. A section model (B=300 mm, D=20 mm, L=450 mm) of the bridge section with end plates was placed in an open-return wind tunnel, Bill James Wind Tunnel (0.915m width by 0.762m height), for the extraction of aeroelastic load functions such as Rational Function Coefficients or Rational Functions and the buffeting indicial functions with two separate sets of experiments. The Rational Function Coefficients, as extracted using the forced-vibration method described in Cao and Sarkar (2010), are given below:

$$\underline{A}_0 = \begin{bmatrix} 0.3273 & -6.2384 \\ -0.0970 & 1.3818 \end{bmatrix}, \underline{A}_1 = \begin{bmatrix} -3.7549 & -1.4947 \\ 0.8510 & -0.3819 \end{bmatrix}, \underline{F} = \begin{bmatrix} -0.9484 & 1.3397 \\ 0.2689 & -0.1682 \end{bmatrix}, \lambda_{\mathrm{L}} = 0.1843, \lambda_{\mathrm{M}} = 0.2239$$

The buffeting indicial functions were extracted using the method described in Chang et al. (2010). The derivatives of these functions, $\phi'_{wL}(s)$ and $\phi'_{wM}(s)$, are given below for the given bridge deck section:

$$\phi'_{wL}(s) = 0.0081e^{-0.0058s} - 0.0392e^{-0.0833s}$$

$$\phi'_{wM}(s) = -0.0347e^{-0.0733s} + 0.0072e^{-0.0051s}$$

In these tests, aerodynamic static force coefficients were also measured as follows:

$C_D = 0.037$, $C_L' = 4.639$, $C_M' = 1.085$

Experimental Set-Up

The experiments described here were performed with a larger model in a larger wind tunnel compared to the previous set of experiments used for extraction of Rational Function Coefficients. There were two reasons - the first one being the larger wind tunnel's capability for generation of atmospheric boundary layer associated with a particular terrain and variety of gusts that were used in the study and the second one was to prove that the aeroelastic parameters that were identified in a different setting can be used to predict loads on the bridge model of a larger scale.

Wind Tunnel and Gust Generation Mechanism

The experiments described here were performed in the Aerodynamic/Atmospheric Boundary Layer (AABL) wind tunnel (Figure 1), which is located in the Wind Simulation and Testing Laboratory (WiST Lab) in the Department of Aerospace Engineering at Iowa State University. This wind tunnel has an aerodynamic test section of 2.44m (8.0ft) width by 1.83m (6.0ft) height and an atmospheric boundary layer test section of 2.44m (8.0ft) width by 2.21m (7.25ft) height, and a designed maximum wind speed of 53m/s (173.9ft/s) in the aero section. An active gust generation mechanism was developed and implemented by Haan and Sarkar (2006) on this wind tunnel. The basic design of this mechanism is a bypass duct added to the wind tunnel fan section, as shown in Figures 1 and 2.

The flow could be diverted to and from the main duct to the bypass duct, so that flow velocity in the test section can be increased or reduced in a short duration. The motion of damper vanes inside the bypass duct can be controlled and programed by a computer,

through which mean velocity time histories of gusts can be prescribed. Several types of gust can be generated by this mechanism, such as ramp-up or ramp-down gust, triangular-shaped gust, trapezoidal-shaped gust and sinusoidal-wave-shaped gust. In this paper, results corresponding to a ramp-down gust are presented.

Model and Suspension System

The section model used in the experiment is shown in Figure 3. The model, as described earlier, is composed of a shallow box girder section and two semi-circular fairings at its edges. The length L, chord length B and thickness D of the model are about 1.83m, 0.74m, and 0.051m, respectively, making this model about 2.5 times larger than the section model described earlier that was used for the extraction of the aeroelastic load functions. To reduce the edge effects, two end plates were used as seen in Figure 3. The two-DOF model suspension system used in this experiment is shown in Figures 3. The suspension system enables vertical and torsional motions of the model using twelve linear helical springs, six at each end of the model, while horizontal motion is restricted by two leaf springs attached at both ends of the model shaft, as shown in Figure 3. Before running wind tunnel tests on the model, free vibration tests without wind were performed to identify the stiffness coefficients of the entire vibration system (with the model mounted) for the two degrees of freedom (vertical h and torsional α) as K_h = 2233.5 N/m and K_α = 103.72 Nm/rad, respectively. The natural frequencies of the two degree-of-freedom system at zero wind were measured as f_h = 1.76Hz, and f_α = 1.78Hz, and the damping ratios of the system at zero wind were measured as ζ_h = 0.25% and ζ_α = 0.83%, along the vertical and torsional degrees of freedom, respectively. The mass and mass moment of inertia of the entire dynamic system were M =

18.3kg, and I = 0.8275kgm^2, respectively. To induce vibration of the model, two C-clamps were added as lumped masses, one on each side of the model span at a distance of 0.25m downstream of the model shaft, as can be seen in Figure 3. The total mass of the two C-clamps was 1.57kg.

Wind Velocity Measurement

In this experiment, wind velocity time histories were measured by a Cobra Probe (Turbulent Flow Instrumentation) placed right in front of the bridge deck model, as shown in Figure 3. The sampling rate for wind velocity was set at 156 Hz.

Model Displacement Measurement

The vertical or torsional displacement of the model was measured by measuring the elastic force in each of the four helical springs which is connected to the model at one end and a strain gage force transducer at the other end, as can be seen in Figure 3. The force transducers were mounted at two opposite corner positions at both ends of the model span to eliminate the spurious modes of vibration of the model such as rotation about its centerline. LabView program was used for data acquisition, where the sampling rate was set at 125Hz.

Aerodynamic Pressure Measurement

Aerodynamic pressures were also recorded in the experiment to assess aeroelastic loads for comparison with those obtained from numerical simulation. Surface pressures were measured on the model including the fairings through a row of pressure taps located on the upper and lower surfaces of the model along the mid-plane. In total, forty-two pressure taps were used in this test, equally distributed on both the surfaces. The pressure taps are denser on the

upstream side than the downstream side of the model. Two 64-channel pressure modules (Scanivalve ZOC33/64 Px) were used to measure the pressure. To minimize the error introduced from pressure tubing, pressure modules were placed inside the model, so that tubing length can be significantly shortened, as shown in Figure 4. A separate program (RAD) collected the pressure data. The sampling rate for pressure measurement was 62.5Hz (half of displacement sampling rate for convenience of synchronization) in the experiment.

Data Synchronization

To synchronize the displacement data with the pressure data and the wind velocity data, both the pressure transducers and the Cobra Probe were set to work in an external-trigger mode. The LabView program that was used for displacement data acquisition was programmed to output a digital signal when the displacement data acquisition started, so that the pressure data acquisition system and the Cobra Probe data acquisition system would receive this external signal and get triggered to start the data acquisition.

Results and Discussion

In the wind tunnel tests, the model was given initial displacement to start the vibration, and both the model displacement and pressures or aeroelastic loads were recorded during the vibration. Using model displacement time histories (h(t) and α(t)) measured from wind tunnel tests, their first derivatives $\dot{h}(t)$ and $\dot{\alpha}(t)$ were calculated by finite difference method. After obtaining all these time histories, self-excited lift and moment were calculated from Equations (3) and (4) at each time step. Similarly, using experimentally measured turbulent velocity time history in vertical direction, w(t), buffeting lift and moment were calculated

from Equations (5) and (6) at all time steps. Rational Function Coefficients and Indicial Functions of the bridge deck identified earlier were used in these calculations. The total aeroelastic loads acting on the model were calculated as the sum of self-excited and buffeting loads. To evaluate this load time history prediction procedure, both stationary wind and gusty wind cases were investigated.

Load Prediction for Stationary Wind Case

For stationary wind case, the aeroelastic loads were predicted and measured at a mean wind velocity of about 6.2m/s, as can be seen in velocity time history shown in Figure 5(a). The standard deviation of vertical turbulence component of the velocity (w(t)) was 0.017m/s which gives a turbulence intensity of 0.27%. Thus, this flow condition can be classified as smooth flow which reduces the effects of the buffeting loads. The displacement time histories which were measured from experiment and used in the prediction of aeroelastic loads are plotted in Figures 5(b) and 5(c). The numerically predicted lift and moment coefficients as computed using Equations (8) and (9) are shown and compared with experimentally measured ones in Figures 5(d) and (e).

$$C_l(t) = \frac{L(t)}{1/2\rho U^2(t)B} \tag{8}$$

$$C_m(t) = \frac{M(t)}{1/2\rho U^2(t)B^2} \tag{9}$$

where L(t) and M(t) are aeroelastic lift and moment per unit length obtained numerically or experimentally, and U(t) is instantaneous wind speed in horizontal direction.

As can be observed from the lift and moment comparison plots, the lift coefficient time history predicted by the procedure described here matches well with experimental results, for both amplitude and phase angle. While the amplitude of moment coefficient time history was predicted well, the predicted phase angle was slightly different from that of the measurement. The discrepancy of phase angle for moment coefficient between prediction and measurement might be due to the error in the Rational Function Coefficients that are used here for the prediction of aerodynamic damping in the torsional direction (i.e, A_2^* in flutter derivative formulation). It is known that the phase shift between torsional motion and aerodynamic moment is attributed to aerodynamic torsional damping so an error in this term would manifest itself in the phase shift. In a separate study, when comparing the eight flutter derivatives for this cross section obtained by free vibration method for vertical-torsional motion (Chowdhury and Sarkar, 2005) with those calculated using the Rational Function Coefficients used here, it was observed that the match between the two sets was generally good for all the direct flutter derivatives over their full range of reduced velocities with the exception of A2* which had more error at low reduced velocities. For example, it is noted that A2* had a large error (33%) at reduced velocity of 4.7 (U = 6.2 m/s) at which the current model was tested.

Load Prediction for Ramp-Down Gusty Wind Case

To ultimately validate the feasibility of the time domain formulations in non-stationary wind environment, the wind tunnel tests were carried out in a ramp-down gusty wind, whose horizontal velocity time history is shown in Figure 6(a). The corresponding displacement and force coefficient time histories are plotted in Figures 6(b) to 6(e).

For this gusty wind case, it is observed in Figures 6(d) and 6(e) that the amplitudes of load coefficients are predicted well in the first half of the time intervals and are over-predicted in the later time periods, for both lift and moment coefficient time histories. Moreover, similar to the stationary wind case, the prediction of moment coefficient time history has slight error in phase angle, and is slightly worse than the prediction of lift coefficient time history.

Given the error in the aeroelastic load functions (Rational and Indicial) as extracted from a separate set of experiments on a smaller section model, the errors in the measurements of displacements on the larger section model that were used for the numerical prediction of aeroelastic loads, combined with errors associated with differentiation and integration in the numerical procedure used here, and error in the pressure measurements that were used to calculate the aeroelastic lift and moment, the comparison between the predicted and measured time histories of the aeroelastic loads seems quite encouraging.

Conclusion

In this paper, time domain method was used to predict aeroelastic loads on a streamlined bridge section model while it is vibrating in stationary and gusty straight-line winds. The Rational Functions and buffeting indicial functions were used to calculate self-excited forces and buffeting forces, respectively. The numerically simulated loads were compared with experimental measurements for both stationary wind case and gusty wind case. It was demonstrated here that the prediction of aeroelastic loads using the time-domain formulation can be made. The comparison between predictions and measurements was quite well in the stationary wind case, while a similar comparison in the gusty wind case was not as good but reasonable within the error bounds expected. The slightly worse performance of time domain

method in gusty wind case is explainable since all the formulations used in this paper were originally proposed for stationary wind and the aeroelastic parameters used here were also extracted in stationary wind. However, a better performance is expected if the time domain formulation used here is revised to include the effect of time-varying mean wind as in the gusty wind cases which could be investigated in future studies. In future, the performance of this time-domain load prediction method for winds that are non-uniform with height such as boundary-layer wind, more turbulent, and not straight-line but highly non-stationary, such as microbursts or tornadoes, will be investigated.

References

Cao, B., Sarkar, P.P. (2010). "Identification of rational functions by forced vibration method for time-domain analysis of flexible structures," In Proceedings: The Fifth International Symposium on Computational Wind Engineering, Chapel Hill, May 23-27.

Caracoglia, L. and Jones, N.P. (2003). "Time domain vs. frequency domain characterization of aeroelastic forces for bridge deck sections," J. of Wind Eng. and Ind. Aero., 91, 371-402.

Chang, B., Sarkar, P.P. and Phares, B.M. (2010). "A time-domain model for predicting aerodynamic loads on a slender support structures for fatigue design." J. Eng. Mech., ASCE. 136(6), 736-746.

Chen, X., Matsumoto, M., Kareem, A. (2000). "Time domain flutter and buffeting response analysis of bridges." J. Eng. Mech., ASCE, 126(1), 7-16.

Chen, X. and Kareem, A. (2002). "Advances in modeling of aerodynamic forces on bridge decks," J. Eng. Mech., ASCE, 128 (11), 1193-1205.

Chowdhury, A.G., Sarkar, P.P. (2005). "Experimental identification of rational function coefficients for time-domain flutter analysis," Eng. Struct., 27(9), 1349-1364.

Haan, F.L., Sarkar, P.P. (2006). "Development of an active gust generation mechanism on a wind tunnel for wind engineering and industrial aerodynamics applications," Wind and Struct., 9(5), 369-386.

Karpel, M. (1982). "Design for active flutter suppression and gust alleviation using state-space aeroelastic modeling," J. of Aircraft 19(3), 221–227.

Li, Q.C. and Lin, Y.K. (1995). "New stochastic theory for bridge stability in turbulent flow." J. Eng. Mech., 121(1), 102-116.

Lin, Y.K. and Ariaratnam, S.T. (1980). "Stability of bridge motion in turbulent winds," J. of Struct. Mech., 8 (1), 1-15.

Roger, K. (1977). "Airplane math modeling methods for active control design," AGARD-CP-228.

Salvatori, L., and Borri, C. (2007). "Frequency and time-domain methods for the numerical modeling of full-bridge aeroelasticity." Comput. Struct., 85, 675-687.

Scanlan, R.H., Tomko, J.J. (1971). "Airfoil and bridge deckflutter derivatives," J. Eng. Mech. Div., 97(6), 1717-1733.

Scanlan, R.H. (1984). "Role of indicial functions in buffeting analysis of bridges," J. of Struc. Eng., 110 (7).

Scanlan, R.H. (1993). "Problematics in formulation of wind-force models for bridge decks," J. Eng. Mech., ASCE, 119 (7), 1353-1375.

Scanlan, R.H. and Jones, N.P. (1999). "A form of aerodynamic admittance for use in bridge aeroelastic analysis. J. Fluids and Struct., 13, 1017-1027.

Scanlan, R.H. (2000). “Motion-related body force functions in two-dimensional low-speed flow.” J. Fluids Struct., 14, 49-63.

Simiu, E. and Scanlan, R.H. (1996). “Wind effects on structures: fundamentals and applications to design,” 3rd ed., John Wiley & Sons, New York, NY.

Tsiatas, G. and Sarkar, P.P. (1988). “Motion stability of long-span bridges under gusty winds,” J. of Eng. Mech., ASCE, 114(2).

Zhang, Z., Chen, Z., Cai, Y., Ge, Y. (2011). “Indicial functions for bridge aeroelastic forces and time-domain flutter analysis.” J. Bridge Eng., ASCE, 16(4), 546-557.

LIST OF FIGURES

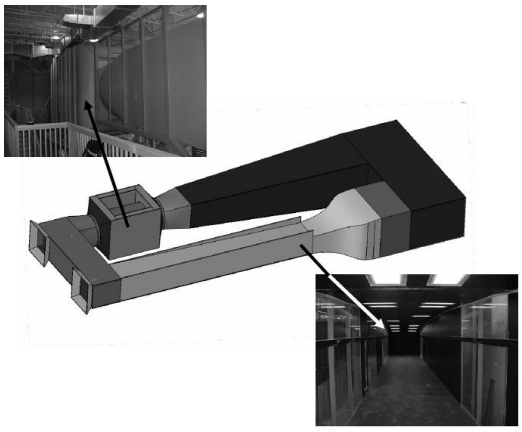

Figure 1. Diagram of AABL Wind and Gust Tunnel at Iowa State University. The bypass duct for gust generator is shown in upper left corner and the aerodynamic test section is shown in the lower right corner. (Haan and Sarkar, 2006)

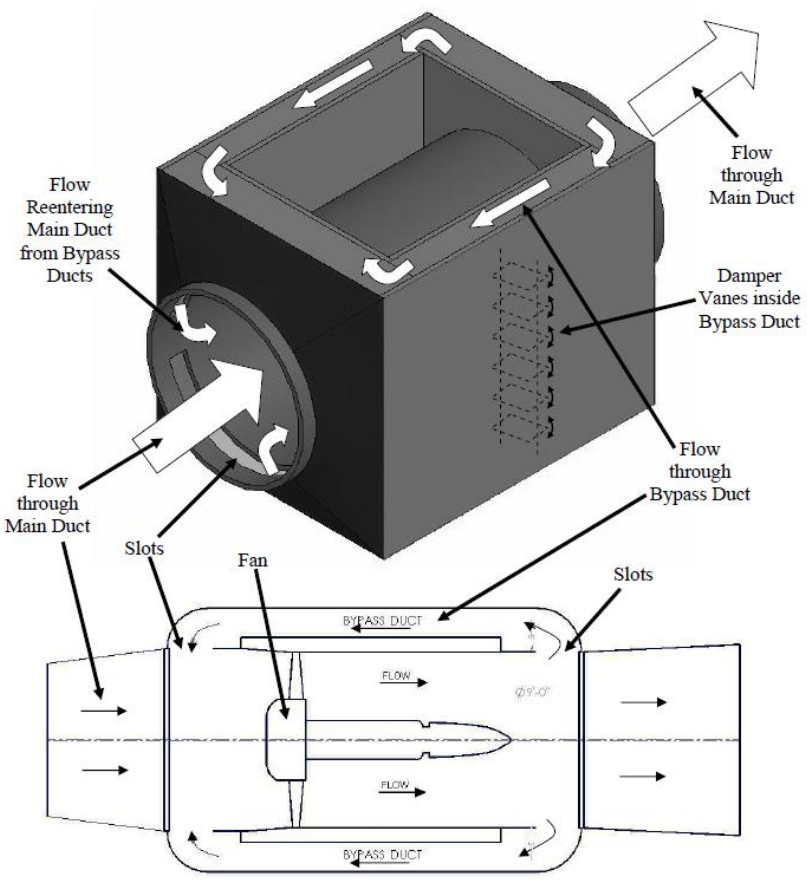

Figure 2. Diagram of the bypass duct surrounding the portion of the main duct containing the fan. The upper diagram is a 3D illustration of the bypass ducts surrounding the fan section. The lower diagram is a top view of the system showing the fan and its relation to the bypass ducts (Haan and Sarkar, 2006).

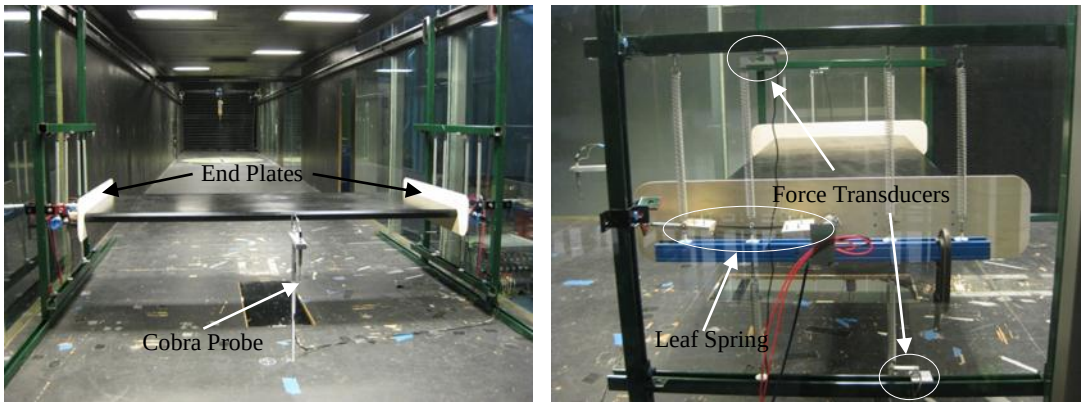

(a) View from upstream (b) View from side

Figure 3. Section model and experimental set-up

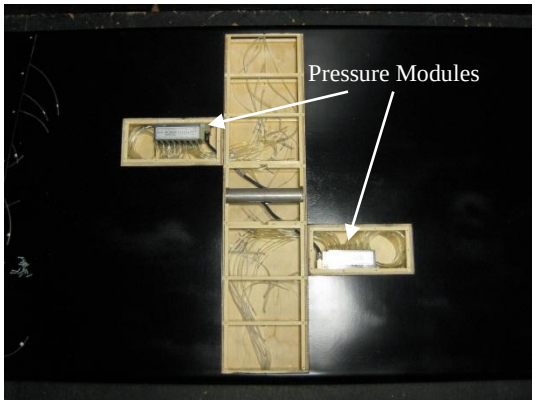

Figure 4. Pressure modules (Scanivalve ZOC 33/64 Px) mounted inside the model

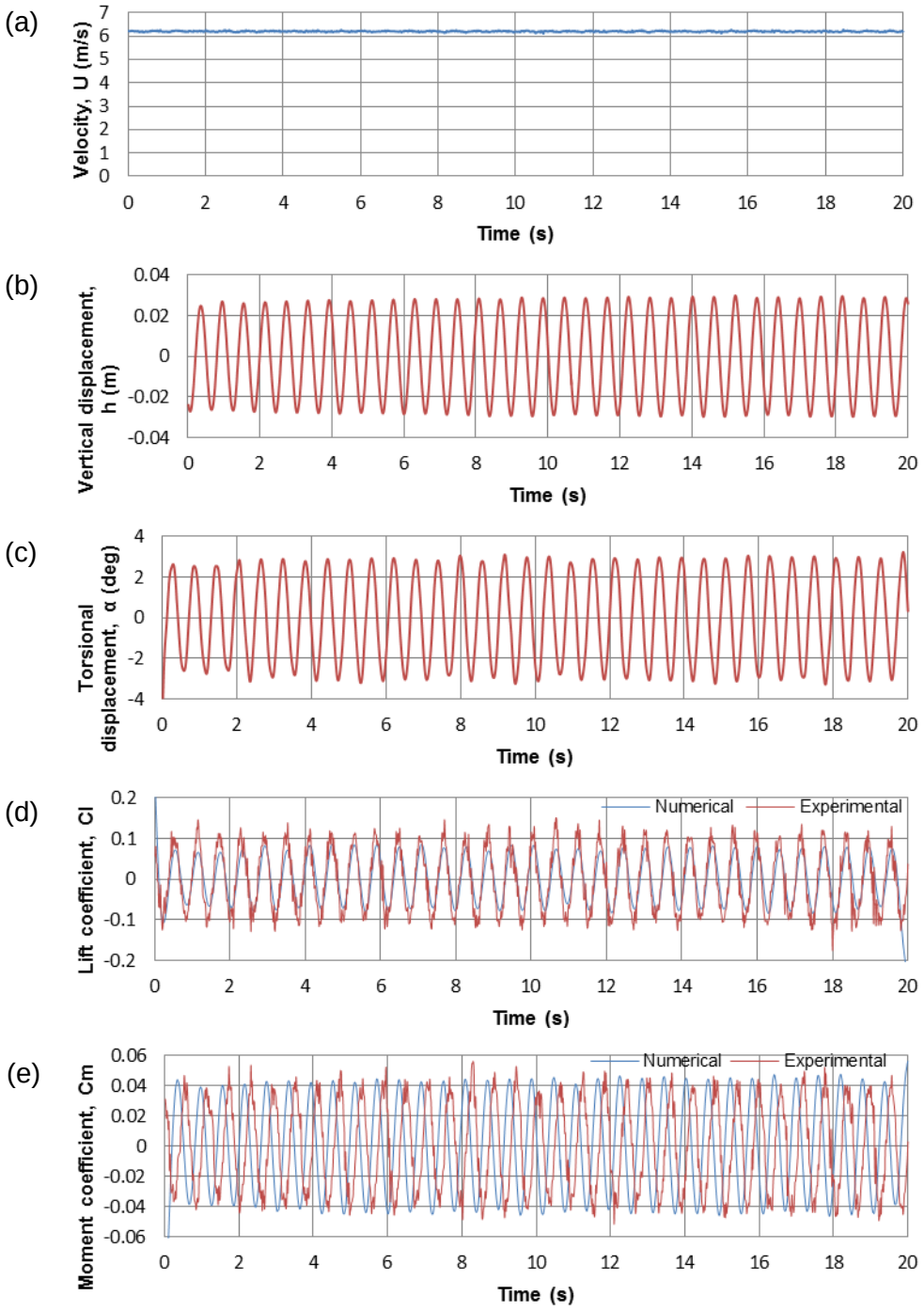

Figure 5. (a) Horizontal velocity time history, (b) Vertical displacement time history, (c) Torsional displacement time history, (d) Aeroelastic lift coefficient comparison, (e) Aeroelastic moment coefficient comparison, for stationary wind case

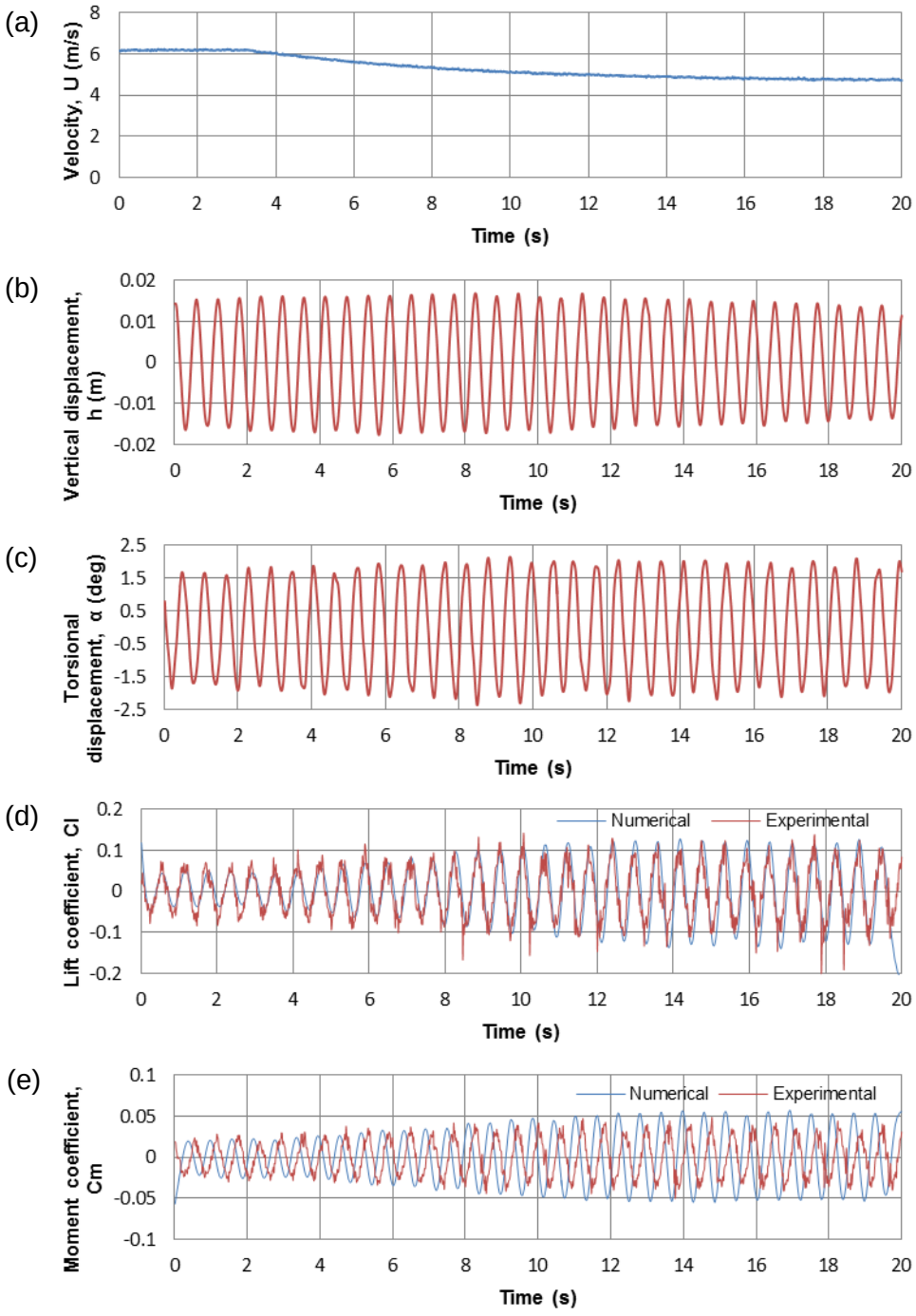

Figure 6. (a) Horizontal velocity time history, (b) Vertical displacement time history, (c) Torsional displacement time history, (d) Aeroelastic lift coefficient comparison, (e) Aeroelastic moment coefficient comparison, for gusty wind case

CHAPTER 5. DYNAMIC WIND LOADS ON BRIDGE DECKS IN TURBULENT WIND ENVIRONMENT

Bochao Cao[2] and Partha P. Sarkar[2]

Abstract: In time domain analysis of structures subjected to wind loads, Rational Function formulation and buffeting indicial formulation can be used to predict self-excited and buffeting wind loads acting on the structure, respectively. In an earlier study, it has already been shown that these formulations can work very well in predicting wind loads for smooth wind cases through section model vibration tests in a wind tunnel. In current research, to validate time domain formulations in turbulent wind environment, wind tunnel tests are performed with turbulence generated by two different boundary layer set-ups in the up-stream of the section model. To incorporate gust effects simultaneously on the prediction of wind loads, different types of gusts (ramp-up, ramp-down and bump-shaped) are also generated in the tests.

Introduction

Flexible structures like long-span bridges or tall buildings are vulnerable to wind loads and could become unstable at certain wind speed (flutter speed). Based on the flutter derivative formulation derived by Scanlan and Tomko (1971), frequency domain method has been proposed to predict flutter speeds of structures. In the following decades, many methods (Huston, 1988, Scanlan and Jones, 1990, Sarkar et al., 1994, Gu et al., 2000, Brownjohn and Jakobsen, 2001, Zhu et al., 2002, Gan Chowdhury and Sarkar, 2004, Chen et al., 2008, Chen

[2] Graduate Research Assistant, Dept. of Aerospace Engineering; cbc@iastate.edu
[2] Professor, Dept. of Aerospace Engineering; corresponding author; *ppsarkar@iastate.edu*
2271 Howe Hall, Iowa State University, Ames, IA 50011-2271

and Kareem, 2008, Batoli et al., 2009, Ding et al., 2010) have been developed to extract flutter derivative from either free vibration or forced vibration wind tunnel tests. However, frequency domain methods cannot be applied to the analysis of interaction between flexible structures and non-stationary winds, especially for extreme winds such as tornadoes and microbursts, which frequently cause loss of human lives and serious economic damages every year. Thus, to enable time domain structural analysis which can be used to investigate problems with non-stationary winds or nonlinear structures, time domain formulations have been developed to evaluate aeroelastic wind loads. To express self-excited wind loads in time domain, indicial function formulation (Tsiatas and Sarkar, 1988; Caracoglia and Jones, 2003) or the formulation as transformed from Laplace domain Rational Function formulation (Roger, 1977; Karpel, 1982) were derived. Methods have been developed to identify indicial functions or Rational Functions through free vibration (Gan Chowdhury and Sarkar, 2005) or forced vibration (Cao and Sarkar, 2010) techniques. While for the calculation of buffeting wind loads, frequency domain admittance functions (Davenport, 1962) and equivalent time domain buffeting indicial functions are widely used. The admittance functions can be extracted using a section model where the aerodynamic loads on the model are measured when fluctuating wind at a distinct frequency is generated using two parallel plates oscillating sinusoidally in front of the model (Chang et al., 2010) and tests repeated at several reduced frequencies. Recently, Sarkar and Cao (2011) have performed a validation study for time domain formulations, in which self-excited and buffeting wind loads were predicted using Rational Functions and buffeting indicial functions, respectively, and compared with experimentally measured wind loads in stationary and ramp-down gusty winds without turbulence, and the results from this study are quite encouraging. However, turbulence in the

wind flow could be a significant factor that affects the aeroelastic parameters and prediction of aeroelastic wind loads and structural responses (Scanlan and Lin, 1978, Scanlan, 1988, Diana et al., 1993, Scanlan, 1997, Gu et al., 2001, Batroli and Righi, 2006). In the current validation study, to test time domain formulations in turbulent winds, the section model is placed in the atmospheric boundary layer section of the wind tunnel with two types of boundary layers generated in the upstream of the model using spires, chains and roughness blocks. Besides the stationary wind, ramp-up, ramp-down and bump-shaped gusts are also tested in this study.

Time domain equations for dynamic wind loads

In most analysis, without considering vortex shedding effect, wind loads acting on a flexible bridge can be represented in two parts: self-excited loads and buffeting loads.

Time domain formulation for self-excited loads, as transformed from Laplace domain Rational Function formulation, can be written as:

$$L_{se}(t)=\frac{1}{2}\rho U^2 B\left[\left(\left(\underline{A}_0\right)_{11}+\left(\underline{F}\right)_{11}\right)\frac{h}{B}+\left(\underline{A}_1\right)_{11}\frac{\dot{h}}{U}-\left(\underline{F}\right)_{11}\frac{\lambda_L U}{B^2}\int_0^t e^{-\frac{U}{B}\lambda_L(t-\tau)}h(\tau)d\tau\right.$$
$$\left.+\left(\left(\underline{A}_0\right)_{12}+\left(\underline{F}\right)_{12}\right)\alpha+\left(\underline{A}_1\right)_{12}\frac{B}{U}\dot{\alpha}-\left(\underline{F}\right)_{12}\frac{\lambda_L U}{B}\int_0^t e^{-\frac{U}{B}\lambda_L(t-\tau)}\alpha(\tau)d\tau\right] \quad (1)$$

$$M_{se}(t)=\frac{1}{2}\rho U^2 B^2\left[\left(\left(\underline{A}_0\right)_{21}+\left(\underline{F}\right)_{21}\right)\frac{h}{B}+\left(\underline{A}_1\right)_{21}\frac{\dot{h}}{U}-\left(\underline{F}\right)_{21}\frac{\lambda_M U}{B^2}\int_0^t e^{-\frac{U}{B}\lambda_M(t-\tau)}h(\tau)d\tau\right.$$
$$\left.+\left(\left(\underline{A}_0\right)_{22}+\left(\underline{F}\right)_{22}\right)\alpha+\left(\underline{A}_1\right)_{22}\frac{B}{U}\dot{\alpha}-\left(\underline{F}\right)_{22}\frac{\lambda_M U}{B}\int_0^t e^{-\frac{U}{B}\lambda_M(t-\tau)}\alpha(\tau)d\tau\right] \quad (2)$$

where ρ= air density, B= width of the bridge deck, U= mean wind velocity, $\underline{A}_0, \underline{A}_1$ are stiffness matrix and damping matrix, respectively, and $\underline{F}$ is a lag matrix, all of order 2×2, λ_L and λ_M are lag coefficients. The elements of $\underline{A}_0, \underline{A}_1, \underline{F}$ matrices and λ_L, λ_M are known as Rational Function Coefficients.

The buffeting wind loads can be formulated using buffeting indicial functions in time domain, as follows:

$$L_b(s) = \frac{1}{2}\rho U^2 B \frac{C_D + C_L^{'}}{U} \int_0^s w(\sigma)\phi_{wL}^{'}(s-\sigma)d\sigma \tag{3}$$

$$M_b(s) = \frac{1}{2}\rho U^2 B^2 \frac{C_M^{'}}{U} \int_0^s w(\sigma)\phi_{wM}^{'}(s-\sigma)d\sigma \tag{4}$$

where s = Ut/B = non-dimensional time, $\phi_{wL}^{'}(s)$ and $\phi_{wM}^{'}(s)$ = derivatives of buffeting indicial functions, $\phi_{wL}(s)$ and $\phi_{wM}(s)$, respectively, C_L = lift coefficient, α = angle of attack, C_M' = $dC_M/d\alpha$, C_M = moment coefficient, w(s) = turbulent velocity in vertical direction. Since the section model used in the current work is symmetric, the lift and moment coefficients C_L and C_M are both zero at angle of attack α=0. Thus, as can be seen in Equations (3) and (4), the along-wind turbulence (u) term that enters through C_L and C_M does not appear.

The derivatives of given buffeting indicial functions, $\phi_{wL}^{'}(s)$ and $\phi_{wM}^{'}(s)$, are functions of non-dimensional time, s, as below:

$$\phi_{xx}^{'} = A_1 \cdot e^{-A_2 \cdot s} + A_3 \cdot e^{-A_4 \cdot s} \tag{5}$$

where A_1 to A_4 are constants, which can be extracted from wind tunnel buffeting tests.

A streamlined bridge deck section that is a thin rectangular section with semi-circular fairings at its both edges with an aspect ratio (B/D, B = total width and D = depth) of 15:1(B=300mm, D=20mm) was used in the experiments described in this paper. To extract aeroelastic parameters used in Equation (1)-(4) for this bridge deck section, two separate tests were carried out on a section model with end plates equipped in Bill James Wind Tunnel (0.915m width by 0.762m height). Forced-vibration method described in Cao and Sarkar (2010) was used to extract the Rational Function Coefficients, while method described in Chang et al. (2010) was used to extract the buffeting indicial functions. The parameters were extracted as below:

$$\underline{A}_0 = \begin{bmatrix} 0.3273 & -6.2384 \\ -0.0970 & 1.3818 \end{bmatrix}, \underline{A}_1 = \begin{bmatrix} -3.7549 & -1.4947 \\ 0.8510 & -0.3819 \end{bmatrix}, \underline{F} = \begin{bmatrix} -0.9484 & 1.3397 \\ 0.2689 & -0.1682 \end{bmatrix}, \lambda_{\mathrm{L}} = 0.1843, \lambda_{\mathrm{M}} = 0.2239$$

$$\phi'_{wL}(s) = 0.0081e^{-0.0058s} - 0.0392e^{-0.0833s}$$

$$\phi'_{wM}(s) = -0.0347e^{-0.0733s} + 0.0072e^{-0.0051s}$$

The static force and moment coefficients and their derivatives that are used in the buffeting load formulation are also measured in smooth wind tests as follows:

C_L =0, C_M =0, C_D = 0.037, C_L' = 4.639, C_M' = 1.085

Experimental Set-Up

Wind Tunnel and Gust Generation Mechanism

The experiments described here were performed in the Aerodynamic/Atmospheric Boundary Layer (AABL) Wind and Gust Tunnel, which is located in the Wind Simulation and Testing Laboratory (WiST Lab) in the Department of Aerospace Engineering at Iowa State University. This wind tunnel has an aerodynamic test section of 2.44m (8.0ft) width by 1.83m (6.0ft) height and an atmospheric boundary layer test section of 2.44m (8.0ft) width by 2.21m (7.25ft) height, and a designed maximum wind speed of 53m/s (173.9ft/s) in the aero section. An active gust generation mechanism was developed and implemented by Haan and Sarkar (2006) on this wind tunnel. Several types of gust can be generated by this mechanism, such as ramp-up or ramp-down gust, bump-shaped gust and sinusoidal-wave-shaped gust. In the experiment of current research, ramp-up, ramp-down and bump-shaped gusts were generated and investigated.

Model Suspension System and Boundary Layer Set-Up

The section model used in the experiment, as described earlier, is composed of a shallow box girder section and two semi-circular fairings at its edges. The length L, chord length B and thickness D of the model are about 1.83m, 0.74m, and 0.051m, respectively, making this model about 2.5 times larger than the section model described earlier that was used for the extraction of the aeroelastic load functions. The scale of this model to a real bridge deck in the field is about 1:50, considering a bridge deck could have a width of about 37m. A cross section diagram of current model is shown in Figure 1.

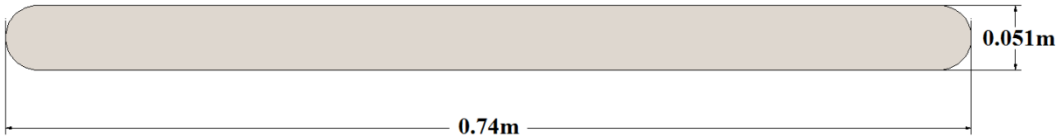

Figure 1. Cross section of the experimental model

To reduce the edge effects, two end plates were used as seen in Figure 2. The two-DOF model suspension system used in this experiment is shown in Figures 2 and 3. The suspension system enables vertical and torsional motions of the model using twelve linear helical springs, six at each end of the model, while horizontal motion is restricted by two leaf springs attached at both ends of the model shaft, as shown in Figure 3. Before running wind tunnel tests on the model, free vibration tests without wind were performed to identify the stiffness coefficients of the entire vibration system (with the model mounted) for the two degrees of freedom (vertical h and torsional α) as K_h = 2843.8 N/m and K_α = 119.5 Nm/rad, respectively. The natural frequencies of the two degree-of-freedom system at zero wind were measured as f_h = 2.015Hz, and f_α = 1.954Hz, and the damping ratios of the system at zero wind were measured as ζ_h = 1.02% and ζ_α = 0.69%, along the vertical and torsional degrees of freedom, respectively. The mass and mass moment of inertia of the entire dynamic system were M = 18.3kg, and I = 0.8275kgm^2, respectively.

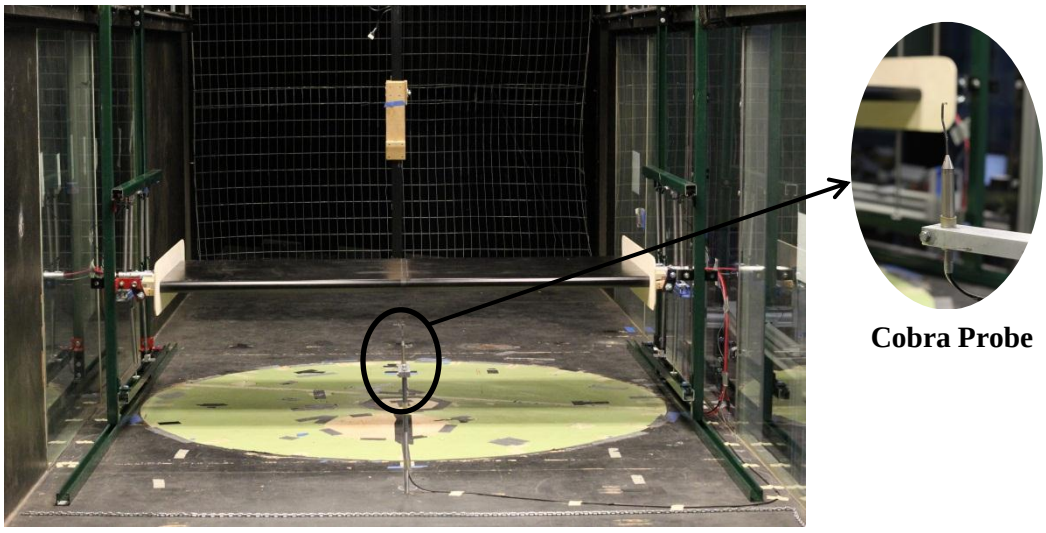

Figure 2. Experimental model and set-up (view from upstream)

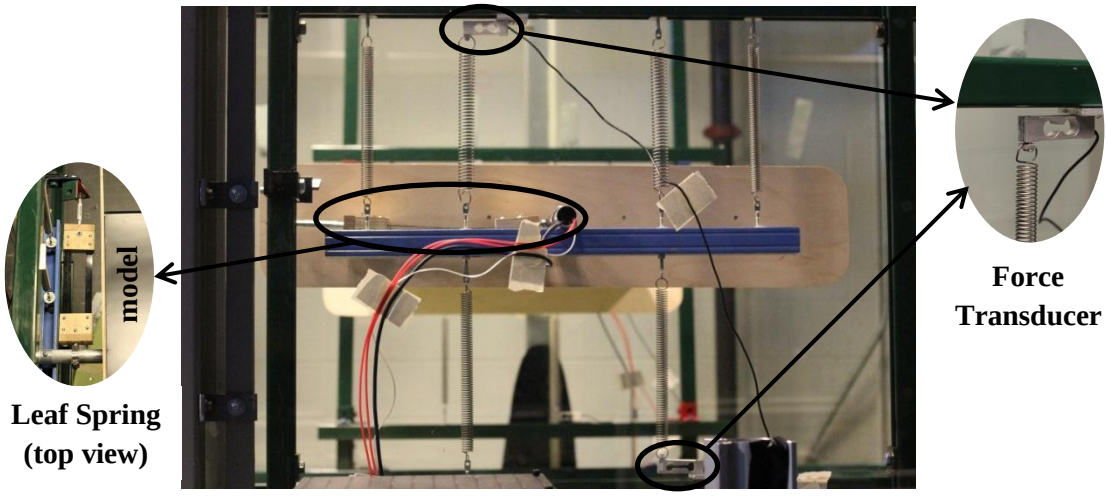

Figure 3. Experimental model and set-up (view from side)

In the current research, to investigate effect of turbulence on time-domain wind load prediction, two different types of set-up were used to generate boundary layers in front of the experimental model. The boundary layer set-ups are shown in Figure 4 and Figure 5. The first set-up consists of three spires, a wall and equally-spaced chains all the way to the

position of the model. The second set-up consists of three spires, a wall, and equally-spaced chains in the first half of the fetch and arranged in staggered configurations in rest of the fetch up to the position of the model.

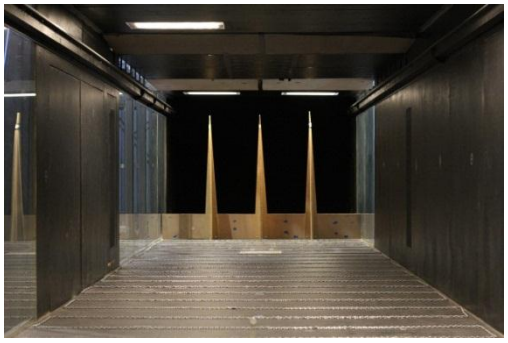

Figure 4. Boundary layer set-up 1

Figure 5. Boundary layer set-up 2

Wind Velocity Measurement

In this experiment, wind velocity time histories in three directions (u(t), v(t) and w(t)) were measured by a Cobra Probe (Turbulent Flow Instrumentation) placed right in front of the bridge deck model, as shown in Figure 2. The sampling rate for wind velocity was set at 312.5 Hz.

Model Displacement Measurement

The vertical or torsional displacement of the model was measured by measuring the elastic force in each of the four helical springs which is connected to the model at one end and a strain gage force transducer at the other end, as can be seen in Figure 3. The force transducers were mounted at two opposite corner positions at both ends of the model span to eliminate the spurious modes of vibration of the model such as rotation about its centerline. LabView program was used for data acquisition, where the sampling rate was set at 125Hz.

Aerodynamic Pressure Measurement

Aerodynamic pressures were also recorded in the experiment to assess aeroelastic loads for comparison with those obtained from numerical simulation. Surface pressures were measured on the model including the fairings through a row of pressure taps located on the upper and lower surfaces of the model along the mid-plane. In total, forty-two pressure taps were used in this test, equally distributed on both the surfaces. The pressure taps are denser on the upstream side than the downstream side of the model. Two 64-channel pressure modules (Scanivalve ZOC33/64 Px) were used to measure the pressure. To minimize the error introduced from pressure tubing, pressure modules were placed inside the model, so that tubing length can be significantly shortened, as shown in Figure 6.

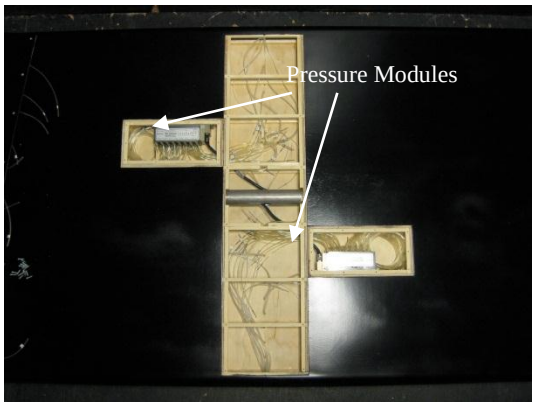

Figure 6. Pressure modules (Scanivalve ZOC 33/64 Px) mounted inside the model

A separate program (RAD) collected the pressure data. The sampling rate for pressure measurement was 62.5Hz (half of displacement sampling rate for convenience of synchronization) in the experiment.

Data Synchronization

To synchronize the displacement data with the pressure data and the wind velocity data, both the pressure transducers and the Cobra Probe were set to work in an external-triggered mode. The LabView program that was used for displacement data acquisition was programmed to output a digital signal when the displacement data acquisition started, so that the pressure data acquisition system and the Cobra Probe data acquisition system would receive this external signal and get triggered to start the data acquisition.

Results and Discussion

Before performing tests on the bridge deck model, to obtain the information about the wind field generated from two types of boundary layer set-ups, wind velocity profiles were measured using Cobra Probe mounted on a traverse system as shown in Figure 7. With the traverse system which is driven by the motor mounted on the top, the Cobra Probe can move continuously in vertical direction. In the experiment, the wind velocity was measured starting from the floor to the height of 0.65m. The height of the equilibrium position of the bridge deck model is about 0.55m which falls in the range of wind velocity measurement. Considering the length scale of this model (1:50) as mentioned earlier, the height of the model in the wind tunnel approximately corresponds to a height of 27.5m in the field which is reasonable for a bridge. The measured mean wind velocity profiles in horizontal direction for two different boundary layer set-ups are plotted in Figure 8. Turbulence intensity profiles in horizontal and vertical directions are plotted in Figure 9 and 10, respectively. It can be seen that the Boundary Layer 2, which has a section of chains replaced by roughness blocks,

has a lower mean wind velocity and higher turbulence intensity than Boundary Layer 1 at the height where the model is placed (0.55m), though the difference is not significant.

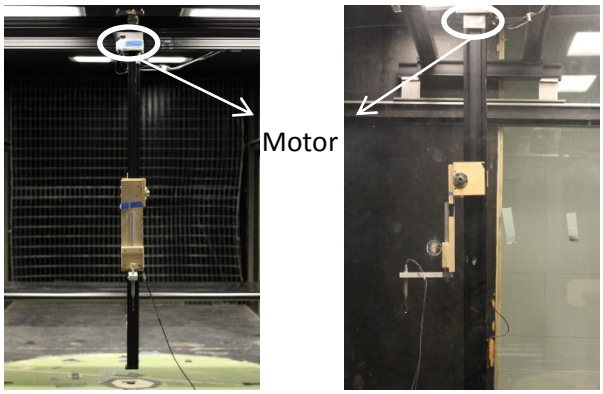

Figure 7. Traverse system used in velocity profile measurement

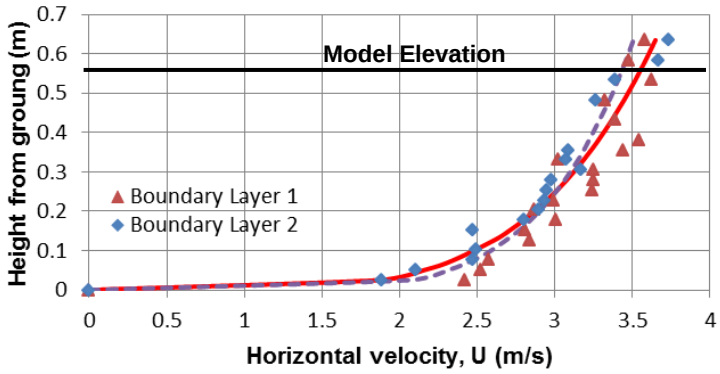

Figure 8. Profile of mean velocity in horizontal direction

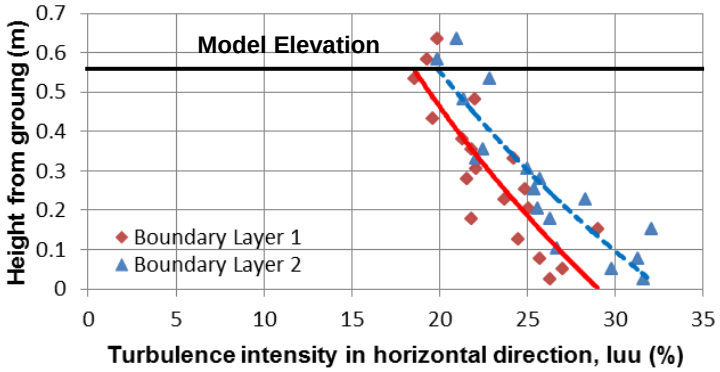

Figure 9. Profile of turbulence intensity in horizontal direction

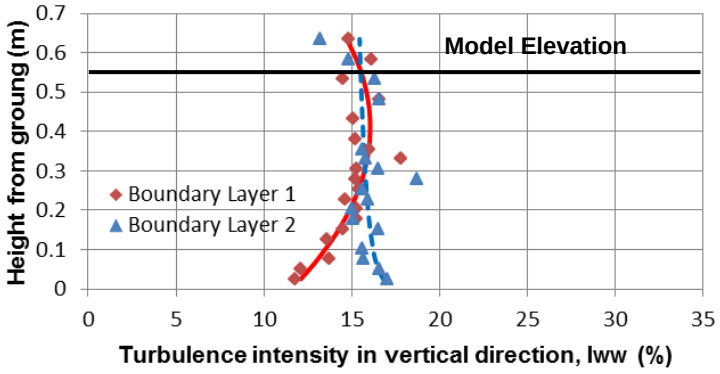

Figure 10. Profile of turbulence intensity in vertical direction

In model vibration tests, stationary wind and three other types of gusty winds (ramp-up, ramp-down and bump-shaped) were generated and applied on the model. From observation of experimental results, ramp-down gust case is similar to ramp-up gust case. Thus, for conciseness, the time histories measured in ramp-down gust case are not shown here. Time histories for stationary wind case, ramp-up gust case and bump-shaped gust case with first boundary layer set-up are shown in Figure 11-13, and those with second boundary layer set-up are shown in Figure 14-16. In the plots, the aeroelastic lift and moment coefficients are calculated using Equation (6) and (7).

$$C_l(t) = \frac{L(t)}{1/2\rho U^2(t)B} \tag{6}$$

$$C_m(t) = \frac{M(t)}{1/2\rho U^2(t)B^2} \tag{7}$$

where L(t) and M(t) are aeroelastic lift and moment per unit length obtained numerically or experimentally, and U(t) is the moving average of horizontal wind speed time history.

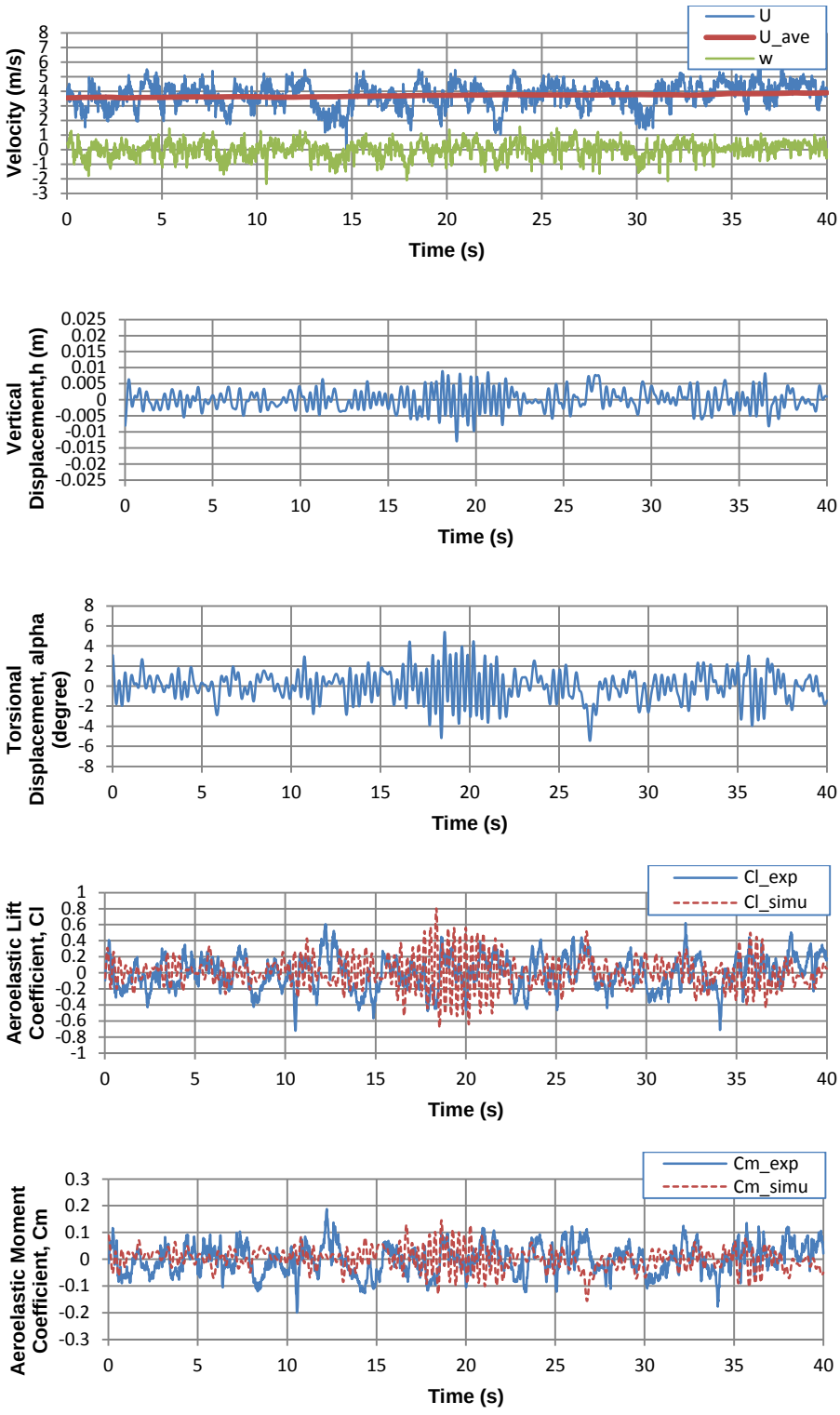

Figure 11. Time histories for stationary wind with first boundary layer set-up

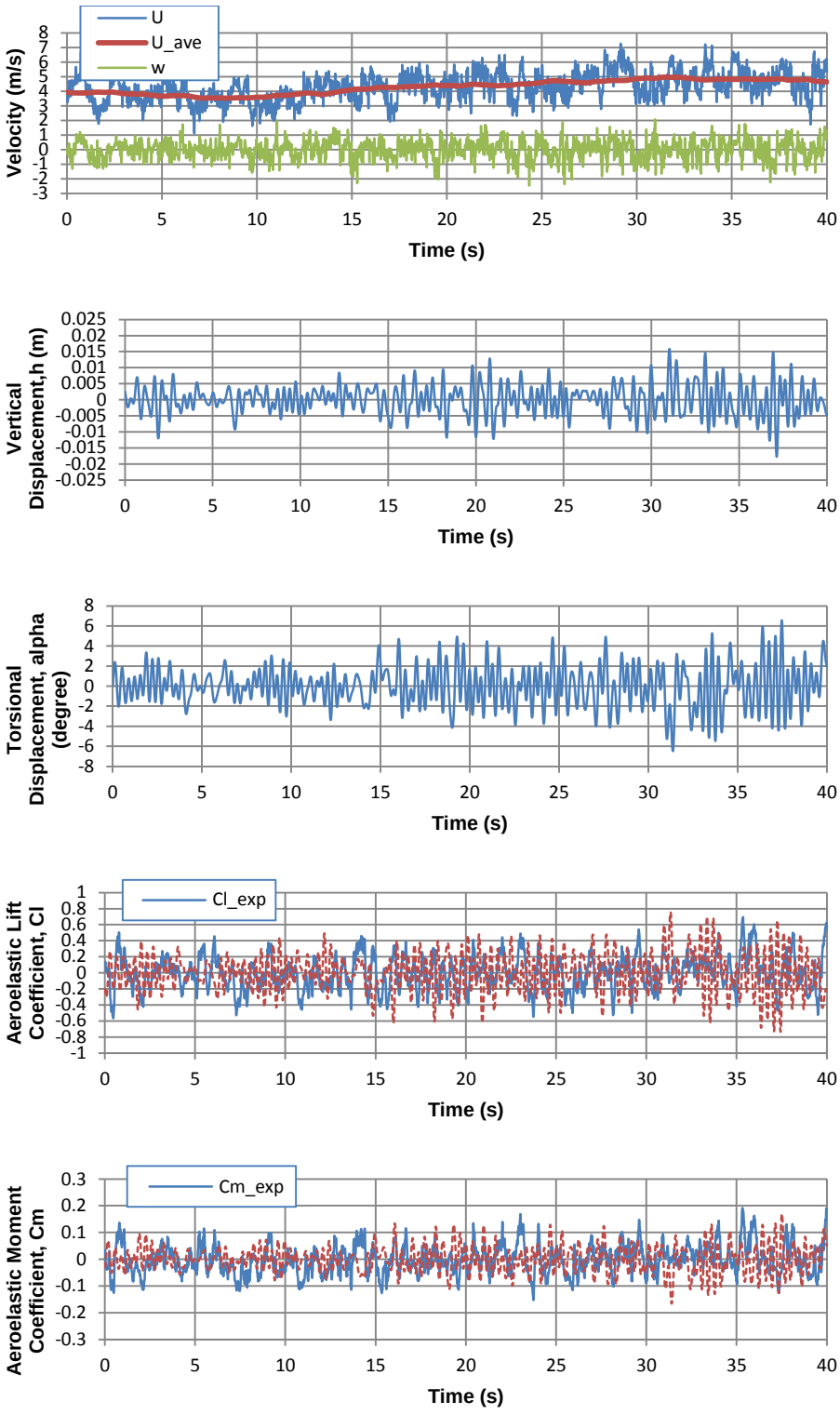

Figure 12. Time histories for ramp-up wind with first boundary layer set-up

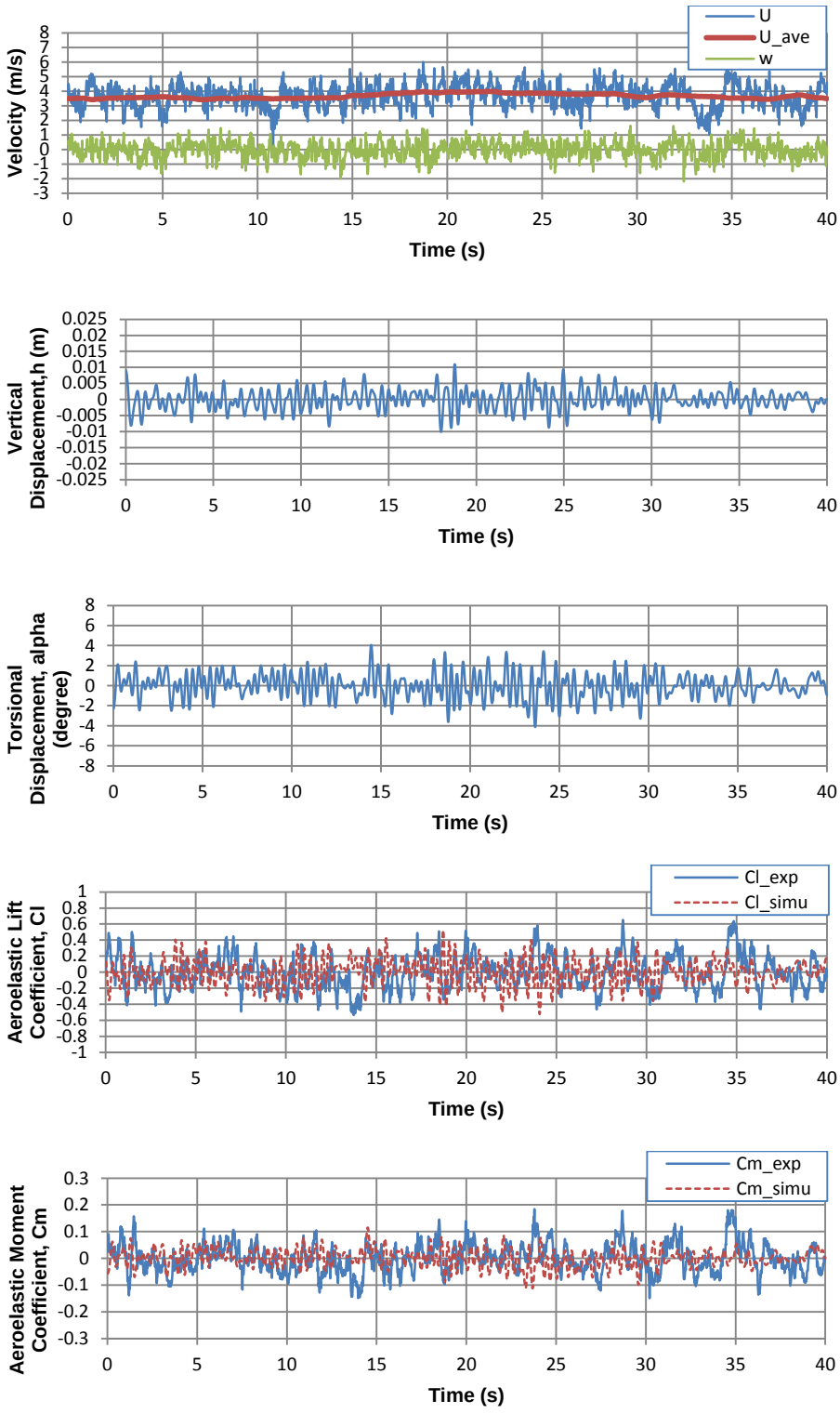

Figure 13. Time histories for bump-shaped wind with first boundary layer set-up

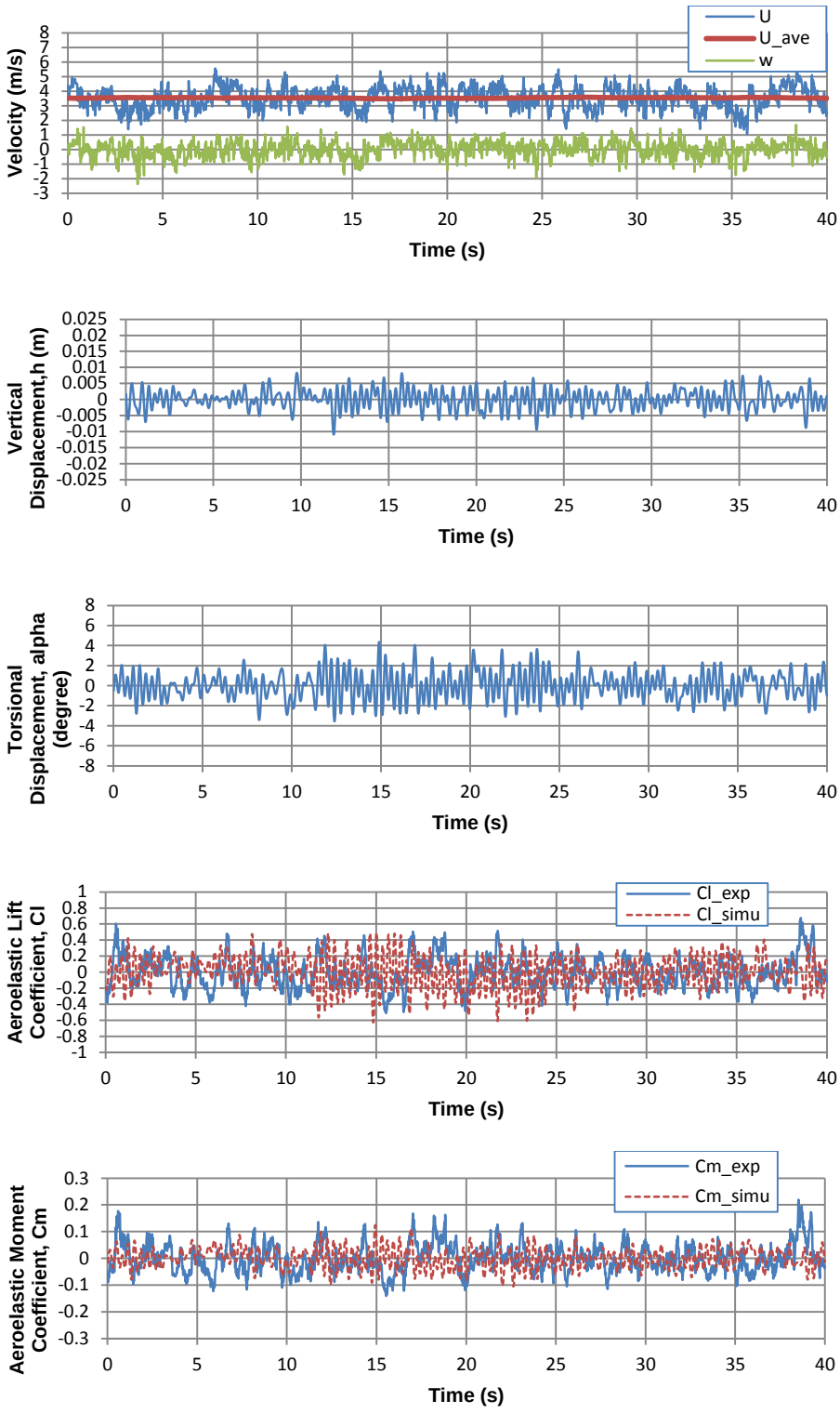

Figure 14. Time histories for stationary wind with second boundary layer set-up

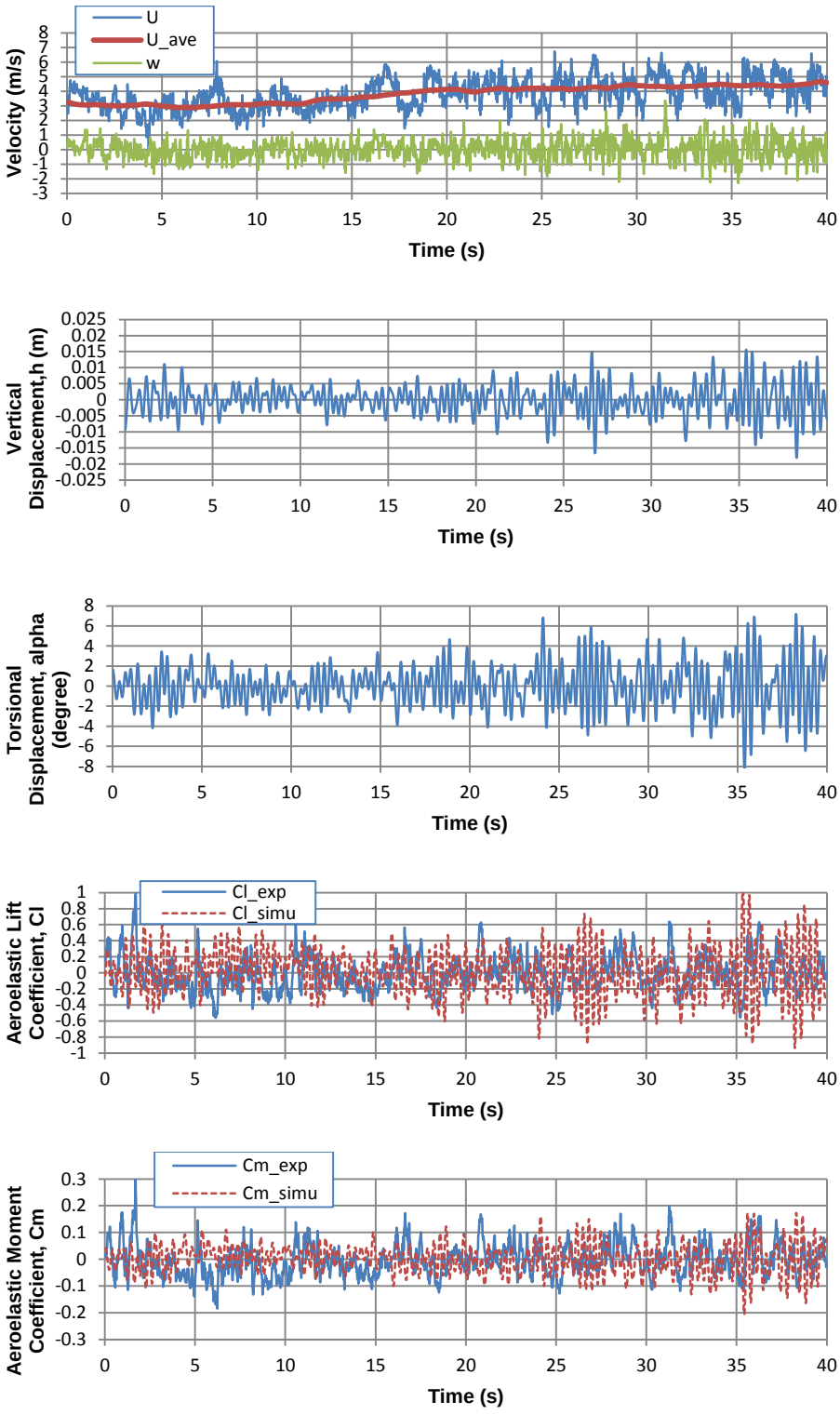

Figure 15. Time histories for ramp-up wind with second boundary layer set-up

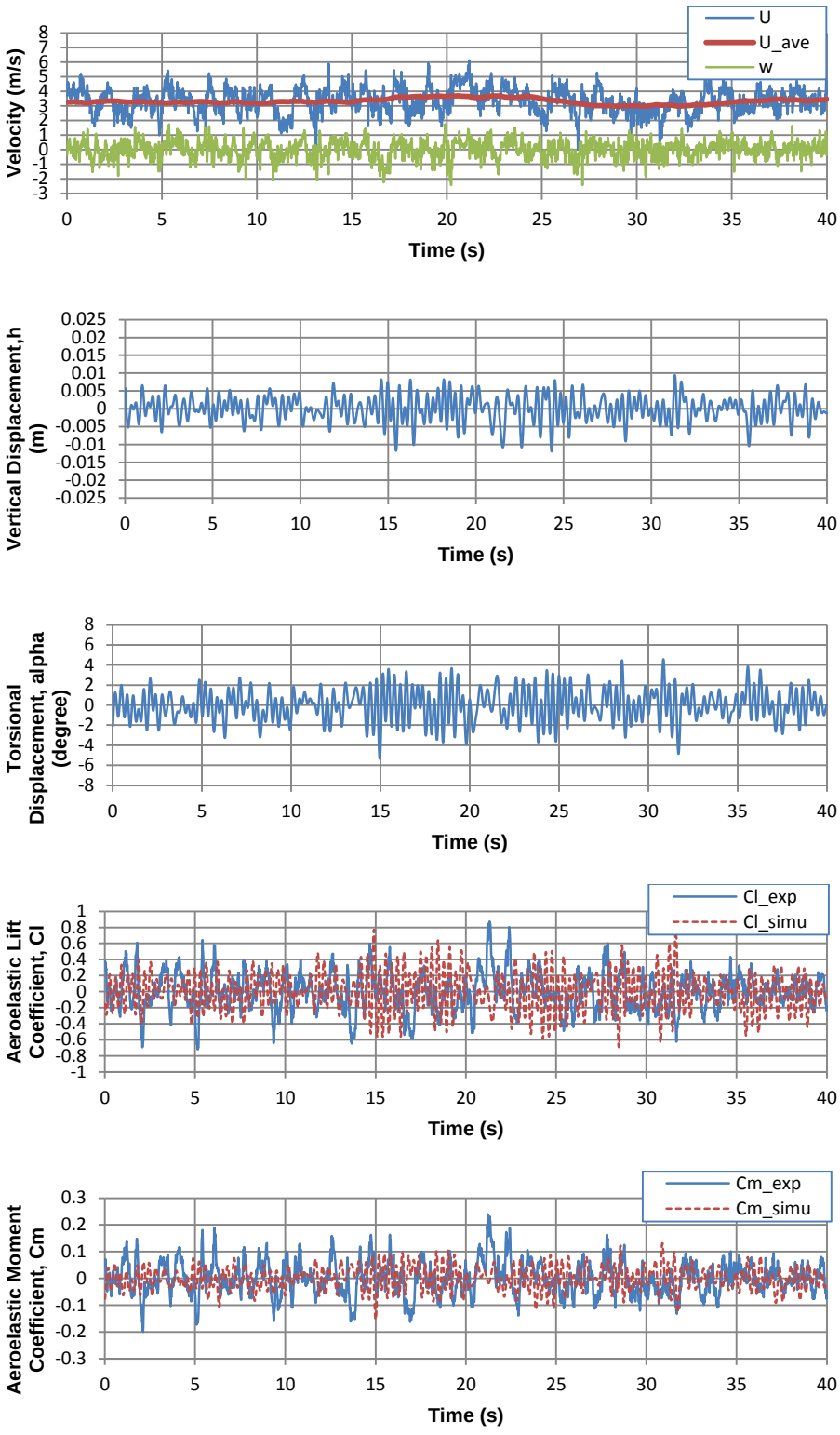

Figure 16. Time histories for bump-shaped wind with second boundary layer set-up

It can be seen from all the plots that the phase angles of aeroelastic load time histories cannot be well predicted for these turbulent wind cases. However, the changing of amplitude of load time histories as shown in ramp-up and bump-shaped gust cases can be reasonably predicted. Since the mean velocities and turbulence intensities of the winds generated by two types of boundary layers are close to each other, the obtained displacement and load time histories are also similar, except that the model vibrates with slightly larger amplitude in the second boundary layer, due to the slightly higher turbulence intensities as shown in Figure 9-10. Moreover, it is shown in the plots that load amplitude can be well predicted when model rotation angle is within +/-5 degree region, while the amplitude is over-predicted when the rotation angle exceeds this range, especially for the lift prediction, which can be seen in ramp-up gust cases. The existence of this valid region is expectable, since in the derivation of the self-excited load formulation used in current paper, it is assumed that the vibration of the structure is in small amplitudes so that the structural displacements and wind loads have a linear relationship.

In an earlier study by Cao and Sarkar (2011), using the same model and set-up, it has already been shown that the time domain method works very well in predicting aeroelastic wind loads for stationary and gusty winds with very low turbulence intensities. Since the buffeting wind loads are very small in smooth wind cases, the research by Cao and Sarkar (2011) mainly shows the self-excited wind loads can be predicted accurately by Rational Function formulation. Thus, the worse prediction shown in current study should come from the poor prediction of the buffeting part of wind loads. Considering the very high turbulence intensities generated in current experiment ($I_{uu} \approx 20\%$, $I_{ww} \approx 15\%$), it is possible that the

buffeting indicial formulation could not give good predictions for buffeting wind loads since the formulation is derived based on the assumption that the turbulent wind velocities are very small comparing to mean wind speed which is obviously not true in current experiment.

To quantitatively compare load coefficient time histories that obtained from experimental measurement and numerical simulation, standard deviations and peak values (first/second peak) of load coefficient time histories for two different boundary layers were computed and listed in Table 1-4. Since each case was repeated three times in the experiment, the results listed in the tables are average values calculated from three repeated tests to reduce randomness in the results.

Table 1. Comparison of standard deviation of time histories for the first boundary layer

	Standard Deviation		
	Stationary	Ramp-up	Bump-shaped
Cl_exp	0.21	0.21	0.21
Cl_simu	0.20	0.24	0.17
Cm_exp	0.06	0.05	0.05
Cm_simu	0.04	0.05	0.03

Table 2. Comparison of peak values of time histories for the first boundary layer

	Peak Value (first peak)			Peak Value (second peak)		
	Stationary	Ramp-up	Bump-shaped	Stationary	Ramp-up	Bump-shaped
Cl_exp	0.73	0.83	0.70	0.70	0.81	0.68
Cl_simu	0.93	0.84	0.54	0.92	0.83	0.54
Cm_exp	0.20	0.22	0.18	0.19	0.21	0.18
Cm_simu	0.19	0.18	0.11	0.19	0.18	0.11

Table 3. Comparison of standard deviation of time histories for the second boundary layer

	Standard Deviation		
	Stationary	Ramp-up	Bump-shaped
Cl_exp	0.21	0.20	0.22
Cl_simu	0.20	0.27	0.21
Cm_exp	0.06	0.06	0.06
Cm_simu	0.04	0.05	0.04

Table 4. Comparison of peak values of time histories for the second boundary layer

	Peak Value (first peak)			Peak Value (second peak)		
	Stationary	Ramp-up	Bump-shaped	Stationary	Ramp-up	Bump-shaped
Cl_exp	0.74	0.81	0.76	0.73	0.79	0.73
Cl_simu	0.68	1.01	0.79	0.66	0.99	0.78
Cm_exp	0.23	0.26	0.21	0.22	0.24	0.20
Cm_simu	0.14	0.19	0.16	0.14	0.19	0.16

According to the definition of standard deviation, it is used here to evaluate the prediction of average amplitudes of whole time histories. As can be seen from Table 1 and 3, with two different boundary layer set-ups, the average amplitudes of load coefficient time histories for both stationary wind cases and gusty wind (ramp-up and bump-shaped) cases are well predicted. The average amplitudes for lift coefficient time histories in ramp-up gust cases are predicted worst, especially for the second boundary layer set-up. As mentioned in earlier discussion for time history plots, this could be caused by the large amplitude vibration exists in the second half of ramp-up wind time histories, especially for the second boundary layer set-up in which the model vibrates with an even larger amplitude, since the self-excited load formulation cannot work well for large amplitude motions.

The peak values in the tables are used to evaluate the prediction of largest amplitudes which could be a major concern in the design process of structures. As shown in Table 2 and 4, the largest amplitude prediction for all the cases are reasonably well, even for lift coefficients in

ramp-up gust cases where the average amplitude prediction is slightly worse as discussed in the last paragraph.

Conclusion

Rational Function formulation and buffeting indicial formulation have been validated in predicting wind loads in stationary and gusty winds with high turbulence intensities. Two types of boundary layers generated in this research are similar, except the second boundary layer induced slightly larger amplitude vibration of the model in the tests, due to the slightly higher turbulence intensity. As shown in the experimental results of both boundary layer set-ups, the phase angles of load time histories cannot be well predicted, while the amplitude prediction is reasonable. It has been observed that the wind loads are over-predicted in amplitude when the model rotation angle is out of region of +/-5 degree which could result from the linearity assumption made in the derivation of time domain formulations. As a result, the predicted wind loads for ramp-up gust cases are not as good as other cases, since the model starts to vibrate in very large amplitude after wind velocity reaches a higher value in second half time period of the test. In the future, to evaluate buffeting load prediction separately, fixed model tests could be carried out in winds with several different turbulence levels. Some modification might be made to the current buffeting indicial function formulation so that the accuracy of buffeting load prediction and hence the total aeroelastic load prediction in turbulent wind environment can be improved.

References

Bartoli, G., Contri, S., Mannini, C., Righi, M. (2009). "Toward an improvement in the identification of bridge deck flutter derivatives," J. Eng. Mech., ASCE, 135(8), 771-785.

Batroli, G., Righi, M. (2006). "Flutter mechanism for rectangular prisms in smooth and turbulent flow," J. of Wind Eng. and Ind. Aero., 94(5), 275-291.

Brownjohn, J.M.W., Jakobsen, J.B. (2001). "Strategies for aeroelastic parameter identification from bridge deck free vibration data," J. of Wind Eng. and Ind. Aero., 89, 1113-1136.

Cao, B., Sarkar, P.P. (2010). "Identification of rational functions by forced vibration method for time-domain analysis of flexible structures," In Proceedings: The Fifth International Symposium on Computational Wind Engineering, Chapel Hill, May 23-27.

Chang, B., Sarkar, P.P. and Phares, B.M., (2010). "A time-domain model for predicting aerodynamic loads on a slender support structures for fatigue design," Journal of Engineering Mechanics, 136(6), 736-746.

Caracoglia, L., Jones, N.P. (2003). "Time domain vs. frequency domain characterization of aeroelastic forces for bridge deck sections," J. of Wind Eng. and Ind. Aero., 91, 371-402.

Chen, C., Wu, J., Chen, J. (2008). "Prediction of flutter derivatives by artificial neural networks," J. Wind Eng. Ind. Aerodyn., 96, 1925-1937.

Chen, X., Kareem, A. (2008). "Identification of critical structural modes and flutter derivatives for predicting coupled bridge flutter," J. Wind Eng. Ind. Aerodyn., 96, 1856-1870.

Davenport, A.G. (1962). “Buffeting of a suspension bridge by storm winds,” J. Structural Eng., ASCE, 88 (3), 233-268.

Diana, G., Bruni, S., Cigada, A., Collina, A. (1993). “Turbulence effect on flutter velocity in long span suspended bridges,” J. of Wind Eng. and Ind. Aero., 48(2-3), 329-342.

Ding, Q., Zhou, Z., Zhu, L., Xiang, H. (2010). “Identification of flutter drivatives of bridge decks with free vibration technique,” J. Wind Eng. Ind. Aerodyn., 98, 911-918.

Gan Chowdhury, A., Sarkar, P.P. (2004). “Identification of eighteen flutter derivatives of an airfoil and a bridge deck,” Wind and Struct., 7(3), 187-202.

Gan Chowdhury, A., Sarkar, P.P. (2005). “Experimental identification of rational function coefficients for time-domain flutter analysis,” Eng. Struct., 27(9), 1349-1364.

Gu, M., Zhang, R., Xiang, H. (2000). “Identification of flutter derivatives of bridge decks.” J. Wind Eng. Ind. Aerodyn., 84, 151-162.

Gu, M., Zhang, R., Xiang, H. (2001). “Parametric study on flutter derivatives of bridge decks,” Eng. Struct., 23(12), 1607-1613.

Huston D.R., Bosch, H.R., Scanlan, R.H. (1988). “The effects of fairings and of turbulence on the flutter derivatives of a notably unstable bridge deck,” J. of Wind Eng. and Ind. Aero., 29(1-3), 339-349.

Karpel, M. (1982). “Design for active flutter suppression and gust alleviation using state-space aeroelastic modeling,” J. of Aircraft 19(3), 221–227.

Roger, K. (1977). “Airplane math modeling methods for active control design,” AGARD-CP-228.

Sarkar, P.P., Cao, B. (2011) “Time-domain loads and response of flexible bridges in gusts: wind-tunnel model validation,” Engineering Mechanics Institute Conference, Boston, June 2-4.

Sarkar, P.P., Jones, N.P., Scanlan, R.H. (1994). “Identification of aeroelastic parameters of flexible bridges,” J. Eng. Mech., 120(8), 1718-1742.

Scanlan, R.H., Jones, N.P. (1990). “A minimum design methodology for evaluating bridge flutter and buffeting response,” J. of Wind Eng. and Ind. Aero.,36(2), 1341-1353.

Scanlan, R.H., Lin, W.H. (1978). “Effects of turbulence on bridge flutter derivatives,” J. of Eng. Mech., ASCE, 104(4), 719-733.

Scanlan, R.H., Tomko, J.J. (1971). “Airfoil and bridge deckflutter derivatives,” J. Eng. Mech. Div., 97(6), 1717-1733.

Scanlan, R.H. (1988). “On flutter and buffeting mechanisms in long-span bridges,” Prob. Eng. Mech., 3(1), 22-27.

Scanlan, R.H. (1997). “Amplitude and turbulence effects on bridge flutter derivatives,” J. of Struc. Eng., 123(2), 232-236.

Tsiatas, G., Sarkar, P.P. (1988). “Motion stability of long-span bridges under gusty winds,” J. of Eng. Mech., ASCE, 114(2).

Zhu, L.D., Xu, Y.L., Zhang, F., Xiang, H.F. (2002). “Tsing Ma bridge deck under skew winds- Part II: flutter derivatives.” J. Wind Eng. Ind. Aerodyn., 90, 807-837.

CHAPTER 6. GENERAL CONCLUSIONS

GENERAL DISCUSSION

The current research work includes following three parts: (a) the development of an algorithm to extract time domain Rational Function Coefficients using phase lags identified from forced vibration experiment which is then validated by one-DOF vibration tests on a streamlined section model, (b) the development of an improved algorithm which is based on direct least squares method to extract Rational Function Coefficients using forced vibration technique and applications on both a streamlined and a bluff cross section model with two-DOF motions, and (c) the validation of time domain method for aeroelastic wind load prediction through free vibration tests of a section model in smooth/turbulent and stationary/gusty winds.

Extraction of rational functions by forced vibration method for time-domain analysis of long-span bridges

A new method has been introduced to directly extract rational function coefficients or rational functions from forced vibration experiment. Through numerical tests, it has been shown that the algorithm is feasible for extraction of rational function coefficients and it is quite robust. The validation results of the obtained rational functions show that flutter derivatives extracted from this RFA method are generally in good agreement with those from earlier free vibration experimental results, given their sensitivity to noise in the signals.

Identification of Rational Functions using Two-Degree-of-Freedom Model by Forced Vibration Method

A new algorithm has been developed for direct extraction of all the Rational Function Coefficients for one, two or three-DOF forced vibration wind tunnel tests on a section model. The algorithm does not use phase angle difference between displacement and aeroelastic force time histories in the extraction procedure like in previous methods available in the literature. Thus, the error introduced in all the parameters from error in identification of one parameter, i.e. phase angle difference, is eliminated in this algorithm. Rather this new algorithm uses all the recorded data points to identify the unknown parameters in a least square sense that minimizes the error originating from the noisy signals. The proposed algorithm is more efficient than others since it requires data collected at two wind speeds only to extract the full set of Rational Function Coefficients for a two-DOF system. As part of the validation process, the Rational Functions obtained in this paper were converted into flutter derivatives and were compared with directly extracted ones obtained in earlier experiments by other scholars, for both streamlined and bluff section models. The comparison is well, especially for the streamlined model case. Moreover, it was shown that the Rational Function Coefficients obtained using this algorithm can be used to accurately predict the self-excited forces acting on a section model at a given wind speed, for both a streamlined cross section and a bluff cross section. Further, the flutter speed of the streamlined cross section bridge deck model was predicted using Rational Function Coefficients obtained here and has been shown to match with earlier results.

Time-Domain Aeroelastic Loads and Response of Flexible Bridges in Gusty and Turbulent Wind: Prediction and Experimental Validation

Time domain method was used to predict aeroelastic loads on a streamlined bridge section model while it is vibrating in stationary and gusty straight-line winds. The Rational Functions and buffeting indicial functions were used to calculate self-excited forces and buffeting forces, respectively. The numerically simulated loads were compared with experimental measurements for both stationary wind case and gusty wind case. It was demonstrated here that the prediction of aeroelastic loads using the time-domain formulation can be made. The comparison between predictions and measurements was quite well in the stationary wind case, while a similar comparison in the gusty wind case was not as good but reasonable within the error bounds expected. The slightly worse performance of time domain method in gusty wind case is explainable since all the formulations used in this paper were originally derived for stationary wind problems and the aeroelastic parameters used here were also extracted in stationary winds. However, a better prediction is expected if the time domain formulations are revised to fit for the gusty wind cases which could be investigated in future work.

Rational Function formulation and buffeting indicial formulation have been validated in predicting wind loads in stationary and gusty winds with high turbulence intensities. Two types of boundary layers generated in this research are similar, except the second boundary layer induced slightly larger amplitude vibration of the model in the tests, due to the slightly higher turbulence intensity. As shown in the experimental results of both boundary layer set-ups, the phase angles of load time histories cannot be well predicted, while the amplitude

prediction is reasonable. It has been observed that the wind loads are over-predicted in amplitude when the model rotation angle is out of region of +/-5 degree which could result from the linearity assumption made in the derivation of time domain formulations. As a result, the predicted wind loads for ramp-up gust cases are not as good as other cases, since the model starts to vibrate in very large amplitude after wind velocity reaches a higher value in second half time period of the test.

RECOMMENDATIONS FOR FUTURE WORK

In current research, the improved algorithm for extraction of Rational Function Coefficients has been applied on a two-DOF motion system and with smooth wind environment. However, the algorithm itself can be simply extended to three-DOF motion system, where the lateral motion could also be included. Thus, once a driving mechanism for three-DOF motion could be designed and set up in the wind tunnel, the forced vibration experiment could be performed to extract all the Rational Function Coefficients for the three-DOF system simultaneously using the algorithm developed in current research. Moreover, since the algorithm is based on forced vibration technique which can be used in turbulent wind environment, it can be applied to investigate if the Rational Function Coefficients are consistent or will change in the winds with different turbulence intensities.

In the future, to evaluate buffeting load prediction separately, fixed model tests could be carried out in the winds with several different turbulence levels. In this way, time domain formulations for aeroelastic wind loads could be investigated more clearly, and it will be known that which part of formulation needs to be modified to improve the total prediction of wind loads. Furthermore, the performance of the time-domain load prediction method for

winds that are non-uniform with height such as boundary-layer wind, and not straight-line but highly non-stationary, such as microbursts or tornadoes, could be investigated.

ACKNOWLEGEMENTS

I would like to express my heartily gratitude to my Ph.D. advisor, Dr. Partha P. Sarkar. I would like to firstly thank him for offering me the opportunity to pursue my Ph.D. study and continuously support me through the end of this study. I also would like to thank his patience, his enthusiasm, and his great efforts during my Ph.D. study which enabled me to go through this whole journey. It is really a great honor for me to pursue my study under his guidance.

I would like to thank my committee members, Dr. Hui Hu, Dr. Peter J. Sherman, Dr. William A. Gallus, and Dr. Sivalingam Sritharan, for evaluating my research work and giving insightful comments. I also thank them to give me valuable suggestions on my Ph.D. study.

I would like to thank laboratory technicians, William L. Rickard and James D. Benson, for offering me countless kind help in my wind tunnel tests.

I would like to thank department secretaries, Dee Pfeiffer and Gayle Fay, for their help on all of my paper works and material processing during my study.

I especially wish to thank my wife, Yuan Feng, for her continuous support on my study and research, and for letting me know there are lots of wonderful things in the world other than research works. I would like to thank my new born son, Lanhao, for bringing tons of happiness in my life, even though he just met me several weeks ago.

Lastly, and most importantly, I wish to thank my parents, Yiming Xiao and Xiaolin Cao, for giving me life to come to this wonderful world, raising me up to become who I am today, and always supporting me through my life.